Two- and three-gluon glueballs within the helicity formalism

Cyrille Chevalier[*]
Service de Physique Nucléaire et Subnucléaire, Université de Mons, UMONS Research Institute for Complex Systems, Place du Parc 20, 7000 Mons, Belgium

Vincent Mathieu[†]
Departament de Física Quàntica i Astrofísica and Institut de Ciències del Cosmos, Universitat de Barcelona, E08028, Barcelona, Spain

(Received 25 March 2025; accepted 14 May 2025; published 8 July 2025)

Both positive and negative charge conjugation glueball spectra are computed with a constituent gluon approach. We first compute the spectrum of the Hamiltonian describing two-gluon bound states having $C = +$, before tackling the three-gluon bound states having $C = -$. We review the construction of two and three particle helicity states in order to build totally symmetric wave functions for our glueball states. In the literature, two different couplings schemes are used to build three particle states. We derive for the first time the relation between these two three-body state definitions. The glueball spectra are compared with those obtained from quantum chromodynamics simulations on a lattice. The two-gluon glueball spectra show a good agreement with the constituent approach and the numerical lattice simulations. The three-gluon spectrum is in overall agreement with the masses observed on the lattice but also predicts additional low-lying states.

DOI: 10.1103/cvld-kwkd

I. INTRODUCTION

One of the earliest predictions of quantum chromodynamics (QCD) is the existence of color-singlet pure-gauge states known as glueballs [1]. Despite this theoretical prediction, a consensus on their properties and definitive experimental evidence remains elusive. Two-gluon glueball states have been extensively studied both theoretically [2,3] and experimentally [3,4]. Theoretical results have been obtained using various phenomenological approaches, functional methods, and lattice QCD (LQCD). On the experimental side, notable experimental efforts by collaborations such as PANDA, Crystal Barrel, WA102, or BESIII continue the search for these states. In contrast, three-gluon glueballs have received relatively little attention due to the technical complexity involved. On the theory side, the LQCD spectrum is expected to include three-gluon states [5–8]. Experimentally, the possible observation of odderon exchange at TOTEM is still debated [9].

This work aims to describe two- and three-gluon systems within the framework of constituent models. In these approaches, hadronic states are treated as colorless bound states of several constituent quarks, antiquarks, and/or gluons. The requirement of color neutrality determines whether a given combination of constituent particles can form a hadron. Constituent gluons transform under $SU(3)_c$ with its adjoint representation denoted 8, leading to the following decompositions for two- and three-gluon systems [10]

$$8 \otimes 8 = 1 \oplus \ldots, \qquad 8 \otimes 8 \otimes 8 = 1 \oplus \ldots. \tag{1}$$

These decompositions indicate the possibility of forming bound states of two and three constituent gluons, so-called two- and three-gluon glueballs, in constituent approaches. The dynamics of these bound states are implemented using a phenomenological but QCD inspired Hamiltonian. Properties of constituent particles often differ from their QCD counterparts (for instance, constituent quarks are often treated as heavier than their QCD equivalents). For two-gluon glueballs, it has been shown in Ref. [11] that constituent gluons have to be considered as massless particles with helicity degrees of freedom in order to reproduce results from LQCD calculations. As a result, extending this approach to three-gluon glueballs seems to necessitate addressing the three-body helicity formalism.

[*]Contact author: cyrille.chevalier@umons.ac.be
[†]Contact author: vmathieu@ub.edu

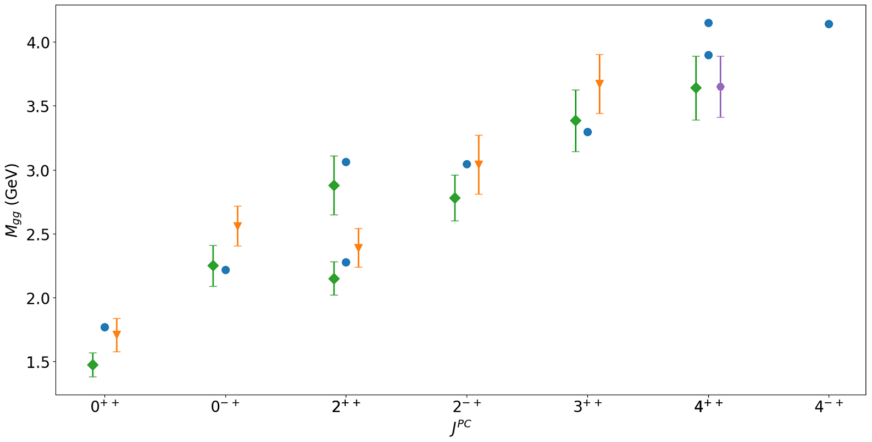

FIG. 1. Comparison of two-gluon glueball spectra. Upper bounds obtained with the current approach (blue circles) are compared to LQCD results from [5] (orange triangles), [7] (green diamonds), and [8] (purple hexagon).

The article is organized as follows. Section II introduces the helicity formalism for one- and two-body systems. Given its important role in most of the subsequent calculations and because the management of three-gluon glueballs requires us to demonstrate novel properties within this formalism, this section provides a relatively detailed overview. Additionally, for pedagogical purpose and for the sake of generality, the case of massive particles is included in the description. Section III applies these results to compute the spectrum of two-gluon glueballs. As already mentioned, a detailed study of two-gluon glueballs in the constituent approach already exists in the literature [11–13]. However, the extension to three-gluon glueballs necessitates revisiting the two-gluon spectrum and introducing a methodology better suited for three-gluons systems. Section IV develops the helicity formalism for three-body systems. Section V investigates three-gluon glueballs. This section is decomposed into three parts: First, helicity states with proper symmetry properties are constructed, second, expressions to compute Hamiltonian matrix elements (MEs) on these states are prepared, and, lastly, the spectrum is obtained and analyzed. The manuscript closes in Sec. VI with a recap of the key results and suggestions for prospects.

In a few words, the use of helicity degrees of freedom proves to allow for an accurate reproduction of the two-gluon glueball spectrum observed in LQCD, as illustrated in Fig. 1. Extending this approach to three-gluon systems yields the spectrum shown in Fig. 2. Overall, each state identified by LQCD has a corresponding counterpart in the spectrum obtained with the helicity formalism, but additional low-lying states are also predicted by the method. While definitive explanations for these discrepancies remain elusive, possible interpretations are suggested at the end of Sec. V.

II. THE HELICITY FORMALISM FOR ONE- AND TWO-BODY SYSTEMS

This section reviews the main concepts underlying the helicity formalism for one- and two-body systems. A

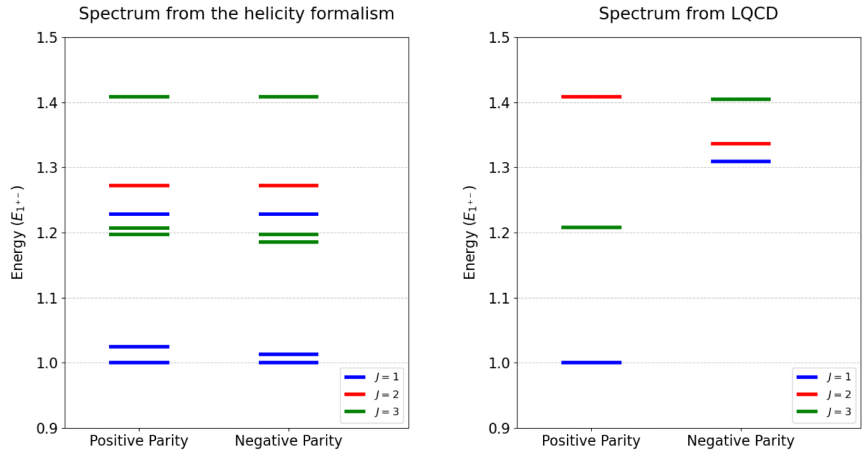

FIG. 2. Comparison of glueball spectra obtained using the helicity formalism (left, this work) and LQCD (right, Refs. [5,6]). In both cases, spectra are provided in units of the lowest mass.

detailed recap is provided, as the analysis of three-body systems requires demonstrating new properties of helicity states. The discussion is kept general to enable application to a variety of systems. Glueball-specific considerations are deferred to the next section.

A. One-body helicity states

To start with, let us focus on massive particles. Massive particles are classified according to their eigenvalue for both Casimir operators of the Poincaré group (PG), namely the mass operator P^2 and the spin operator W^2 (also known as the Pauli-Lubanski Casimir). Any state $|\psi; m; s\rangle$ such that[1]

$$\begin{aligned} P^2|\psi;m;s\rangle &= m^2|\psi;m;s\rangle \\ \text{and}\quad W^2|\psi;m;s\rangle &= -m^2 s(s+1)|\psi;m;s\rangle \end{aligned} \tag{2}$$

is a possible state to describe a particle of mass m and spin s. The current work uses the mostly minus convention for the Minkowski metric. To write the actual state of the particle, one has to resort to complete sets of states in which it can be decomposed. In the current work, two different complete sets will be used.

1. The one-body canonical states

The first set is filled with the common eigenstates of the third component of the Pauli-Lubanski W_3 and of the four P_μ operators. In the following, such common eigenstates, referred to as one-body canonical states, will be denoted $|m; p\theta\phi; sm_s\rangle$. The labels in the notation provide the eigenvalues of the aforementioned operators,

$$\begin{aligned} P^2|m;p\theta\phi;sm_s\rangle &= m^2|m;p\theta\phi;sm_s\rangle, \\ W^2|m;p\theta\phi;sm_s\rangle &= -m^2 s(s+1)|m;p\theta\phi;sm_s\rangle, \end{aligned} \tag{3}$$

$$\begin{aligned} P_0|m;p\theta\phi;sm_s\rangle &= \sqrt{m^2+p^2}|m;p\theta\phi;sm_s\rangle, \\ P_1|m;p\theta\phi;sm_s\rangle &= p\cos\phi\sin\theta|m;p\theta\phi;sm_s\rangle, \\ P_2|m;p\theta\phi;sm_s\rangle &= p\sin\phi\sin\theta|m;p\theta\phi;sm_s\rangle, \\ P_3|m;p\theta\phi;sm_s\rangle &= p\cos\theta|m;p\theta\phi;sm_s\rangle, \end{aligned} \tag{4}$$

$$W_3|m;p\theta\phi;sm_s\rangle = mm_s|m;p\theta\phi;sm_s\rangle. \tag{5}$$

Physically speaking, each p-canonical state has a definite mass, spin, four-momentum, and spin projection along the z axis. The associated Lorentz-invariant orthonormality and completeness relations are written below,

$$\begin{aligned} &\langle m;\bar{p}\,\bar{\theta}\,\bar{\phi};s\bar{m}_s|m;p\theta\phi;sm_s\rangle \\ &\quad = 2w\delta(p-\bar{p})\delta(\phi-\bar{\phi})\delta(\cos\theta-\cos\bar{\theta})\delta_{m_s\bar{m}_s}, \end{aligned} \tag{6}$$

$$\sum_{m_s=-s}^{s}\int |m;p\theta\phi;sm_s\rangle\frac{\mathrm{d}^3p}{2w}\langle m;p\theta\phi;sm_s| = \mathbb{1}, \tag{7}$$

where $w=\sqrt{m^2+p^2}$. Normalization conventions used in this document follow the ones from [14]. In the literature, one-body canonical states are often decomposed as the application of a so-called canonical boost on a rest state $|m; sm_s\rangle$,

$$\begin{aligned} |m;p\theta\phi;sm_s\rangle &= U(L(m,p,\theta,\phi))|m;sm_s\rangle \\ &= U(R(\phi,\theta,0)L_z(m,p)R(\phi,\theta,0)^{-1})|m;sm_s\rangle. \end{aligned} \tag{8}$$

Above, $R(\alpha,\beta,\gamma)$ refers to a rotation of Euler angles (α,β,γ) while $L_z(m,p)$ is a boost that provides a spatial momentum of modulus p and along the z axis to particle of mass m initially at rest. Hereinabove, these transformations are combined to produce a so-called canonical boost denoted $L(m,p,\theta,\phi)$. The notation U reminds us that whenever space-time transformations are applied on states, their action follows a given unitary representation of the PG. By construction, rest states $|m; sm_s\rangle$ transform under rotations using the spin s irreducible representation of $SO(3)$. As a result, whenever applied on a rest state, rotations are concretely represented by the well-known Wigner D matrices [15],

$$U(R(\alpha,\beta,\gamma))|m;sm_s\rangle = \sum_{m_s'=-s}^{s} D^s_{m_s'm_s}(\alpha,\beta,\gamma)|m;sm_s'\rangle. \tag{9}$$

Formula (8) provides an intuitive graphic interpretation for one-body canonical states which is illustrated in Fig. 3. In the left-hand part of the diagram, the rest state is represented with a single green arrow which stands for its spin projection. The state is then subjected to a rotation and a boost which, notably, alter its momentum represented by a red arrow. After successive transformations, as expected, the state ends with a momentum direction (θ,ϕ) and with a definite spin projection along the z axis. Apart from its visualization use, this expression combined with relation (8) also enables easy derivations of transformation rules under operations such as rotations, boosts, and parity. The interested reader is referred to [16] for more details.

2. The one-body helicity states

Although one-body canonical states are abundantly used in quantum mechanics, especially in the nonrelativistic limit, this set cannot encompass massless particles. For this reason, a second set of states is introduced. The states are

[1]We are using natural units, $\hbar = c = 1$, throughout this work.

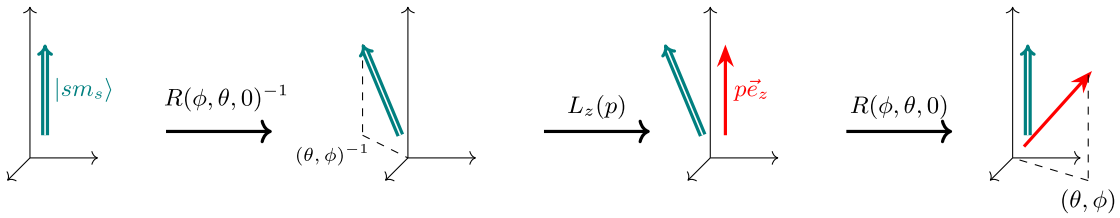

FIG. 3. Graphic illustration for the definition (8) of one-body p-canonical states.

still chosen as the common eigenstates of the four P_μ generators but, instead of W_3, these are taken as eigenstates of Λ, the helicity operator,

$$\Lambda = \frac{\boldsymbol{J}\cdot\boldsymbol{P}}{\sqrt{\boldsymbol{P}^2}}. \tag{10}$$

Above, $\boldsymbol{P}$ and $\boldsymbol{J}$ collect the spatial components of the momentum and angular momentum, respectively. These states are named one-body helicity states and are denoted $|m;p\theta\phi;s\lambda\rangle$. Relations (3) and (4) remain true in terms of one-body helicity states, but (5) is replaced by

$$\Lambda|m;p\theta\phi;s\lambda\rangle = \lambda|m;p\theta\phi;s\lambda\rangle. \tag{11}$$

States now have a definite spin projection along their momentum direction. The completeness and orthonormality relations for one-body helicity states are similar to the ones for one-body canonical states (same conventions are used),

$$\begin{aligned}&\langle m;\bar{p}\,\bar{\theta}\,\bar{\phi};s\bar{\lambda}|m;p\theta\phi;s\lambda\rangle\\&\quad= 2w\delta(p-\bar{p})\delta(\phi-\bar{\phi})\delta(\cos\theta-\cos\bar{\theta})\delta_{\lambda\bar{\lambda}},\end{aligned} \tag{12}$$

$$\sum_{\lambda=-s}^{s}\int |m;p\theta\phi;s\lambda\rangle\frac{\mathrm{d}^3p}{2w}\langle m;p\theta\phi;s\lambda| = \mathbb{1}. \tag{13}$$

As well as canonical states, helicity ones can also be expressed in terms of a rest state on which boosts and rotations are applied,

$$\begin{aligned}|m;p\theta\phi;s\lambda\rangle &= U(L_h(m,p,\theta,\phi))|m;s\lambda\rangle\\&= U(R(\phi,\theta,0)L_z(m,p))|m;s\lambda\rangle.\end{aligned} \tag{14}$$

In comparison with relation (8), the canonical boost L has here been replaced by a helicity boost L_h which differs by a rotation. The graphic interpretation set up for relation (8) in Fig. 3 can be adapted to fit with formula (14). The result is shown in Fig. 4. Referring to the same graphical conventions, one can see that the state ends with a definite projection of the spin along the momentum direction instead of along the z axis. This feature is in agreement with the definition of the helicity operator. Before we discuss the properties of one-body helicity states, let us draw the reader's attention to the convention used for relation (14). In the current definition, the third angle of the rotation has been settled to zero, a choice which will be denoted as the zero convention in the following. Some other references consider $-\phi$ for this angle [14,17,18],

$$|m;p\theta\phi;s\lambda\rangle_{-\phi} = U(R(\phi,\theta,-\phi)L_z(m,p))|m;s\lambda\rangle. \tag{15}$$

A priori, such a modified relation should result in a different definition for one-body helicity states. However, these two different definitions are shown to simply differ by a phase factor,

$$|m;p\theta\phi;s\lambda\rangle = e^{-i\lambda\phi}|m;p\theta\phi;s\lambda\rangle_{-\phi}. \tag{16}$$

Because physics is contained in the modulus squared of the state, this phase factor proves to be irrelevant in assessing a physical interpretation for one-body helicity states. Nevertheless, the user has to be conscious and consistent with the convention he employs, especially if he wants to superpose different helicity states. The current work will always use the zero convention.

The decomposition (14) also allows one to prove many properties about helicity states. Only a few of them will be recapped here. For more properties and demonstrations, the

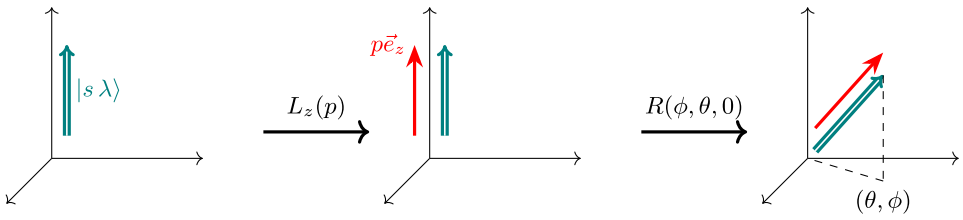

FIG. 4. Graphic illustration for the definition (14) of one-body p-helicity states.

interested reader is referred to [14,16,17,19]. The first property to be investigated is the transformation rule of helicity states under rotations. Simple algebra allows us to show that

$$U(R(\alpha,\beta,\gamma))|m;p\theta\phi;s\lambda\rangle = \pm e^{-i\xi\lambda}|m;p\theta'\phi';s\lambda\rangle \tag{17}$$

where θ', ϕ', and ξ satisfy $R(\phi',\theta',\xi) = R(\alpha,\beta,\gamma)R(\phi,\theta,0)$. The phase $\exp(-i\xi\lambda)$ comes out while ensuring that the state, initially in 0 convention, ends in that same convention. Concerning the plus or minus sign, it is included to account for the fact that any hypothetical 2π rotation must be identified with minus the identity for fermions. Property (17) is sometimes referred to as helicity rotational invariance, because the quantum number λ remains unchanged despite the rotation.

Second, the action of the parity transformation, Π, on one-body helicity states can be determined by making use of the commutation relations between parity, boosts, and rotations. The following formula is obtained:

$$\Pi|m;p\theta\phi;s\lambda\rangle = \eta(-1)^{-s}|m;p(\pi-\theta)(\pi+\phi);s-\lambda\rangle. \tag{18}$$

Notice that the classical intuition that parity inverts the particle's momentum and helicity is respected. Above, η refers to the intrinsic parity of the particle. This quantity defines how parity acts on the particle rest state,

$$\Pi|m;s\lambda\rangle = \eta|m;s\lambda\rangle. \tag{19}$$

It depends on the nature of the particle. In relation (18), both left- and right-hand-side states are written in the zero convention. However, in many references, the right-hand side is written in a different convention, such as the π convention

$$\begin{aligned}|m;p(\pi-\theta)(\pi+\phi);s\lambda\rangle_\pi &= U(R(\pi+\phi,\pi-\theta,\pi))U(L_z(m,p))|m;s\lambda\rangle\\ &= U(R(\phi,\theta,0))U(R(0,\pi,0))U(L_z(m,p))|m;s\lambda\rangle\end{aligned} \tag{20}$$

or the opposite convention

$$\begin{aligned}|m;p(\pi-\theta)(\pi+\phi);s\lambda\rangle_- &= U(R(\phi,\theta,0))U(L_{-z}(m,p))|m;s-\lambda\rangle\\ \text{with}\quad L_{-z}(m,p) &= R(0,\pi,0)L_z(m,p)R(0,-\pi,0).\end{aligned} \tag{21}$$

All these conventions being equal up to phase factors, they convey the same physical meaning,

$$\begin{aligned}|m;p(\pi-\theta)(\pi+\phi);s\lambda\rangle &= (-1)^\lambda|m;p(\pi-\theta)(\pi+\phi);s\lambda\rangle_\pi\\ &= (-1)^s|m;p(\pi-\theta)(\pi+\phi);s\lambda\rangle_-.\end{aligned} \tag{22}$$

These various conventions are introduced to simplify calculations that mix helicity states with opposed directions. Such situations will for example be encountered in Sec. II B where helicity states for two-body systems in their center-of-mass frame (c.m.f.) are introduced.

Third, we focus on the application of a general Lorentz transformation L on an helicity state $|m;p\theta\phi;s\lambda\rangle$. The corresponding transformation rule reads as follows:

$$U(L)|m;p\theta\phi;s\lambda\rangle = \sum_{\lambda'=-s}^{s} D^s_{\lambda'\lambda}(\alpha_W,\beta_W,\gamma_W)|m;p'\theta'\phi';s\lambda'\rangle. \tag{23}$$

Hereinabove, primed variables denote the components of the boosted momentum which are obtained by applying L on the initial four-momentum. In addition, $(\alpha_W,\beta_W,\gamma_W)$ denotes the Euler angles of a rotation R_W, named Wigner rotation, defined by the following combination of boosts:

$$R_W = (L_h(m,p',\theta',\phi'))^{-1}LL_h(m,p,\theta,\phi). \tag{24}$$

Relation (23) illustrates that, in general, the helicity of a massive state is not invariant under Lorentz transformations. The invariance of helicity under rotation (17) can be seen as a special case of property (23).

Finally, it is possible to switch from the one-body helicity basis to the one-body canonical one. Comparing relation (14) for the helicity state to relation (8) for the canonical state and using relation (9) provides the following transformation rule:

$$|m;p\theta\phi;s\lambda\rangle = \sum_{m_s=-s}^{s} D^s_{m_s\lambda}(\phi,\theta,0)|m;p\theta\phi;sm_s\rangle. \tag{25}$$

This property allows the user to switch the complete set, based on its intended use.

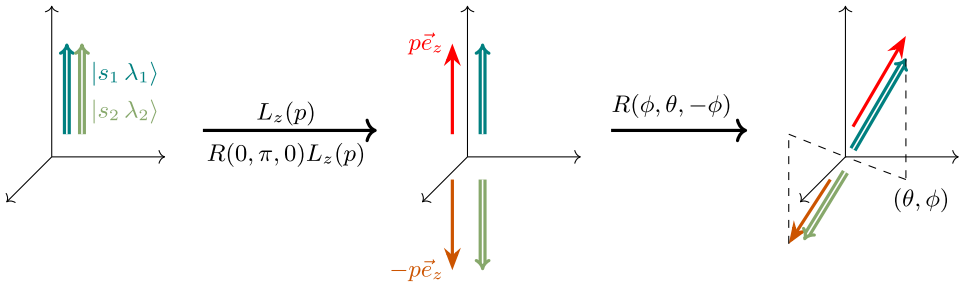

FIG. 5. Schematic illustration for the definition of two-body p-helicity state (26a).

Before closing this section, let us insist on the fact that helicity states generalize very well to massless particles. In a common simplification of reality, massless particles are considered to behave as massive particles with only two spin projections, $+s$ and $-s$. This rule allows us to infer the massless behavior from the massive one. Appendix A goes beyond this simplification and provides more details about the distinction between massive and massless particles.

B. Two-body helicity states

One-body helicity states (14) can be used to build a complete set of states for two-body systems. Because, in the following, these many-body states will be used to describe composite particles, we will focus on obtaining helicity states in the c.m.f. of the entire many-body system (the e.c.m.f.). Properties of composite particles are most easily obtained in this frame: Mass is given by the total energy of the state while spin is given by its total angular momentum. Before we dive into this description, let us shorten a bit the notations. In the previous section, one-body states at rest where denoted $|m, sm_s\rangle$, a notation in which the mass, the spin, and the spin projection of the particle were specified. In the following, the mass of the particle will be frequently omitted. By default, it will be assumed that the state $|s_i\lambda_i\rangle$ possesses the mass of the ith particle. Similarly, in the following sections, boosts along the z axis will be written without specifying any mass parameter. By default, this parameter will be assumed equal to the mass of the state on which the boost acts.

1. Helicity bases for two-body systems

Again, our analysis starts at the level of massive particle states. Differences in the presence of massless particles will be discussed subsequently. Two particles are brought in their c.m.f. by boosting them back to back,

$$|p\theta\phi; s_1\lambda_1 s_2\lambda_2\rangle = (-1)^{\lambda_2 - s_2} U(R(\phi,\theta,0))[U(L_z(p))|s_1\lambda_1\rangle \otimes U(R(0,\pi,0)L_z(p))|s_2\lambda_2\rangle] \tag{26a}$$

$$= (-1)^{\lambda_2 - s_2} U(R(\phi,\theta,0)L_z(p))|s_1\lambda_1\rangle \otimes U(R(\pi+\phi,\pi-\theta,\pi)L_z(p))|s_2\lambda_2\rangle. \tag{26b}$$

Above, p, θ, and ϕ respectively denote the modulus, the polar, and the azimuthal angle of the momentum of the first particle in the e.c.m.f. Helicities λ_1 and λ_2 are defined in that same frame. The phase in front of the definition is mainly conventional [17] and results from the choice to assign to the one-body state with opposed momentum the opposite convention (21). Figure 5 schematically decomposes the successive transformations in definition (26a). By construction, states (26a) are eigenstates of particle 1 and 2 momentum operators. In the following, they will be referred to as two-body p-helicity states. Their orthonormalization relation is

$$\langle \bar{p}\,\bar{\theta}\,\bar{\phi}; s_1\bar{\lambda}_1 s_2\bar{\lambda}_2|p\theta\phi; s_1\lambda_1 s_2\lambda_2\rangle = \frac{4W}{p}\delta(\bar{W}-W)\delta(\cos\bar{\theta}-\cos\theta)\delta(\bar{\phi}-\phi)\delta_{\bar{\lambda}_1\lambda_1}\delta_{\bar{\lambda}_2\lambda_2} \tag{27}$$

$$= \frac{4w_1(p)w_2(p)}{p^2}\delta(\bar{p}-p)\delta(\cos\bar{\theta}-\cos\theta)\delta(\bar{\phi}-\phi)\delta_{\bar{\lambda}_1\lambda_1}\delta_{\bar{\lambda}_2\lambda_2} \tag{28}$$

where $w_i(p)$ serves as a notation shortcut for $\sqrt{m_i^2+p^2}$ and where $W = w_1(p) + w_2(p)$ is the total energy of the two-body state. If expression (26b) is more convenient for practical purposes, (26a) unveils that these states present a specific structure: They are obtained by rotating two-body states at rest with a reference orientation, here along the z axis,

$$|p; s_1\lambda_1 s_2\lambda_2\rangle = (-1)^{\lambda_2 - s_2}(U(L_z(p))|s_1\lambda_1\rangle \otimes U(R(0,\pi,0)L_z(p))|s_2\lambda_2\rangle). \tag{29}$$

A similar structure will reappear in the definition of helicity states for three-body systems in Sec. IV.

As already mentioned, states with a definite total angular momentum are expected. Such a property can be provided to two-body p-helicity states by weighting them with a Wigner D matrix and by integrating the result on angular degrees of freedom,

$$|p;JM;s_1\lambda_1 s_2\lambda_2\rangle = \sqrt{\frac{2J+1}{4\pi}}\int \mathrm{d}\cos\theta \mathrm{d}\phi D^{J*}_{M\lambda_1-\lambda_2}(\phi,\theta,0)|p\theta\phi;s_1\lambda_1 s_2\lambda_2\rangle. \tag{30}$$

In the following, these states will be referred to as two-body J-helicity states. The prefactor is introduced to ensure a standard normalization,

$$\langle \bar{p};\bar{J}\,\bar{M};s_1\bar{\lambda}_1 s_2\bar{\lambda}_2|p;JM;s_1\lambda_1 s_2\lambda_2\rangle = \frac{4W}{p}\delta(\bar{W}-W)\delta_{\bar{J}J}\delta_{\bar{M}M}\delta_{\bar{\lambda}_1\lambda_1}\delta_{\bar{\lambda}_2\lambda_2} \tag{31}$$

$$= \frac{4w_1(p)w_2(p)}{p^2}\delta(\bar{p}-p)\delta_{\bar{J}J}\delta_{\bar{M}M}\delta_{\bar{\lambda}_1\lambda_1}\delta_{\bar{\lambda}_2\lambda_2}. \tag{32}$$

Of course, definition (30) is only relevant for $J \geq |\lambda_1-\lambda_2|$. It can be shown that, under rotations, two-body J-helicity states follow the spin J irreducible representation of $SO(3)$ [16,20], meaning that this state indeed has a total angular momentum J. For further use, let us mention that definition (30) can be inverted, expressing two-body p-helicity states as a linear combination of two-body J-helicity states [19],

$$|p\theta\phi;s_1\lambda_1 s_2\lambda_2\rangle = \sum_{J=|\lambda_1-\lambda_2|}^{\infty}\sum_{M=-J}^{J}\sqrt{\frac{2J+1}{4\pi}}D^{J}_{M\lambda_1-\lambda_2}(\phi,\theta,0)|p;JM;s_1\lambda_1 s_2\lambda_2\rangle. \tag{33}$$

Other properties of these states are abundantly described in the literature [11,14,16,17,19]. Their behavior under parity and permutation of particles, denoted $\mathbb{P}_{12}$, will be reminded here for further use,

$$\Pi|p;JM;s_1\lambda_1 s_2\lambda_2\rangle = \eta_1\eta_2(-1)^{J-s_1-s_2}|p;JM;s_1-\lambda_1 s_2-\lambda_2\rangle, \tag{34}$$

$$\mathbb{P}_{12}|p;JM;s\lambda_1 s\lambda_2\rangle = (-1)^{J+2s}|p;JM;s\lambda_2 s\lambda_1\rangle. \tag{35}$$

Above, η_i is the intrinsic parity of the ith particle. Symmetry having to be implemented only for identical particles, s_1 and s_2 have been taken equal to each other in relation (35). These two properties illustrate that two-body J-helicity states are neither parity eigenstates nor (anti) symmetric by themselves. Parity eigenstates are obtained by superposing states with opposed helicity signs. Non-normalized symmetric (antisymmetric) states are obtained by applying the two-body symmetrizer $\mathbb{S}_2$ (anti-symmetrizer $\mathbb{A}_2$),

$$\mathbb{S}_2 = \mathbb{1}+\mathbb{P}_{12}, \qquad \mathbb{A}_2 = \mathbb{1}-\mathbb{P}_{12}. \tag{36}$$

As agreed, helicity states have been written in the zero convention. Switching the convention to the "$-\phi$" one results in a different phase convention for p-helicity states. Nevertheless, provided that angles of the Wigner D matrix in definition (30) are adapted consequently, it can be shown that two-body J-helicity states are not affected.

In the presence of massless particles, the results presented above remain correct up to a few adjustments. First in definition (26a) and (26b), the conventional phase has to be adapted to remove any spin occurrence, such a quantum number being formally undefined for massless particles. Following the usual misuse that massless particles have spin degrees of freedom with forbidden intermediary projections, it seems appropriate to replace s_2 by $|\lambda_2|$. Second, relations (34) and (35) only account for massive particles. It can be shown that, for massless ones, the factor $(-1)^{-s_1-s_2}$ has to be replaced by $(-1)^{\lambda_1+\lambda_2}$ while the $(-1)^{2s}$ factor from (35) has to be replaced by $(-1)^{2|\lambda_1|}$. Notice that, as long as helicities are integers, one can naively use massive relations with $\lambda_i = \pm s_i$ to deal with massless particles. The case of helicity states for two massless particles is also briefly discussed at the end of Appendix A.

Two-body p- and J-helicity states are not the two only complete sets able to describe two-body systems at rest. For massive particles, one can replace in definition (26b) each occurrence of p-helicity states by p-canonical ones. It

results in the following definition for the so-called two-body p-canonical states [16]:

$$|p\phi\theta; s_1 m_{s_1} s_2 m_{s_2}\rangle = U(R(\phi,\theta,0)L_z(p)R^{-1}(\phi,\theta,0))|s_1 m_{s_1}\rangle \otimes U(R(\pi+\phi,\pi-\theta,0)L_z(p)R^{-1}(\pi+\phi,\pi-\theta,0))|s_2 m_{s_2}\rangle. \tag{37}$$

These states are then used to define two-body J-canonical states through intermediary spin and spatial angular momentum couplings,

$$|p; JM; \ell s; s_1 s_2\rangle = \sum_{m_\ell, m_s, m_{s_1}, m_{s_2}} (\ell m_\ell s m_s | JM)(s_1 m_{s_1} s_2 m_{s_2}|s m_s) \int \mathrm{d}\cos\theta \mathrm{d}\phi Y^\ell_{m_\ell}(\theta,\phi)|p\theta\phi; s_1 m_{s_1} s_2 m_{s_2}\rangle. \tag{38}$$

Above, $(j_1 m_1 j_2 m_2|j_3 m_3)$ refers to a Clebsh-Gordan coefficient and $Y^\ell_{m_\ell}(\theta,\phi)$ to a spherical harmonic. Because of the appearance of an orbital angular momentum quantum number ℓ, this definition is often used in nonrelativistic treatments. The interested reader will find a description of the properties of two-body canonical states in Ref. [16]. It is possible to relate two-body J-canonical states to two-body J-helicity states,

$$|p; JM; s_1\lambda_1 s_2\lambda_2\rangle = \sum_{s=|s_1-s_2|}^{s_1+s_2} \sum_{\ell=|J-s|}^{J+s} \sqrt{\frac{2\ell+1}{2J+1}}(s_1\lambda_1 s_2 -\lambda_2|s\lambda_1-\lambda_2)(\ell 0 s\lambda_1-\lambda_2|J\lambda_1-\lambda_2)|p; JM; \ell s; s_1 s_2\rangle. \tag{39}$$

This relation allows us to easily switch from one to the other set of states. For instance, it has been used in [11] to describe two-gluon glueballs in constituent approaches.

2. Decomposition of a physical two-body state in J-helicity states

Two-body J-helicity states can be used to model two-body composite particles. In the e.c.m.f., any two-body state with spin J and helicity quantum numbers can be decomposed as an integral on internal momentum degree of freedom of two-body p-helicity states. For two-body systems, the internal motion is ruled by the relative momentum $\boldsymbol{p} = (\boldsymbol{p_1} - \boldsymbol{p_2})/2$ whose modulus and angles have already been denoted p, θ, and ϕ. Let us start by decomposing a generic two-body state in the e.c.m.f., denoted $|\Phi; s_1\lambda_1 s_2\lambda_2\rangle$, as a combination of two-body p-helicity states. Using the completeness relation of the latter, one gets

$$|\Phi; s_1\lambda_1 s_2\lambda_2\rangle = \int \frac{p^2 \mathrm{d}p \mathrm{d}\cos\theta \mathrm{d}\phi}{4 w_1(p) w_2(p)} \Phi(p,\theta,\phi)|p\theta\phi; s_1\lambda_1 s_2\lambda_2\rangle \tag{40}$$

where

$$\Phi(p,\theta,\phi) = \langle p\theta\phi; s_1\lambda_1 s_2\lambda_2|\Phi; s_1\lambda_1 s_2\lambda_2\rangle \tag{41}$$

is the two-body helicity-momentum wave function of the state. The Jacobian factor in (40) ensures consistency with the normalization of two-body p-helicity states (28). Without additional requirements, this state does not have the expected definite total angular momentum J. However, the definition of two-body J-helicity states proved that this property can be supplied by imposing the angular dependence of $\Phi(p,\theta,\phi)$,

$$\Phi^J_M(p,\theta,\phi) = \sqrt{\frac{2J+1}{4\pi}}\Psi(p) D^{J*}_{M\lambda_1-\lambda_2}(\phi,\theta,0). \tag{42}$$

The function $\Psi(p)$ can be understood as a radial helicity-momentum wave function. Replacing Φ by Φ^J_M in expression (40) results in the decomposition of a generic two-body helicity state with total angular momentum J, denoted $|\Psi; JM; s_1\lambda_1 s_2\lambda_2\rangle$, in two-body J-helicity states,

$$|\Psi; JM; s_1\lambda_1 s_2\lambda_2\rangle = \int \frac{p^2 \mathrm{d}p}{4 w_1(p) w_2(p)} \Psi(p)|p; JM; s_1\lambda_1 s_2\lambda_2\rangle. \tag{43}$$

States $|\Psi; JM; s_1\lambda_1 s_2\lambda_2\rangle$ can be used to model spin J two-body composite particles. If the composite state is made of identical particles or is expected to possess a parity quantum number, the hereinabove discussion has to be slightly adapted. The structure (43) still applies but two-body J-helicity states on the right-hand side have to be replaced by parity and/or symmetry eigenstates which are obtained using properties (34) and (35). Concerning normalization, states $|\Psi; JM; s_1\lambda_1 s_2\lambda_2\rangle$ are expected to have a unit normalization,

$$\langle \Psi; JM; s_1\lambda_1 s_2\lambda_2|\Psi; JM; s_1\lambda_1 s_2\lambda_2\rangle = 1. \tag{44}$$

Using expression (43) and orthonormalization of two-body J-helicity states (32), one can transfer this normalization condition to the $\Psi(p)$ wave function,

$$\int \frac{p^2 \mathrm{d}p}{4w_1(p)w_2(p)} |\Psi(p)|^2 = 1. \tag{45}$$

For convenience, it is worth introducing a modified radial helicity-momentum wave function denoted $\Xi(p)$ that includes the Jacobian factors from (45),

$$\Xi(p) = \frac{p\Psi(p)}{2\sqrt{w_1(p)w_2(p)}}. \tag{46}$$

In terms of $\Xi(p)$, the normalization condition (45) significantly simplifies

$$\int \mathrm{d}p |\Xi(p)|^2 = 1, \tag{47}$$

while (43) has to be slightly adapted,

$$|\Psi; JM; s_1\lambda_1 s_2\lambda_2\rangle = \int \frac{p\mathrm{d}p}{2\sqrt{w_1(p)w_2(p)}} \times \Xi(p)|p; JM; s_1\lambda_1 s_2\lambda_2\rangle. \tag{48}$$

Notice that, Ψ having to remain finite for all p, Ξ must necessarily cancel at $p = 0$ for massive particles. Further tests show that this condition stays required in the massless case.

3. Calculations with physical two-body states

The following developments aim to evaluate the MEs of observables, such as Hamiltonians, on composite particle states. It focuses on unsymmetrical two-body J-helicity states (48) but can easily be adapted to symmetrized odd/even helicity states. Since states (48) are decomposed in a momentum representation, observables that depend on momentum variables prove easier to evaluate. Let us consider an observable $\mathcal{O}(\hat{p})$ that only depends on the modulus of the relative momentum (we are only interested in spherically symmetric variables). Let us evaluate $\mathcal{O}(\hat{p})$ on $|\Psi; JM; \lambda_1\lambda_2\rangle$,

$$\begin{aligned}&\langle\Psi; JM; s_1\bar{\lambda}_1 s_2\bar{\lambda}_2|\mathcal{O}(\hat{p})|\Psi; JM; s_1\lambda_1 s_2\lambda_2\rangle \\ &= \int \frac{\bar{p}\mathrm{d}\bar{p}}{2\sqrt{w_1(\bar{p})w_2(\bar{p})}} \frac{p\mathrm{d}p}{2\sqrt{w_1(p)w_2(p)}} \Xi(\bar{p})^*\Xi(p)\langle\bar{p}; JM; s_1\bar{\lambda}_1 s_2\bar{\lambda}_2|\mathcal{O}(\hat{p})|p; JM; s_1\lambda_1 s_2\lambda_2\rangle.\end{aligned} \tag{49}$$

In two-body J-helicity states, being by construction eigenstates of p, the action of $\mathcal{O}(p)$ reduces to a simple scalar multiplication. Using orthonormality relation (32), one gets

$$\langle\Psi; JM; s_1\bar{\lambda}_1 s_2\bar{\lambda}_2|O(\hat{p})|\Psi; JM; s_1\lambda_1 s_2\lambda_2\rangle = \delta_{\lambda_1\bar{\lambda}_1}\delta_{\lambda_2\bar{\lambda}_2} \int \mathrm{d}p |\Xi(p)|^2 \mathcal{O}(p). \tag{50}$$

A similar expression accounts for symmetrized odd/even helicity state as long as these are correctly orthonormalized.

The evaluation of operators that depend on position variables proves to be more difficult to handle. Let us consider $\mathcal{O}(\hat{r})$ an operator that only depends on the modulus of the relative position (again, the emphasis is put on spherically symmetric observables), one may require to evaluate it on the composite particle state,

$$\begin{aligned}&\langle\Psi\bar{J}\,\bar{M}; s_1\bar{\lambda}_1 s_2\bar{\lambda}_2|\mathcal{O}(\hat{r})|\Psi; JM; s_1\lambda_1 s_2\lambda_2\rangle \\ &= \int \frac{\bar{p}\mathrm{d}\bar{p}}{2\sqrt{w_1(\bar{p})w_2(\bar{p})}} \frac{p\mathrm{d}p}{2\sqrt{w_1(p)w_2(p)}} \Xi(\bar{p})^*\Xi(p)\langle\bar{p}; \bar{J}\,\bar{M}; s_1\bar{\lambda}_1 s_2\bar{\lambda}_2|\mathcal{O}(\hat{r})|p; JM; s_1\lambda_1 s_2\lambda_2\rangle.\end{aligned} \tag{51}$$

Above, different total angular momenta J and $\bar{J}$ were considered. This modification has been implemented for further use while studying the case of three-body systems. Because two-body J-helicity states are not position eigenstates, the evaluation of $\mathcal{O}(\hat{r})$ on $|\bar{p}; JM; s_1\lambda_1 s_2\lambda_2\rangle$ requires more developments than the evaluation of $\mathcal{O}(\hat{p})$. Let us first switch the basis and develop two-body J-helicity states into the canonical basis using relation (39),

$$\begin{aligned}&\langle\bar{p}; \bar{J}\,\bar{M}; s_1\bar{\lambda}_1 s_2\bar{\lambda}_2|\mathcal{O}(\hat{r})|p; JM; s_1\lambda_1 s_2\lambda_2\rangle \\ &= \sum_{\bar{s}=|s_1-s_2|}^{s_1+s_2} \sum_{\bar{\ell}=|J-\bar{s}|}^{J+\bar{s}} \mathcal{C}^{\bar{J};s_1 s_2}_{\bar{\ell}\,\bar{s};\bar{\lambda}_1\bar{\lambda}_2} \sum_{s=|s_1-s_2|}^{s_1+s_2} \sum_{\ell=|J-s|}^{J+s} \mathcal{C}^{J;s_1 s_2}_{\ell s;\lambda_1\lambda_2} \langle\bar{p}; \bar{J}\,\bar{M}; \bar{\ell}\,\bar{s}; s_1 s_2|\mathcal{O}(\hat{r})|p; JM; \ell s; s_1 s_2\rangle\end{aligned} \tag{52}$$

with the following notation shortcut:

$$\mathcal{C}^{J;s_1s_2}_{\ell s;\lambda_1\lambda_2} = \sqrt{\frac{2\ell+1}{2J+1}}(s_1\lambda_1 s_2 - \lambda_2|s\lambda_1 - \lambda_2)(\ell 0 s\lambda_1 - \lambda_2|J\lambda_1 - \lambda_2). \tag{53}$$

The problem now reduces to the evaluation of $\mathcal{O}(\hat{r})$ on the more traditional canonical states. Using the definition (38) of two-body J-canonical states in terms of p ones, one obtains

$$\begin{aligned}\langle \bar{p};\bar{J}\,\bar{M};\overline{\ell}\,\bar{s};s_1s_2|\mathcal{O}(\hat{r})|p;JM;\ell s;s_1s_2\rangle = &\sum_{\bar{m}'_\ell\bar{m}'_s\bar{m}'_{s_1}\bar{m}'_{s_2}} (\overline{\ell}\bar{m}'_\ell\bar{s}\bar{m}'_s|\bar{J}\,\bar{M})(s_1\bar{m}'_{s_1}s_2\bar{m}'_{s_2}|\bar{s}\bar{m}'_s)\int \mathrm{d}\cos\bar{\theta}'\mathrm{d}\bar{\phi}' Y^{\overline{\ell}*}_{\bar{m}'_\ell}(\bar{\theta}',\bar{\phi}')\\ &\times\sum_{m'_\ell m'_s m'_{s_1} m'_{s_2}} (\ell m'_\ell s m'_s|JM)(s_1 m'_{s_1}s_2 m'_{s_2}|s m'_s)\int \mathrm{d}\cos\theta'\mathrm{d}\phi' Y^{\ell}_{m'_\ell}(\theta',\phi')\\ &\times\langle \bar{p}\bar{\theta}'\bar{\phi}';s_1\bar{m}'_{s_1}s_2\bar{m}'_{s_2}|\mathcal{O}(\hat{r})|p\theta'\phi';s_1m'_{s_1}s_2m'_{s_2}\rangle.\end{aligned} \tag{54}$$

Because spin degrees of freedom are uncorrelated from spatial ones in canonical states and because the observable $\mathcal{O}(\hat{r})$ does not affect them, the right-hand-side residual MEs are proportional to $\delta_{\bar{m}'_{s_1}m'_{s_1}}\delta_{\bar{m}'_{s_2}m'_{s_2}}$. Concerning spatial degrees of freedom, the action of the observable can be evaluated using a result from Ref. [21],[2]

$$\begin{aligned}&\langle \bar{p}\bar{\theta}'\bar{\phi}';s_1\bar{m}'_{s_1}s_2\bar{m}'_{s_2}|\mathcal{O}(\hat{r})|p\theta'\phi';s_1m'_{s_1}s_2m'_{s_2}\rangle\\ &= \delta_{\bar{m}'_{s_1}m'_{s_1}}\delta_{\bar{m}'_{s_2}m'_{s_2}}4\sqrt{w_1(\bar{p})w_2(\bar{p})w_1(p)w_2(p)}\sum_{\ell''m''_\ell} Y^{\ell''}_{m''_\ell}(\bar{\theta}',\bar{\phi}')Y^{\ell''*}_{m''_\ell}(\theta',\phi')\mathcal{O}_{\ell''}(\bar{p},p)\end{aligned} \tag{55}$$

where

$$\mathcal{O}_\ell(\bar{p},p) = \frac{2}{\pi}\int_0^\infty j_\ell(\bar{p}r)\mathcal{O}(r)j_\ell(pr)r^2\mathrm{d}r, \tag{56}$$

with $j_\ell(x)$ being spherical Bessel functions. Making use of spherical harmonics and Clebsh-Gordan coefficients properties, one gets

$$\langle \bar{p};\bar{J}\,\bar{M};\overline{\ell}\,\bar{s};s_1s_2|\mathcal{O}(\hat{r})|p;JM;\ell s;s_1s_2\rangle = 4\sqrt{w_1(\bar{p})w_2(\bar{p})w_1(p)w_2(p)}\mathcal{O}_\ell(\bar{p},p)\delta_{\bar{J}J}\delta_{\bar{M}M}\delta_{\overline{\ell}\ell}\delta_{\bar{s}s}. \tag{57}$$

This expression is inserted in (52) and leads to the following formula for the evaluation of $\mathcal{O}(\hat{r})$ on two-body J-helicity states:

$$\begin{aligned}&\langle \bar{p};\bar{J}\,\bar{M};s_1\bar{\lambda}_1s_2\bar{\lambda}_2|\mathcal{O}(\hat{r})|p;JM;s_1\lambda_1s_2\lambda_2\rangle\\ &= \delta_{\bar{J}J}\delta_{\bar{M}M}\sum_{s=|s_1-s_2|}^{s_1+s_2}\sum_{\ell=|J-s|}^{J+s}\mathcal{C}^{J;s_1s_2}_{\ell s;\bar{\lambda}_1\bar{\lambda}_2}\mathcal{C}^{J;s_1s_2}_{\ell s;\lambda_1\lambda_2}4\sqrt{w_1(\bar{p})w_2(\bar{p})w_1(p)w_2(p)}\mathcal{O}_\ell(\bar{p},p).\end{aligned} \tag{58}$$

Finally, back to the state for the composite particle, expression (51) becomes

$$\begin{aligned}&\langle \Psi;\bar{J}\,\bar{M};s_1\bar{\lambda}_1s_2\bar{\lambda}_2|\mathcal{O}(\hat{r})|\Psi;JM;s_1\lambda_1s_2\lambda_2\rangle\\ &= \delta_{\bar{J}J}\delta_{\bar{M}M}\sum_{s=|s_1-s_2|}^{s_1+s_2}\sum_{\ell=|J-s|}^{J+s}\mathcal{C}^{J;s_1s_2}_{\ell s;\bar{\lambda}_1\bar{\lambda}_2}\mathcal{C}^{J;s_1s_2}_{\ell s;\lambda_1\lambda_2}\int p\mathrm{d}p\,\bar{p}\mathrm{d}\bar{p}\Xi(\bar{p})^*\Xi(p)\mathcal{O}_\ell(\bar{p},p).\end{aligned} \tag{59}$$

As expected due to angular momentum conservation, the MEs for central potentials are proportional to $\delta_{\bar{J}J}\delta_{\bar{M}M}$. Moreover, as soon as they are nonzero, these MEs are also independent of the total angular momentum projection M. The evaluation of

[2]The result from [21] must slightly be adapted in two different ways. First, our normalization conventions being different, a kinematic factor has been added. Second, a property of Legendre polynomials is used to get spherical harmonics back.

such MEs on symmetrized odd/even helicity states differs from that on two-body J-helicity only by the coefficients of the expansion in canonical states. Relation (59) remains valid provided that the expression (53) for $\mathcal{C}$ coefficients is correctly adapted.

Analytical expressions of $\mathcal{O}_l(\bar{p},p)$ for different potentials are given in [21]. For instance, in the presence of a Yukawa potential $\mathcal{O}(r)=-\alpha e^{-\eta r}/r$, one gets

$$\mathcal{O}_\ell(\bar{p},p)=-\frac{\alpha}{\pi\bar{p}p}Q_\ell\left(\frac{\bar{p}^2+p^2+\eta^2}{2\bar{p}p}\right) \tag{60}$$

with $Q_l(x)$ a second kind of Legendre function [22]. This expression can be naively plugged into the integral from (59) without any extra precaution, even for $\eta=0$. As a result, the treatment of Coulombic interactions only requires the evaluation of the following integrals:

$$\begin{aligned}&\int p\mathrm{d}p\,\bar{p}\mathrm{d}\bar{p}\Xi(\bar{p})^*\Xi(p)\mathcal{O}_\ell(\bar{p},p)\\&=-\frac{\alpha}{\pi}\int \mathrm{d}p\mathrm{d}\bar{p}\Xi(\bar{p})^*\Xi(p)Q_\ell\left(\frac{\bar{p}^2+p^2}{2\bar{p}p}\right).\end{aligned} \tag{61}$$

Although they present a logarithmic divergence for $p=\bar{p}$, Gaussian quadrature allows for a reasonably efficient evaluation of these integrals. This is even easier by introducing a new set of coordinates,

$$v=\bar{p}+p,\qquad \bar{v}=\bar{p}-p,\qquad \mathrm{d}v\mathrm{d}\bar{v}=2\mathrm{d}p\mathrm{d}\bar{p}. \tag{62}$$

As a result, Eq. (61) becomes

$$\begin{aligned}&\int p\mathrm{d}p\,\bar{p}\mathrm{d}\bar{p}\Xi(\bar{p})^*\Xi(p)\mathcal{O}_\ell(\bar{p},p)\\&=-\frac{\alpha}{2\pi}\int_0^\infty \mathrm{d}v\int_{-v}^{v}\mathrm{d}\bar{v}\,\Xi\left(\frac{v+\bar{v}}{2}\right)^*\Xi\left(\frac{v-\bar{v}}{2}\right)Q_\ell\left(\frac{v^2+\bar{v}^2}{v^2-\bar{v}^2}\right).\end{aligned} \tag{63}$$

The situation is more delicate concerning linear potentials. The Fourier transforms of these potentials are not traditional functions but are distributions [23]. To overcome this difficulty, the $\mathcal{O}_\ell$ function associated with this potential is defined by screening the linear potential with a decreasing exponential,

$$\mathcal{O}(r)=\lambda r=\lim_{\eta\to0}\lambda re^{-\eta r}=-\lim_{\eta\to0}\frac{\partial^2}{\partial\eta^2}\left(-\lambda\frac{e^{-\eta r}}{r}\right). \tag{64}$$

The second equality relates the linear potential to a derivative of the Yukawa potential whose $\mathcal{O}_\ell$ function is provided hereinabove. Using this relation, before taking the limit for η, one gets

$$\begin{aligned}\mathcal{O}^\eta_\ell(\bar{p},p)&=\frac{\lambda}{\pi\bar{p}p}\frac{\partial^2}{\partial\eta^2}(Q_\ell(z_\eta))\quad\text{with}\quad z_\eta=\frac{\bar{p}^2+p^2+\eta^2}{2\bar{p}p}\\&=\frac{\lambda}{\pi\bar{p}p}\frac{\partial}{\partial\eta}\left(\frac{\eta Q'_\ell(z_\eta)}{p\bar{p}}\right)=\frac{\lambda}{\pi}\left(\frac{Q'_\ell(z_\eta)}{(p\bar{p})^2}+\eta^2\frac{Q''_\ell(z_\eta)}{(p\bar{p})^3}\right)\end{aligned} \tag{65}$$

where Q'_ℓ and Q''_ℓ denote the first and second derivatives of Q_ℓ with respect to its argument. The limit on η is taken after integration and has to be considered carefully to ensure a finite result. Reference [23] develops formulas for this ME with arbitrary ℓ,

$$\lim_{\eta\to0}\int p\mathrm{d}p\,\bar{p}\mathrm{d}\bar{p}\Xi(\bar{p})^*\Xi(p)\mathcal{O}^\eta_\ell(\bar{p},p)=\frac{\lambda}{\pi}\int_0^\infty \mathrm{d}\bar{p}\Xi(\bar{p})^*P\int_0^\infty\left(\frac{4\bar{p}^2\Xi(\bar{p})}{(\bar{p}^2-p^2)^2}+Q'_\ell\left(\frac{p^2+\bar{p}^2}{2p\bar{p}}\right)\frac{\Xi(p)}{p\bar{p}}\right)\mathrm{d}p \tag{66}$$

where P denotes the Cauchy principal value of the integral. The left-hand side of relation (66) presents an apparent difference with its equivalent in [23]. This is because what is called $V^\ell_\eta(p,\bar{p})$ in [23] is actually equal to $p\bar{p}\mathcal{O}^\eta_\ell(\bar{p},p)$. Integrals from (66) are quite difficult to handle, mainly due to the Cauchy principal value. To overcome this problem, coordinates (62) are again introduced. Performing the change, (66) becomes

$$\lim_{\eta\to0}\int p\mathrm{d}p\,\bar{p}\mathrm{d}\bar{p}\Xi(\bar{p})^*\Xi(p)\mathcal{O}^\eta_\ell(\bar{p},p)=\frac{\lambda}{\pi}\int_0^\infty \mathrm{d}vP\int_{-v}^{v}\mathrm{d}\bar{v}\Xi\left(\frac{v+\bar{v}}{2}\right)^*\left(\frac{(v+\bar{v})^2}{2v^2\bar{v}^2}\Xi\left(\frac{v+\bar{v}}{2}\right)+Q'_\ell\left(\frac{v^2+\bar{v}^2}{v^2-\bar{v}^2}\right)\frac{2\Xi(\frac{v-\bar{v}}{2})}{v^2-\bar{v}^2}\right). \tag{67}$$

With these coordinates, the Cauchy principal value in the integration on $\bar{v}$ can naturally be taken into account by performing a Gauss-Legendre quadrature with an even number of points [23,24]. Formulas (63) and (67) allow for an efficient evaluation of the MEs with (59). Appendix B illustrates the calculation of Hamiltonian matrix elements using formulas (50), (63), and (67).

III. TWO-GLUON GLUEBALLS

The previous section defined two-body helicity states and introduced a way to compute the corresponding ME. In the current section, this formalism is applied to the description of glueballs in the framework of constituent approaches. Glueballs are modeled by colorless bound states of several constituent gluons. The latter are considered as bosons with helicity degrees of freedom $\lambda = \pm 1$ and negative intrinsic parity. The mass of the constituent gluon remains a controversial subject. Although formally massless, the QCD gluon has proven to acquire a dynamical mass in the nonperturbative regime [25–31]. This incited some studies to consider a massive kinetic energy for constituent gluons (with a mass around 0.5 GeV) [32,33]. On the other hand, Ref. [11] tends to indicate that the challenge in modeling glueballs consists more in the correct use of the helicity formalism than in the choice of the kinematics. In addition, it has already been observed in other constituent approaches that a modification in the kinematics of the system can be absorbed in modifications of the parameters from the potential [34]. For these reasons, the current work will consider an ultrarelativistic kinetic energy for the constituent gluon. This section limits the discussion to two-gluon bound states that produce the so-called two-gluon glueballs. The colorless constraint on the wave function implies for two-gluon glueballs a positive charge conjugation and a symmetric color part of the state [10]. Gluons having a bosonic nature, the spin-space part of the two-body state, must also be symmetrical.

To start with, let us focus on the construction of symmetrical two-body J-helicity states with $\lambda_i = \pm 1$ and having a definite parity. Making use of properties (34) and (35), Ref. [11] constructs four sets of such symmetric parity eigenstates,

$$|p; S_+; J^P = (2k)^+\rangle = \frac{1}{\sqrt{2}}(|p; JM; +1+1\rangle + |p; JM; -1-1\rangle), \tag{68a}$$

$$|p; S_-; J^P = (2k)^-\rangle = \frac{1}{\sqrt{2}}(|p; JM; +1+1\rangle - |p; JM; -1-1\rangle), \tag{68b}$$

$$|p; D_+; J^P = (2k+2)^+\rangle = \frac{1}{\sqrt{2}}(|p; JM; +1-1\rangle + |p; JM; -1+1\rangle), \tag{68c}$$

$$|p; D_-; J^P = (2k+3)^+\rangle = \frac{1}{\sqrt{2}}(|p; JM; +1-1\rangle - |p; JM; -1+1\rangle) \tag{68d}$$

with $k \in \mathbb{N}$. For readability, s_1 and s_2 labels have been omitted from the notation. One can show that these states are correctly orthonormalized. In each of the four sets, the parity and signature of J had to be constrained to ensure a correct symmetry of the state. In addition, the constraint $J \geq |\lambda_1 - \lambda_2|$ in definition (30) forbade the occurrence of total angular momenta smaller than 2 in $|D_\pm; J^P\rangle$ sets. The linear combinations of helicity states (68a)–(68d) can be expanded in terms of two-body J-canonical states making use of (39). This calculation has been performed in Ref. [11]. The resulting expansions are displayed in Table I.

As suggested in the previous section, these two-gluon states $|p; S_\pm/D_\pm; J^P\rangle$ are integrated on their momentum degree of freedom to produce a generic glueball state,

$$|\Psi; S_\pm/D_\pm; J^P\rangle = \int \frac{\mathrm{d}p}{2} \Xi(p) |p; S_\pm/D_\pm; J^P\rangle, \tag{69}$$

where $\Xi(p)$ satisfies the normalization condition (47). Compared to (48), expression (69) replaces $\sqrt{w_1(p)w_2(p)}$ by p because both gluons are assumed to be massless. One can now go back over the demonstration of relations

TABLE I. Expansion of symmetrized parity eigenstate two-body J-helicity states in canonical J-helicity states from [11]. A condensed notation for J-canonical states has been used, $|p; {}^{2s+1}l_J\rangle = |p; JM; ls; s_1 s_2\rangle$.

$$|p; S_+; (2k)^+\rangle = \sqrt{\tfrac{2}{3}}|p; {}^1 2k_{2k}\rangle - \sqrt{\tfrac{2k(2k+1)}{3(4k-1)(4k+3)}}|p; {}^5 2k_{2k}\rangle + \sqrt{\tfrac{k(2k-1)}{(4k+1)(4k-1)}}|p; {}^5 2k-2_{2k}\rangle + \sqrt{\tfrac{(k+1)(2k+1)}{(4k+3)(4k+1)}}|p; {}^5 2k+2_{2k}\rangle,$$

$$|p; S_-; (2k)^-\rangle = \sqrt{\tfrac{2k}{4k+1}}|p; {}^3 2k-1_{2k}\rangle - \sqrt{\tfrac{2k+1}{4k+1}}|p; {}^3 2k+1_{2k}\rangle,$$

$$|p; D_+; (2k+2)^+\rangle = \sqrt{\tfrac{(k+2)(2k+3)}{(4k+3)(4k+5)}}|p; {}^5 2k_{2k+2}\rangle + \sqrt{\tfrac{6(k+2)(2k+1)}{(4k+3)(4k+7)}}|p; {}^5 2k+2_{2k+2}\rangle + \sqrt{\tfrac{(k+1)(2k+1)}{(4k+5)(4k+7)}}|p; {}^5 2k+4_{2k+2}\rangle,$$

$$|p; D_-; (2k+3)^+\rangle = -\sqrt{\tfrac{2k+5}{4k+7}}|p; {}^5 2k+2_{2k+3}\rangle - \sqrt{\tfrac{2(k+1)}{4k+7}}|p; {}^5 2k+4_{2k+3}\rangle.$$

TABLE II. Comparison of two-gluon glueball spectra. Upper bounds obtained with the original SGA, $E_{\text{or.SGA}}$, are compared to the modified SGA, $E_{\text{mod.SGA}}$, and to the spectrum from [11] for which instanton contributions have been removed for the comparison. Some LQCD results from [5,7] are added as points of comparison. A supplementary LQCD calculation [8] that predicts a $|\Psi; D_+, 4^+\rangle$ state of $3.650 \pm 0.060 \pm 0.180$ GeV can be mentioned. Energy results are provided in GeV. Relative differences with [11], δ, are indicated in square brackets.

State	$E_{\text{or.SGA}}$	$[\delta]$	$E_{\text{mod.SGA}}$	$[\delta]$	Ref. [11]	LQCD [5]	LQCD [7]
$\|\Psi; S_+, 0^+\rangle$	1.769	[19%]	2.216	[2%]	2.174	$1.710 \pm 0.050 \pm 0.080$	$1.475 \pm 0.030 \pm 0.065$
$\|\Psi; S_-, 0^-\rangle$	2.216	[2%]	2.216	[2%]	2.174	$2.560 \pm 0.035 \pm 0.120$	$2.250 \pm 0.060 \pm 0.100$
$\|\Psi; D_+, 2^+\rangle$	2.279	[12%]	2.651	[2%]	2.588	$2.390 \pm 0.030 \pm 0.120$	$2.150 \pm 0.030 \pm 0.100$
$\|\Psi; S_+, 2^+\rangle$	3.060	[1%]	3.194	[4%]	3.077	⋯	$2.880 \pm 0.100 \pm 0.130$
$\|\Psi; S_-, 2^-\rangle$	3.043	[1%]	3.194	[4%]	3.077	$3.040 \pm 0.040 \pm 0.150$	$2.780 \pm 0.050 \pm 0.130$
$\|\Psi; D_-, 3^+\rangle$	3.297	[1%]	3.393	[4%]	3.254	$3.670 \pm 0.050 \pm 0.180$	$3.385 \pm 0.090 \pm 0.150$
$\|\Psi; D_+, 4^+\rangle$	3.897	[3%]	3.981	[6%]	3.768	⋯	$3.640 \pm 0.090 \pm 0.160$
$\|\Psi; S_+, 4^+\rangle$	4.150	[5%]	4.204	[6%]	3.961	⋯	⋯
$\|\Psi; S_-, 4^-\rangle$	4.139	[4%]	4.204	[6%]	3.961	⋯	⋯

(50) and (59) to generalize them for the symmetrical $|\Psi; S_\pm/D_\pm; J^P\rangle$ states. On the one hand, the generalization of (50) is immediate. Symmetrical states being similarly orthonormalized, the demonstration does not require any modification and one gets

$$\langle \Psi; S_\pm/D_\pm; J^P | O(\hat{p}) | \Psi; S_\pm/D_\pm; J^P \rangle = \int \mathrm{d}p |\Xi(p)|^2 \mathcal{O}(p). \tag{70}$$

Kinetic energy MEs that mix states with different labels are shown to cancel. Because states are naturally written in momentum space, angular momentum does not play any role in the calculation. It results in the left-hand side of Eq. (70) independent of S/D and J. This was not the case in [11] where calculations were performed in coordinate space. On the other hand, relation (59) requires a slight modification. Because symmetrized states satisfy a different expansion in canonical states, coefficients $\mathcal{C}^{J;s_1 s_2}_{\ell s;\lambda_1\lambda_2}$ from relation (59) have to be replaced by the expansion coefficients from Table I. Denoting the latter $\mathcal{C}^J_{\ell s}$, one gets the following analog to (59):

$$\langle \Psi; S_\pm/D_\pm; J^P | \mathcal{O}(\hat{r}) | \Psi; S_\pm/D_\pm; J^P \rangle = \sum_{s=0}^{2} \sum_{\ell=|J-s|}^{J+s} (\mathcal{C}^J_{\ell s})^2 \int p\mathrm{d}p\, \bar{p}\mathrm{d}\bar{p}\, \Xi(\bar{p})^* \Xi(p) \mathcal{O}_\ell(\bar{p}, p). \tag{71}$$

These two formulas can now be used to concretely compute a glueball spectrum by means of a variational approach. A Gaussian shape supplemented by a p factor that cancels at $p = 0$ is suggested as a trial helicity-momentum wave function,

$$\Xi_a(p) = A p e^{-a p^2}. \tag{72}$$

In the following, the approximation provided by this trial state will be referred to as the single Gaussian approximation (SGA). To enable a comparison, the Hamiltonian considered is the same as the one in [11],

$$\mathcal{H}_{\text{GB}} = 2\sqrt{p^2} + \frac{9\sigma}{4} r - 3\frac{\alpha_s}{r} \tag{73}$$

where $\alpha_s = 0.450$ is the strong coupling constant and $\sigma = 0.185\ \text{GeV}^2$ is the mesonic string tension. The factor $9/4$ comes from the Casimir scaling hypothesis [35] and the factor 3 corresponds to the color charge associated with a pair of constituent gluons in a color singlet. Instanton contributions added in [11] to split the degeneracy of the lowest states are not considered at first. Masses obtained using the SGA for the low-lying angular momenta are displayed in the second column of Table II. These results are compared to energies from Ref. [11] (instanton contribution is manually removed). At first sight, both values seem incompatible. Energies from the SGA, a variational method supposed to provide upper bounds, lies below the ones from Ref. [11], where a very accurate resolution method has been used (namely, the Lagrange mesh method [36]). This incompatibility is left noticing that Ref. [11] solves the same Hamiltonian using a fundamentally different approach. First of all, the total orbital angular momentum of the system is evaluated on the symmetric parity eigenstates from Table I. The matrix obtained in this way turns out to be diagonal with the respective diagonal elements $J(J+1)+2$ for $|p; S_\pm, J^P\rangle$ states and $J(J+1)-2$ for $|p; D_\pm, J^P\rangle$ states. Consequently, Ref. [11] suggests to replace the $|p; S_\pm/D_\pm, J^P\rangle$ states with canonical ones with effective angular momenta ℓ_{eff} such that

$$\ell_{\text{eff}}(\ell_{\text{eff}} + 1) = J(J+1) \pm 2. \tag{74}$$

The Hamiltonian matrix is then evaluated on these effective canonical states rather than on the true two-body helicity states. Mimicking this strategy with the SGA gives rise to the third column of Table II. Such calculations require the evaluation of a second kind of Legendre function for

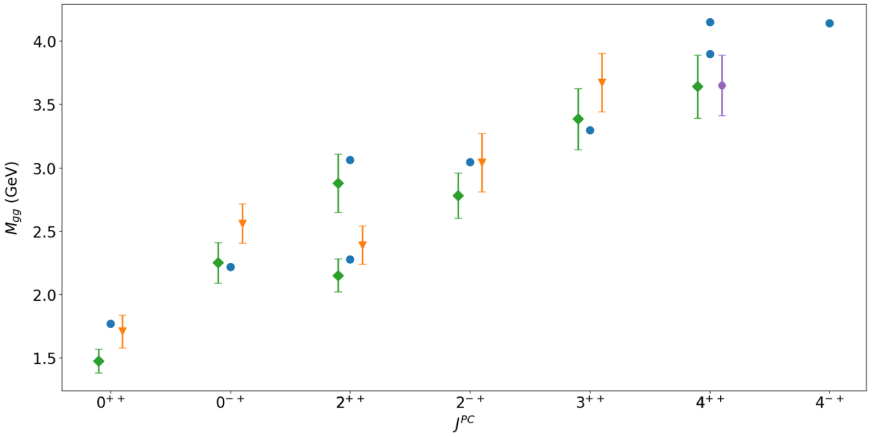

FIG. 6. Comparison of two-gluon glueball spectra. Upper bounds obtained with the SGA (blue circles) are compared to LQCD results from [5] (orange triangles), [7] (green diamonds), and [8] (purple hexagon).

noninteger ℓ values. As expected, this modified SGA provides upper bounds of the energies from [11].

The second and fourth columns are compared with LQCD results in Table II and in Fig. 6. First of all, one notices that most of the masses provided by the original SGA lie below the ones from [11]. Nevertheless, in most cases, relative differences between both methods lie around a few percent. The main exception to this claim occurs for the 0^+ state. In Ref. [11], the 0^+ and 0^- states prove to be degenerated thereby requiring the introduction of instanton interactions to split both levels. The original SGA naturally raises this degeneracy. It does not mean that the instanton does not contribute in the glueball spectrum but that their effects may be overestimated by the use of the method from [11]. All results seem in global agreement with LQCD results [5–8], no matter which methodology is used.

It can be worth considering an extension of the SGA by incorporating a second Gaussian trial wave function (72) within the variational approach [37]. The single Hamiltonian ME to compute in the SGA is replaced by the evaluation of a 2 by 2 Hamiltonian and overlap matrices, which form the core of a generalized eigenvalue problem,

$$\begin{pmatrix} \langle\Psi_a|\mathcal{H}_{\rm GB}|\Psi_a\rangle & \langle\Psi_a|\mathcal{H}_{\rm GB}|\Psi_b\rangle \\ \langle\Psi_b|\mathcal{H}_{\rm GB}|\Psi_a\rangle & \langle\Psi_b|\mathcal{H}_{\rm GB}|\Psi_b\rangle \end{pmatrix} \begin{pmatrix} C_1 \\ C_2 \end{pmatrix} = E \begin{pmatrix} \langle\Psi_a|\Psi_a\rangle & \langle\Psi_a|\Psi_b\rangle \\ \langle\Psi_b|\Psi_a\rangle & \langle\Psi_b|\Psi_b\rangle \end{pmatrix} \begin{pmatrix} C_1 \\ C_2 \end{pmatrix} \tag{75}$$

where $|\Psi_a\rangle$ serves as shorthand for any symmetric helicity state $|\Psi; S_\pm/D_\pm; J^P\rangle$, with a being the nonlinear variational parameter considered. This double Gaussian approximation (DGA) serves two purposes: to assess the accuracy of the SGA, and to explore first radially excited states. The nonlinear variational parameters of each

TABLE III. Comparison of two-gluon glueball spectra. Upper bounds obtained with the original SGA, $E_{\rm or.SGA}$, are compared to the DGA, $E_{\rm DGA}$, and to the spectrum from [11] from which instanton contributions have been removed for the comparison. Labels Ψ_1 and Ψ_2 respectively refer to the fundamental and to the first excited state. Some LQCD results from [5–7] are added as points of comparison. Energy results are provided in GeV.

State	$E_{\rm or.SGA}$	$E_{\rm DGA}$	Ref. [11]	LQCD [5,6]	LQCD [7]
$\|\Psi_1; S_+, 0^+\rangle$	1.769	1.668	2.174	$1.710 \pm 0.050 \pm 0.080$	$1.475 \pm 0.030 \pm 0.065$
$\|\Psi_2; S_+, 0^+\rangle$	⋯	2.808	2.993	$2.670 \pm 0.180 \pm 0.130$	$2.755 \pm 0.070 \pm 0.120$
$\|\Psi_1; S_-, 0^-\rangle$	2.216	2.202	2.174	$2.560 \pm 0.035 \pm 0.120$	$2.250 \pm 0.060 \pm 0.100$
$\|\Psi_2; S_-, 0^-\rangle$	⋯	3.069	2.993	$3.640 \pm 0.060 \pm 0.180$	$3.370 \pm 0.150 \pm 0.150$
$\|\Psi_1; D_+, 2^+\rangle$	2.279	2.241	2.588	$2.390 \pm 0.030 \pm 0.120$	$2.150 \pm 0.030 \pm 0.100$
$\|\Psi_2; D_+, 2^+\rangle$	⋯	3.249	3.325	⋯	⋯
$\|\Psi_1; S_+, 2^+\rangle$	3.060	3.042	3.077	⋯	$2.880 \pm 0.100 \pm 0.130$
$\|\Psi_2; S_+, 2^+\rangle$	⋯	3.852	3.732	⋯	⋯
$\|\Psi_1; S_-, 2^-\rangle$	3.043	3.042	3.077	$3.040 \pm 0.040 \pm 0.150$	$2.780 \pm 0.050 \pm 0.130$
$\|\Psi_2; S_-, 2^-\rangle$	⋯	3.845	3.732	$3.890 \pm 0.040 \pm 0.190$	$3.480 \pm 0.140 \pm 0.160$
$\|\Psi_1; D_-, 3^+\rangle$	3.297	3.295	3.254	$3.670 \pm 0.050 \pm 0.180$	$3.385 \pm 0.090 \pm 0.150$
$\|\Psi_2; D_-, 3^+\rangle$	⋯	4.067	3.882	⋯	⋯

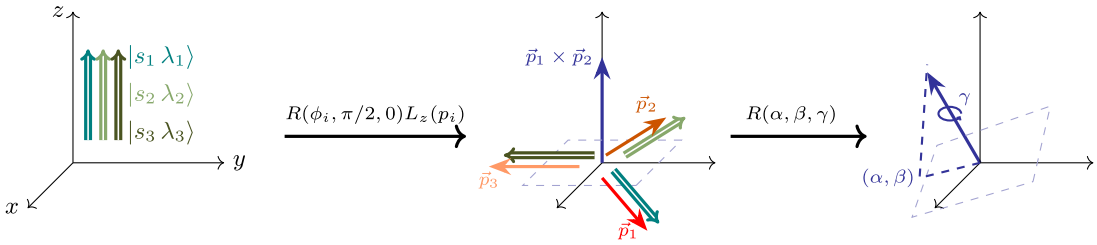

FIG. 7. Visual interpretation for the definition of Berman's p-helicity states (76).

Gaussian denoted a and b above are treated as independent, and optimization is performed on both. Results are presented in Table III. For all considered states, the energy difference between the SGA and DGA does not exceed 0.1 GeV (it even decreases to below 0.01 GeV for high angular momenta). These findings suggest that the SGA is sufficiently accurate to study low-lying two-gluon glueball states. For radially excited states, as expected, the DGA results align in magnitude with those from Ref. [11].

IV. THE HELICITY FORMALISM FOR THREE-BODY SYSTEMS

As for two-body systems, efforts are made to produce complete sets of three-body helicity states possessing a total angular momentum J in the e.c.m.f.. These sets of three-body states are used to decompose the state of composite particles at rest. There are two main ways to define helicity states for three-body systems, both ways having their own strengths and weaknesses. These two definitions are reviewed in the following subsections.

A. Berman's definition

Berman's three-body helicity states definition is based on the observation that, in their c.m.f., any set of three particles always lies and moves in a given plane. This feature allows the following geometrical construction for the tensorial product of three one-body helicity states in the e.c.m.f. [16,38]:

$$\begin{aligned}&|\alpha\beta\gamma; w_1w_2w_3;\lambda_1\lambda_2\lambda_3\rangle\\&= U(R(\alpha,\beta,\gamma))[U(R(\phi_1,\pi/2,0)L_z(p_1))|s_1\lambda_1\rangle\\&\quad\otimes U(R(\phi_2,\pi/2,0)L_z(p_2))|s_2\lambda_2\rangle\\&\quad\otimes U(R(\phi_3,\pi/2,0)L_z(p_3))|s_3\lambda_3\rangle]\end{aligned}\tag{76}$$

where p_i and ϕ_i are fixed combinations of the particle's energies, w_1, w_2, and w_3,

$$p_i=\sqrt{w_i^2-m_i^2},\qquad \cos\varphi_{ij}=\frac{p_k^2-p_i^2-p_j^2}{2p_ip_j},\tag{77}$$

$$\phi_1=\varphi_{13}-\pi/2,\quad \phi_2=\varphi_{13}+\varphi_{12}-\pi/2,\quad \phi_3=3\pi/2.\tag{78}$$

Above, the φ_{ij} angles are always to be taken in between 0 and π. Individual masses m_i and spins s_i are omitted from the notation for the sake of conciseness. As for two-body p-helicity states, definition (76) can be decomposed into two pieces. Inside the square brackets, reference momenta are provided to each of the three particles using helicity convention. Their moduli are defined so that the ith particle has an energy w_i, while their direction is chosen so that it respects four conditions.

(1) Each momentum lies in the xy plane.
(2) The sum of the momenta is the null vector.
(3) The momentum of the third particle is along the y direction toward negatives.
(4) The cross product of the momenta of particles 1 and 2 is along the z axis toward positives.

All these conditions are ensured by definitions (77) and (78). This defines what will be thereafter named Berman's reference state and denoted as follows:

$$\begin{aligned}|w_1w_2w_3;\lambda_1\lambda_2\lambda_3\rangle &= U(R(\phi_1,\pi/2,0)L_z(p_1))|s_1\lambda_1\rangle\\&\quad\otimes U(R(\phi_2,\pi/2,0)L_z(p_2))|s_2\lambda_2\rangle\\&\quad\otimes U(R(\phi_3,\pi/2,0)L_z(p_3))|s_3\lambda_3\rangle.\end{aligned}\tag{79}$$

Once the reference state is built, in a second phase, this state is rotated with Euler angles (α,β,γ) to give its orientation to the plane in which lies the three particles. This decomposition provides its interpretation to the angles (α,β,γ); these are the angles of the normal to particles' plane. A visual interpretation of the aforementioned structure is proposed in Fig. 7. States defined in (76) will be thereafter referred to as Berman's p-helicity states.[3] These satisfy the following orthonormality relation [16,38]:

$$\begin{aligned}&\langle\bar\alpha\bar\beta\bar\gamma;\bar w_1\bar w_2\bar w_3;\bar\lambda_1\bar\lambda_2\bar\lambda_3|\alpha\beta\gamma;w_1w_2w_3;\lambda_1\lambda_2\lambda_3\rangle\\&= 8\delta(w_1-\bar w_1)\delta(w_2-\bar w_2)\delta(w_3-\bar w_3)\\&\quad\delta(\alpha-\bar\alpha)\delta(\cos\beta-\cos\bar\beta)\delta(\gamma-\bar\gamma)\delta_{\lambda_1\bar\lambda_1}\delta_{\lambda_2\bar\lambda_2}\delta_{\lambda_3\bar\lambda_3}.\end{aligned}\tag{80}$$

[3]This name refers to one of the authors of a pioneer work using this definition [38]. Conventions in this work slightly differ from the ones used here, the third particle being taken along the x axis toward negatives. For completeness, let us also mention the names of Werle and Jacob that abundantly contributed to this definition too [38,39].

The normalization announced in [16] differs from this one by a multiplicative constant. It is due to a different choice of convention for the normalization of one-body helicity states (as a reminder, the convention used here is the one of [14]).

The definition (76) introduces three-body helicity states with defined directions for the momenta and therefore no good total angular momentum. It is as straightforward as it is for two-body J-helicity states to combine these states to overcome this deficiency [16,38],

$$\begin{aligned}|JM\mu;w_1w_2w_3;\lambda_1\lambda_2\lambda_3\rangle &= \sqrt{\frac{2J+1}{8\pi^2}}\int \mathrm{d}\alpha\mathrm{d}\cos\beta\mathrm{d}\gamma D^{J*}_{M\mu}(\alpha,\beta,\gamma)|\alpha\beta\gamma;w_1w_2w_3;\lambda_1\lambda_2\lambda_3\rangle \\ &= \sqrt{\frac{2J+1}{8\pi^2}}\int \mathrm{d}\alpha\mathrm{d}\cos\beta\mathrm{d}\gamma D^{J*}_{M\mu}(\alpha,\beta,\gamma)U(R(\alpha,\beta,\gamma))|w_1w_2w_3;\lambda_1\lambda_2\lambda_3\rangle. \end{aligned} \tag{81}$$

States defined hereinabove will be referred to as Berman's J-helicity states and satisfy the following orthonormality relation [16]:

$$\begin{aligned}&\langle \bar{J}\,\bar{M}\,\bar{\mu};\bar{w}_1\bar{w}_2\bar{w}_3;\bar{\lambda}_1\bar{\lambda}_2\bar{\lambda}_3|JM\mu;w_1w_2w_3;\lambda_1\lambda_2\lambda_3\rangle \\ &= 8\delta(w_1-\bar{w}_1)\delta(w_2-\bar{w}_2)\delta(w_3-\bar{w}_3) \\ &\quad \delta_{J\bar{J}}\delta_{M\bar{M}}\delta_{\mu\bar{\mu}}\delta_{\lambda_1\bar{\lambda}_1}\delta_{\lambda_2\bar{\lambda}_2}\delta_{\lambda_3\bar{\lambda}_3}. \end{aligned} \tag{82}$$

This relation can also be compared to the results in Ref. [39], where different orientation conventions are used, and in Ref. [38], where an expression only including space degrees of freedoms is provided. In addition to the total angular momentum J and its projection M, a third quantum number μ is produced. This quantum number corresponds to the projection of the total angular momentum along the normal to the plane [16]. Even if the direction of this normal is not fixed due to the integration on the (α,β,γ) angles, the projection of J along the normal to the plane is well defined. One might wonder whether choosing to set up the reference state in the xy plane truly matters, given that the angles of this plane are integrated over in Berman's J-helicity states. It is demonstrated in Appendix C that a modification of this reference plane truly impacts the definition of Berman's J-helicity states,

$$\begin{aligned}&|JM\mu;w_1w_2w_3;\lambda_1\lambda_2\lambda_3\rangle \\ &= \sum_{\mu'=-J}^{J} D^{J}_{\mu\mu'}(\bar{R}^{-1})|JM\mu';w_1w_2w_3;\lambda_1\lambda_2\lambda_3\rangle_{\bar{R}} \end{aligned} \tag{83}$$

where the state denoted $|JM\mu;w_1w_2w_3;\lambda_1\lambda_2\lambda_3\rangle_{\bar{R}}$ is built from a different initial configuration, with the rotation $\bar{R}$ relating the reference planes used to define the states on either side of Eq. (83). The change of reference plane modified the definition of the μ quantum number.

The action of the parity and permutation operators on Berman's states can be investigated. As for one- and two-body helicity states, Berman's J-helicity states are not parity eigenstates by themselves [16],

$$\begin{aligned}&\Pi|JM\mu;w_1w_2w_3;\lambda_1\lambda_2\lambda_3\rangle \\ &= \eta_1\eta_2\eta_3(-1)^{-s_1-s_2-s_3-\mu}|JM\mu;w_1w_2w_3;-\lambda_1-\lambda_2-\lambda_3\rangle. \end{aligned} \tag{84}$$

Above, η_i is still the intrinsic parity of the ith particle. To get parity eigenstates, linear combinations of Berman's J-helicity states that mix helicity signs have to be considered. Concerning permutations of particles, let $\mathbb{P}_{ij}$ be the operator that represents exchange operations between particles i and j. Berman's J-helicity states are not eigenstates of permutations but

$$\mathbb{P}_{12}|JM\mu;w_1w_2w_3;\lambda_1\lambda_2\lambda_3\rangle = (-1)^{J+\mu+\lambda_1+\lambda_2-\lambda_3}|JM-\mu;w_2w_1w_3;\lambda_2\lambda_1\lambda_3\rangle, \tag{85a}$$

$$\mathbb{P}_{13}|JM\mu;w_1w_2w_3;\lambda_1\lambda_2\lambda_3\rangle = (-1)^{J-\mu-\lambda_1-\lambda_2-\lambda_3}e^{-i\varphi_{13}\mu}|JM-\mu;w_3w_2w_1;\lambda_3\lambda_2\lambda_1\rangle, \tag{85b}$$

$$\mathbb{P}_{23}|JM\mu;w_1w_2w_3;\lambda_1\lambda_2\lambda_3\rangle = (-1)^{J+\mu+\lambda_1-\lambda_2-\lambda_3}e^{i\varphi_{23}\mu}|JM-\mu;w_1w_3w_2;\lambda_1\lambda_3\lambda_2\rangle, \tag{85c}$$

where expressions of φ_{ij} are given in (77). The relation for $\mathbb{P}_{12}$ can be found in [16,38] but results for $\mathbb{P}_{13}$ and $\mathbb{P}_{23}$ are new. The proof of (85b) is given in Appendix C. This proof can easily be adapted to demonstrate (85c). It has been checked that the hereinabove relations are consistent with S_3 multiplication table,

$$\mathbb{P}_{23} = \mathbb{P}_{12}\mathbb{P}_{13}\mathbb{P}_{12}. \tag{86}$$

Non-normalized symmetric (antisymmetric) states can be obtained by applying the three-body symmetrizer $\mathbb{S}_3$ (antisymmetrizer $\mathbb{A}_3$) on each of Berman's J-helicity states (81),

$$\mathbb{S}_3 = \mathbb{1} + \mathbb{P}_{12} + \mathbb{P}_{13} + \mathbb{P}_{12}\mathbb{P}_{13}\mathbb{P}_{12} + \mathbb{P}_{13}\mathbb{P}_{12} + \mathbb{P}_{12}\mathbb{P}_{13}, \quad (87)$$

$$\mathbb{A}_3 = \mathbb{1} - \mathbb{P}_{12} - \mathbb{P}_{13} - \mathbb{P}_{12}\mathbb{P}_{13}\mathbb{P}_{12} + \mathbb{P}_{13}\mathbb{P}_{12} + \mathbb{P}_{12}\mathbb{P}_{13}. \quad (88)$$

Symmetric and antisymmetric parity eigenstates for three-gluon systems are built in Sec. V.

1. Decomposition of a physical three-body state in Berman's J-helicity states

In the same way as for two-body systems, any three-body bound state in the e.c.m.f. with spin J and with helicity quantum numbers can be decomposed as an integral on the internal momentum degrees of freedom of Berman's p-helicity states. But contrary to the two-body case, this integral can be written in many possible variables. Let us first introduce the Jacobi coordinates. These coordinates denoted $\boldsymbol{x}$ and $\boldsymbol{y}$ complemented with the center-of-mass position, $\boldsymbol{R}$, are abundantly used in the literature to deal with bound states of three identical bodies. In terms of individual positions, they read

$$\boldsymbol{x} = \boldsymbol{x_1} - \boldsymbol{x_2}, \quad \boldsymbol{y} = \frac{\boldsymbol{x_1} + \boldsymbol{x_2}}{2} - \boldsymbol{r_3}, \quad \boldsymbol{R} = \frac{\boldsymbol{x_1} + \boldsymbol{x_2} + \boldsymbol{r_3}}{3}. \quad (89)$$

With Berman's states being momentum eigenstates, Jacobi coordinates will take part in the following through their conjugated momenta:

$$\boldsymbol{p_x} = \frac{\boldsymbol{p_1} - \boldsymbol{p_2}}{2}, \quad \boldsymbol{p_y} = \frac{\boldsymbol{p_1} + \boldsymbol{p_2} - 2\boldsymbol{p_3}}{3}, \quad \boldsymbol{P} = \boldsymbol{p_1} + \boldsymbol{p_2} + \boldsymbol{p_3}, \quad (90)$$

where $\boldsymbol{P}$ is the total momentum of the system. This choice of coordinates has the advantage that it does not bring any Jacobian compared to individual momenta,

$$\mathrm{d}^3p_1\mathrm{d}^3p_2\mathrm{d}^3p_3 = \mathrm{d}^3P\mathrm{d}^3p_x\mathrm{d}^3p_y. \quad (91)$$

Another possible system of coordinates that may be used consists of three angles that describe the plane in which the momenta lie as well as the three-momentum length. One will recognize in this set of coordinates the α, β, γ, p_1, p_2, and p_3 variables used in Berman's definition of p-helicity states (76). Equivalently, one can replace the p_i variables by the w_i ones, these being related each other through relation (77). In the following, these coordinates will be called pseudo-momentum perimetric coordinates (PMP coordinates), in analogy with position perimetric coordinates, used, for instance, in [40]. The full change of coordinates from Jacobi to PMP is not mandatory for the sake of this discussion. Let us simply mention that, for three massless particles, the modulus of Jacobi coordinates can be related to the w_i variables as follows:

$$p_x^2 = (2w_1^2 + 2w_2^2 - w_3^2)/4, \qquad p_y^2 = w_3^2, \quad (92)$$

and that, between these variables, a nontrivial Jacobian has to be taken into account,

$$\mathrm{d}^3p_x\mathrm{d}^3p_y = w_1w_2w_3\mathrm{d}w_1\mathrm{d}w_2\mathrm{d}w_3\mathrm{d}\alpha\mathrm{d}\cos\beta\mathrm{d}\gamma. \quad (93)$$

This relation can be demonstrated by considering the intermediary system of coordinates that supplements α, β, γ with the respective moduli of $\boldsymbol{p_x}$ and $\boldsymbol{p_y}$ as well as the angle between these two vectors denoted $\cos\theta_{xy}$ [40].

Out of the two possible sets of coordinates, the momentum perimetric ones clearly fit better with Berman's definition of helicity states. Making use of the completeness relation of Berman's p-helicity states, a generic three-body helicity state in thee.c.m.f., $|\Phi;\lambda_1\lambda_2\lambda_3\rangle$, is naturally decomposed in coordinates w_1, w_2, w_3, α, β, and γ,

$$|\Phi;\lambda_1\lambda_2\lambda_3\rangle = \int \frac{\mathrm{d}w_1\mathrm{d}w_2\mathrm{d}w_3\mathrm{d}\alpha\mathrm{d}\cos\beta\mathrm{d}\gamma}{8} \Phi(\alpha,\beta,\gamma,w_1,w_2,w_3)|\alpha\beta\gamma;w_1w_2w_3;\lambda_1\lambda_2\lambda_3\rangle \quad (94)$$

where

$$\Phi(\alpha,\beta,\gamma,w_1,w_2,w_3) = \langle\alpha\beta\gamma;w_1w_2w_3;\lambda_1\lambda_2\lambda_3|\Phi;\lambda_1\lambda_2\lambda_3\rangle \quad (95)$$

is the three-body helicity-momentum wave function of the state. Above, w_1 and w_2 are integrated along the set of positive real numbers while w_3 is bounded by $|w_1 - w_2|$ and $w_1 + w_2$ so that $\boldsymbol{P} = \boldsymbol{0}$ is possible. This relation is the three-body equivalent to the two-body decomposition (40). Here again, this state has not the expected definite total angular momentum J. But reminding of Berman's definition of J-helicity states, this property can be supplied to the state by imposing the angular dependence of $\Phi(\alpha,\beta,\gamma,w_1,w_2,w_3)$,

$$\Phi^J_{M\mu}(\alpha,\beta,\gamma,w_1,w_2,w_3) = \sqrt{\frac{2J+1}{8\pi^2}}\Psi(w_1,w_2,w_3)D^{J*}_{M\mu}(\alpha,\beta,\gamma). \quad (96)$$

Replacing Φ by $\Phi^J_{M\mu}$ in expression (94) results in the decomposition of a generic three-body helicity state with total angular momentum J denoted $|\Psi;JM\mu;\lambda_1\lambda_2\lambda_3\rangle$, in Berman's J-helicity states,

$$|\Psi; JM\mu; \lambda_1\lambda_2\lambda_3\rangle = \int \frac{\mathrm{d}w_1\mathrm{d}w_2\mathrm{d}w_3}{8}\Psi(w_1, w_2, w_3)|JM\mu; w_1w_2w_3; \lambda_1\lambda_2\lambda_3\rangle. \tag{97}$$

Imposing a unit normalization for $|\Psi; JM\mu; \lambda_1\lambda_2\lambda_3\rangle$ and making use of the orthonormalization of Berman's J-helicity (82) allows us to infer the normalization condition on $\Psi(w_1, w_2, w_3)$,

$$\langle\Psi; JM\mu; \lambda_1\lambda_2\lambda_3|\Psi; JM\mu; \lambda_1\lambda_2\lambda_3\rangle = \int \frac{\mathrm{d}w_1\mathrm{d}w_2\mathrm{d}w_3}{8}|\Psi(w_1, w_2, w_3)|^2 = 1. \tag{98}$$

States $|\Psi; JM\mu; \lambda_1\lambda_2\lambda_3\rangle$ can be used to model spin J three-body composite particles made of three constituents. Although the aforementioned developments considered three identical particles, they can be easily generalized to three different particles. The same commentary for two-body systems (cf. Sec. II B 2) about symmetry and parity applies. In the presence of identical particles and/or if a parity quantum number is expected, Berman's J-helicity states have to be replaced by parity and/or symmetry eigenstates which can be obtained using properties (84)–(85c). This construction will be performed in the special case of three-gluon systems in Sec. V.

B. Wick's definition

Next to Berman's proposal to define three-body helicity states, Wick suggests another scheme based on an intermediate two-body coupling. First, following relation (30), particles 1 and 2 are coupled in a two-body J-helicity state at rest,

$$|p_{12}; j_{12}\lambda_{12}; s_1\lambda_1' s_2\lambda_2'\rangle = \sqrt{\frac{2j_{12}+1}{4\pi}}\int \mathrm{d}\cos\theta_{12}\mathrm{d}\phi_{12}D^{j_{12}*}_{\lambda_{12}\lambda_1'-\lambda_2'}(\phi_{12}, \theta_{12}, 0)|p_{12}\theta_{12}\phi_{12}; s_1\lambda_1' s_2\lambda_2'\rangle. \tag{99}$$

Above, p_{12}, θ_{12}, and ϕ_{12} respectively denote the momentum modulus, polar, and azimuthal angle of particle 1 in the c.m.f. of particles 1 and 2 (12-c.m.f.). Helicities λ_1' and λ_2' are also defined in this frame. By construction, states defined by Eq. (99) possess a definite total angular momentum for particles 1 and 2, denoted j_{12}. The third particle is then taken into account. The subsystem of particles 1 and 2 is considered a composite particle of spin j_{12}, of spin projection λ_{12}, and of mass $m_{12}(p_{12})$ with

$$m_{12}(p_{12}) = \sqrt{p_{12}^2 + m_1^2} + \sqrt{p_{12}^2 + m_2^2}. \tag{100}$$

This mass is necessarily nonzero. The composite particle is then coupled with the third particle in the same way it has been done for particles 1 and 2. Because masses of the different states are less explicit than before, these quantities are temporarily brought back in the notation of the boosts along the z axis. The composite particle and the third one are boosted in their own c.m.f., which coincides with the e.c.m.f.,

$$\begin{aligned}|p\theta\phi; j_{12}\lambda_{12}s_3\lambda_3; p_{12}s_1\lambda_1' s_2\lambda_2'\rangle = (-1)^{\lambda_3-s_3}U(R(\phi, \theta, 0)L_z(m_{12}(p_{12}), p))|p_{12}; j_{12}\lambda_{12}; s_1\lambda_1' s_2\lambda_2'\rangle \\ \otimes U(R(\pi+\phi, \pi-\theta, \pi)L_z(m_3, p))|s_3\lambda_3\rangle.\end{aligned} \tag{101}$$

Above, p, θ, and ϕ respectively denote the modulus, the polar, and the azimuthal angle of the momentum of the composite particle in the e.c.m.f. By construction, this momentum is opposite to that of the third particle, both thereby having the same modulus. For this reason, in the following, the notation p_3 will supplant p. States (101) will be referred to as Wick's p-helicity states. Even if quantum numbers that describe the internal motion of the subsystem have been included in the notations, definition (101) has the exact same structure as (26a). Therefore, a total angular momentum can be provided to the whole system by integrating on momentum angles as well,

$$|p_3; JM; j_{12}\lambda_{12}s_3\lambda_3; p_{12}s_1\lambda_1' s_2\lambda_2'\rangle = \sqrt{\frac{2J+1}{4\pi}}\int \mathrm{d}\cos\theta\mathrm{d}\phi D^{J*}_{M\lambda_{12}-\lambda_3}(\phi, \theta, 0)|p_3\theta\phi; j_{12}\lambda_{12}s_3\lambda_3; p_{12}s_1\lambda_1' s_2\lambda_2'\rangle. \tag{102}$$

These three-body helicity states will be referred to as Wick's J-helicity states. Their orthonormality relation is the following:

$$\langle \bar{p}_3;\bar{J}\,\bar{M};\bar{j}_{12}\bar{\lambda}_{12}s_3\bar{\lambda}_3;\bar{p}_{12}s_1\bar{\lambda}_1's_2\bar{\lambda}_2'|p_3;JM;j_{12}\lambda_{12}s_3\lambda_3;p_{12}s_1\lambda_1's_2\lambda_2'\rangle$$
$$=\frac{8W(p_{12},p_3)}{p_3p_{12}}\delta(\bar{W}-W)\delta(\bar{m}_{12}-m_{12})\delta_{\bar{J}J}\delta_{\bar{M}M}\delta_{\bar{j}_{12}j_{12}}\delta_{\bar{\lambda}_{12}\lambda_{12}}\delta_{\bar{\lambda}_1'\lambda_1'}\delta_{\bar{\lambda}_2'\lambda_2'}\delta_{\bar{\lambda}_3\lambda_3}. \tag{103}$$

Above, W is the total energy of the three-body system in its c.m.f.,

$$W(p_{12},p_3)=\sqrt{m_{12}(p_{12})^2+p_3^2}+\sqrt{m_3^2+p_3^2}. \tag{104}$$

As mentioned above, p_{12} is defined in the 12-c.m.f., whereas p_3 is a momentum in the overall c.m.f. Relation (103) is to be compared to the one provided in Ref. [20]. Both are not directly equivalent because the definition of Wick's J-helicity states from this reference differs by an additional $(p_3p_{12}/Wm_{12})^{1/2}/4$ kinematic factor from ours. For further use, this relation is specified for the case of three massless particles. In that case, the relations between p_{12}, p_3, m_{12}, and W simplifies

$$\begin{cases} W=p_3+\sqrt{4p_{12}^2+p_3^2}, \\ m_{12}=2p_{12} \end{cases} \Leftrightarrow \begin{cases} p_3=(W^2-m_{12}^2)/(2W), \\ p_{12}=m_{12}/2. \end{cases} \tag{105}$$

As a result, in the massless case, relation (103) is shown to become

$$\langle \bar{p}_3;\bar{J}\,\bar{M};\bar{j}_{12}\bar{\lambda}_{12}s_3\bar{\lambda}_3;\bar{p}_{12}s_1\bar{\lambda}_1's_2\bar{\lambda}_2'|p_3;JM;j_{12}\lambda_{12}s_3\lambda_3;p_{12}s_1\lambda_1's_2\lambda_2'\rangle$$
$$=\frac{2^5W^2}{(W^2-m_{12}^2)m_{12}}\delta(\bar{W}-W)\delta(\bar{m}_{12}-m_{12})\delta_{\bar{J}J}\delta_{\bar{M}M}\delta_{\bar{j}_{12}j_{12}}\delta_{\bar{\lambda}_{12}\lambda_{12}}\delta_{\bar{\lambda}_1'\lambda_1'}\delta_{\bar{\lambda}_2'\lambda_2'}\delta_{\bar{\lambda}_3\lambda_3}. \tag{106}$$

For the current purpose, this relation will prove more comfortable to use in terms of p_3 and p_{12}, with these variables being directly the momenta of particles in different frames,[4]

$$\langle \bar{p}_3;\bar{J}\,\bar{M};\bar{j}_{12}\bar{\lambda}_{12}s_3\bar{\lambda}_3;\bar{p}_{12}s_1\bar{\lambda}_1's_2\bar{\lambda}_2'|p_3;JM;j_{12}\lambda_{12}s_3\lambda_3;p_{12}s_1\lambda_1's_2\lambda_2'\rangle$$
$$=\frac{4\sqrt{p_3^2+4p_{12}^2}}{p_3p_{12}}\delta(\overline{p_3}-p_3)\delta(\bar{p}_{12}-p_{12})\delta_{\bar{J}J}\delta_{\bar{M}M}\delta_{\bar{j}_{12}j_{12}}\delta_{\bar{\lambda}_{12}\lambda_{12}}\delta_{\bar{\lambda}_1'\lambda_1'}\delta_{\bar{\lambda}_2'\lambda_2'}\delta_{\bar{\lambda}_3\lambda_3}. \tag{107}$$

Whereas Berman's J-helicity states (81) allows for an easy implementation of symmetry through relations (84)–(85c), Wick's states, thanks to the intermediary two-body coupling, are more convenient to compute the ME for operators related to the internal motion. To exploit the advantages of both definitions, a relationship between the two different sets of states can be constructed,

$$|JM\mu;w_1w_2w_3;\lambda_1\lambda_2\lambda_3\rangle=\sum_{\lambda_1',\lambda_2'}D^{s_1}_{\lambda_1'\lambda_1}(R_W^1)D^{s_2}_{\lambda_2'\lambda_2}(R_W^2)e^{i(2s_2+2s_3+\lambda_2'-\lambda_1'-\mu)\pi/2}$$
$$\times\sum_{j_{12}=|\lambda_1'-\lambda_2'|}^{\infty}\sum_{\lambda_{12}=-j_{12}}^{j_{12}}e^{i\lambda_{12}\pi/2}\sqrt{\frac{2j_{12}+1}{2}}d^{j_{12}}_{\lambda_{12}\lambda_1'-\lambda_2'}(\pi/2-\phi_{12})d^{J}_{\mu\lambda_{12}-\lambda_3}(\pi/2)$$
$$\times|p_3;JM;j_{12}\lambda_{12}s_3\lambda_3;p_{12}s_1\lambda_1s_2\lambda_2\rangle. \tag{108}$$

A demonstration of this property is provided in Appendix D. Above, ϕ_{12} is the azimuthal angle of the first particle in the 12-c.m.f. where the momentum of the third particle is along the y axis toward negatives. This quantity, as well as every other dynamical quantity in this relation, is to be understood as depending on w_1, w_2, and w_3. Rotations R_W^1 and R_W^2 are Wigner rotations given by the following combinations of boosts and rotations:

$$R_W^1=(R(\phi_{12},\pi/2,0)L_z(m_1,p_{12}))^{-1}L_3(R(\phi_1,\pi/2,0)L_z(m_1,p_1)),$$
$$R_W^2=(R(\pi+\phi_{12},\pi/2,0)L_z(m_2,p_{12}))^{-1}L_3(R(\phi_2,\pi/2,0)L_z(m_2,p_2)), \tag{109}$$

[4]The Jacobian determinant related to this change is $\mathrm{d}W\mathrm{d}m_{12}=2W(p_{12},p_3)/\sqrt{p_3^2+4p_{12}^2}\mathrm{d}p_3\mathrm{d}p_{12}$.

where $L_3 = R(3\pi/2,\pi/2,0)L_z(m_{12},p_3)R^{-1}(3\pi/2,\pi/2,0)$. The fact that helicities of particles 1 and 2 are summed in the formula keeps track that the helicities λ_i and λ_i' are not defined in the same frame. The appearance of an infinite sum over j_{12} is also an expected feature. To obtain a given total angular momentum J, one can always choose an arbitrarily large relative angular momentum between particles 1 and 2 and then compensate it with the relative angular momentum between this subsystem and the third particle. Let us mention that formula (108) looks rather similar to a result obtained by Wick in [20]. In this reference, Wick rewrites its states in a more symmetrical way, closer to Berman's definition but where the yz plane is chosen as reference. This rewriting introduces two Wigner rotations and a Wigner d-matrix which depends on a dynamical angle. The formula introduced in the current work presents the same components supplemented by a second Wigner D-matrix that rotates the reference plane, in accordance with property (83). Formula (108) can be seen as a descendant of Wick's rewriting.

In Sec. V, formula (108) will be used to describe systems of three massless gluons. For massless particles, both previous Wigner rotations simplify following expression (A6). The change of basis formula reduces to

$$\begin{aligned}|JM\mu;w_1w_2w_3;\lambda_1\lambda_2\lambda_3\rangle = {}& e^{i(2s_2+2s_3+\lambda_2-\lambda_1-\mu)\pi/2}e^{i(\theta_1\lambda_1+\theta_2\lambda_2)}\\ &\times\sum_{j_{12}=|\lambda_1-\lambda_2|}^{\infty}\sum_{\lambda_{12}=-j_{12}}^{j_{12}} e^{i\pi\lambda_{12}/2}\sqrt{\frac{2j_{12}+1}{2}}d^{j_{12}}_{\lambda_{12}\lambda_1-\lambda_2}(\pi/2-\phi_{12})d^{J}_{\mu\lambda_{12}-\lambda_3}(\pi/2)\\ &\times|p_3;JM;j_{12}\lambda_{12}s_3\lambda_3;p_{12}s_1\lambda_1s_2\lambda_2\rangle.\end{aligned} \tag{110}$$

As expected, since helicity is Lorentz invariant for massless particles, the corresponding quantum numbers are no longer summed. The values for both θ_i angles are found by applying the methodology suggested in Ref. [41]. These two angles are shown to cancel and the phase factor reduces,

$$e^{i(2s_2+2s_3+\lambda_2-\lambda_1-\mu)\pi/2}e^{i(\theta_1\lambda_1+\theta_2\lambda_2)} = (-1)^{s_3+s_2}e^{i(\pi/2)(\lambda_2-\lambda_1-\mu)}. \tag{111}$$

This phase is manifestly independent of the w_1, w_2, or w_3 energies. In the case of massless particles, the expression of ϕ_{12}, p_{12}, and p_3 in terms of w_1, w_2, and w_3 also simplifies,

$$\cos(\pi/2-\phi_{12}) = (w_1-w_2)/w_3, \qquad 2p_{12} = \sqrt{(w_1+w_2)^2-w_3^2}, \qquad p_3 = w_3. \tag{112}$$

Inverting these relations, one gets

$$w_1 = \left(\sqrt{4p_{12}^2+w_3^2}+uw_3\right)/2, \qquad w_2 = \left(\sqrt{4p_{12}^2+w_3^2}-uw_3\right)/2, \qquad w_3 = p_3, \tag{113}$$

where $u = \cos(\pi/2-\phi_{12}) = \sin\phi_{12}$. A consistency check of formula (110) is provided in Appendix D.

V. THREE-GLUON GLUEBALLS

Using the helicity formalism for three-body systems introduced in the previous section, a three-gluon glueball spectrum can be obtained following a methodology similar to the two-gluon case. The developments are carried out in three main steps. First, symmetry and parity are implemented in Berman's basis so that this complete set is ready to be used in the description of three-gluon bound states. Second, this basis is used to develop trial states that should approximate reasonably well the true three-gluon glueball states. Third, Hamiltonian MEs are evaluated on these trial states to obtain the aforementioned spectrum.

A. Berman's basis for three-gluon systems

Let us start with the acquisition of symmetric parity eigenstates from Berman's J-helicity states. Dealing with three spin-1 massless particles, the helicity quantum number λ_i can only take two values, -1 and $+1$. Therefore, there are only eight possible triplets of helicities $(\lambda_1,\lambda_2,\lambda_3)$. In Berman's definition, any consistent set of J, M, μ, w_1, w_2, w_3 quantum numbers can be built from each of these triplets. In other words, for any given energy and angular momentum quantum numbers, eight three-gluon J-helicity states can be obtained:

$$|JM\mu; w_1w_2w_3; +++\rangle, \quad |JM\mu; w_1w_2w_3; --+\rangle, \quad |JM\mu; w_1w_2w_3; -++\rangle, \quad |JM\mu; w_1w_2w_3; -+-\rangle,$$
$$|JM\mu; w_1w_2w_3; +-+\rangle, \quad |JM\mu; w_1w_2w_3; +--\rangle, \quad |JM\mu; w_1w_2w_3; ++-\rangle, \quad |JM\mu; w_1w_2w_3; ---\rangle. \tag{114}$$

For shortness, only the sign of the helicities has been kept in the notation. Let us start by implementing parity quantum numbers in these eight states. Considering that gluons have negative intrinsic parity and using relation (84), the eight states (114) can be recombined into eight parity eigenstates,

$$|JM\mu; w_1w_2w_3; +++\rangle + |JM\mu; w_1w_2w_3; ---\rangle, \quad |JM\mu; w_1w_2w_3; -++\rangle + |JM\mu; w_1w_2w_3; +--\rangle,$$
$$|JM\mu; w_1w_2w_3; +-+\rangle + |JM\mu; w_1w_2w_3; -+-\rangle, \quad |JM\mu; w_1w_2w_3; ++-\rangle + |JM\mu; w_1w_2w_3; --+\rangle,$$
$$|JM\mu; w_1w_2w_3; +++\rangle - |JM\mu; w_1w_2w_3; ---\rangle, \quad |JM\mu; w_1w_2w_3; -++\rangle - |JM\mu; w_1w_2w_3; +--\rangle,$$
$$|JM\mu; w_1w_2w_3; +-+\rangle - |JM\mu; w_1w_2w_3; -+-\rangle, \quad |JM\mu; w_1w_2w_3; ++-\rangle - |JM\mu; w_1w_2w_3; --+\rangle. \tag{115}$$

Their parity eigenvalue is $(-1)^{-\mu}$ for the four left states and $(-1)^{1-\mu}$ for the four right ones. In addition to parity, symmetry is also to be implemented. Depending on the expected charge conjugation of the system, three-gluon states have to be symmetrized (negative charge conjugation) or antisymmetrized (positive charge conjugation) [10]. Applying both the symmetrizer and the antisymmetrizer on the eight states (115) provides states with a definite symmetry under exchange of particles. The result of these applications is presented in Table IV. Fixing respectively $\sigma = +1$ or $\sigma = -1$ provides symmetric or antisymmetric states. Because permutation operators change the sign of μ, (anti)symmetric states mix different states with opposite μ quantum numbers. To avoid any redundancy, μ must be understood as positive in Table IV.

B. Three-gluon glueball states

The eight states from Table IV will now be used to construct states that model J^{PC} three-gluon glueballs. The procedure for this construction was outlined at the

TABLE IV. Combinations of Berman's J helicity states that present a given parity and symmetry. Depending on whether σ is chosen to be $+1$ or -1 the state is symmetric or antisymmetric. The parity eigenvalue of the two first sets of states is $(-1)^{-\mu}$ while it is $(-1)^{1-\mu}$ for the last two.

$$\begin{aligned}
&(|JM\mu; w_1w_2w_3; +++\rangle + |JM\mu; w_1w_2w_3; ---\rangle)\\
&+\sigma(-1)^{J+\mu+1}(|JM-\mu; w_2w_1w_3; +++\rangle + |JM-\mu; w_2w_1w_3; ---\rangle)\\
&+\sigma(-1)^{J+\mu+1}e^{-i\varphi_{13}\mu}(|JM-\mu; w_3w_2w_1; +++\rangle + |JM-\mu; w_3w_2w_1; ---\rangle)\\
&+\sigma(-1)^{J+\mu+1}e^{i\varphi_{23}\mu}(|JM-\mu; w_1w_3w_2; +++\rangle + |JM-\mu; w_1w_3w_2; ---\rangle)\\
&+e^{-i\varphi_{13}\mu}(|JM\mu; w_2w_3w_1; +++\rangle + |JM\mu; w_2w_3w_1; ---\rangle)\\
&+e^{i\varphi_{23}\mu}(|JM\mu; w_3w_1w_2; +++\rangle + |JM\mu; w_3w_1w_2; ---\rangle)
\end{aligned}$$

$$\begin{aligned}
&(|JM\mu; w_1w_2w_3; -++\rangle + |JM\mu; w_1w_2w_3; +--\rangle)\\
&+\sigma(-1)^{J+\mu+1}(|JM-\mu; w_2w_1w_3; +-+\rangle + |JM-\mu; w_2w_1w_3; -+-\rangle)\\
&+\sigma(-1)^{J+\mu+1}e^{-i\varphi_{13}\mu}(|JM-\mu; w_3w_2w_1; ++-\rangle + |JM-\mu; w_3w_2w_1; --+\rangle)\\
&+\sigma(-1)^{J+\mu+1}e^{i\varphi_{23}\mu}(|JM-\mu; w_1w_3w_2; -++\rangle + |JM-\mu; w_1w_3w_2; +--\rangle)\\
&+e^{-i\varphi_{13}\mu}(|JM\mu; w_2w_3w_1; ++-\rangle + |JM\mu; w_2w_3w_1; --+\rangle)\\
&+e^{i\varphi_{23}\mu}(|JM\mu; w_3w_1w_2; +-+\rangle + |JM\mu; w_3w_1w_2; -+-\rangle)
\end{aligned}$$

$$\begin{aligned}
&(|JM\mu; w_1w_2w_3; +++\rangle - |JM\mu; w_1w_2w_3; ---\rangle)\\
&+\sigma(-1)^{J+\mu+1}(|JM-\mu; w_2w_1w_3; +++\rangle - |JM-\mu; w_2w_1w_3; ---\rangle)\\
&+\sigma(-1)^{J+\mu+1}e^{-i\varphi_{13}\mu}(|JM-\mu; w_3w_2w_1; +++\rangle - |JM-\mu; w_3w_2w_1; ---\rangle)\\
&+\sigma(-1)^{J+\mu+1}e^{i\varphi_{23}\mu}(|JM-\mu; w_1w_3w_2; +++\rangle - |JM-\mu; w_1w_3w_2; ---\rangle)\\
&+e^{-i\varphi_{13}\mu}(|JM\mu; w_2w_3w_1; +++\rangle - |JM\mu; w_2w_3w_1; ---\rangle)\\
&+e^{i\varphi_{23}\mu}(|JM\mu; w_3w_1w_2; +++\rangle - |JM\mu; w_3w_1w_2; ---\rangle)
\end{aligned}$$

$$\begin{aligned}
&(|JM\mu; w_1w_2w_3; -++\rangle - |JM\mu; w_1w_2w_3; +--\rangle)\\
&+\sigma(-1)^{J+\mu+1}(|JM-\mu; w_2w_1w_3; +-+\rangle - |JM-\mu; w_2w_1w_3; -+-\rangle)\\
&+\sigma(-1)^{J+\mu+1}e^{-i\varphi_{13}\mu}(|JM-\mu; w_3w_2w_1; ++-\rangle - |JM-\mu; w_3w_2w_1; --+\rangle)\\
&+\sigma(-1)^{J+\mu+1}e^{i\varphi_{23}\mu}(|JM-\mu; w_1w_3w_2; -++\rangle - |JM-\mu; w_1w_3w_2; +--\rangle)\\
&+e^{-i\varphi_{13}\mu}(|JM\mu; w_2w_3w_1; ++-\rangle - |JM\mu; w_2w_3w_1; --+\rangle)\\
&+e^{i\varphi_{23}\mu}(|JM\mu; w_3w_1w_2; +-+\rangle - |JM\mu; w_3w_1w_2; -+-\rangle)
\end{aligned}$$

TABLE V. Total angular momentum, parity, and charge conjugation eigenstates for three-gluon systems. A generic helicity-momentum wave function $\Psi(w_1, w_2, w_3)$ is considered. Labels A_2' and A_2'' differentiate the two symmetrical combinations of helicity triplets possible. These labels are inspired by the notations in Ref. [42] and originate from crystallography [43].

$$
\begin{aligned}
|\Psi; A_2'; JM; C=-\sigma; P=\pm(-1)^\mu\rangle = \int \tfrac{\mathrm{d}w_1\mathrm{d}w_2\mathrm{d}w_3}{8} \Big(&\Psi(w_1,w_2,w_3) + e^{-i\varphi_{23}\mu}\Psi(w_3,w_1,w_2) + e^{i\varphi_{13}\mu}\Psi(w_2,w_3,w_1)\Big)\\
&(|JM\mu; w_1w_2w_3; +++\rangle \pm |JM\mu; w_1w_2w_3; ---\rangle)\\
-\sigma(-1)^{J+\mu} \int \tfrac{\mathrm{d}w_1\mathrm{d}w_2\mathrm{d}w_3}{8} \Big(&\Psi(w_2,w_1,w_3) + e^{-i\varphi_{13}\mu}\Psi(w_3,w_2,w_1) + e^{i\varphi_{23}\mu}\Psi(w_1,w_3,w_2)\Big)\\
&(|JM-\mu; w_1w_2w_3; +++\rangle \pm |JM-\mu; w_1w_2w_3; ---\rangle)
\end{aligned}
$$

$$
\begin{aligned}
|\Psi; A_2''; JM; C=-\sigma; P=\pm(-1)^\mu\rangle = \int \tfrac{\mathrm{d}w_1\mathrm{d}w_2\mathrm{d}w_3}{8} \Big(&\Psi(w_1,w_2,w_3)(|JM\mu; w_1w_2w_3; -++\rangle \pm |JM\mu; w_1w_2w_3; +--\rangle)\\
&+e^{-i\varphi_{23}\mu}\Psi(w_3,w_1,w_2)(|JM\mu; w_1w_2w_3; ++-\rangle \pm |JM\mu; w_1w_2w_3; --+\rangle)\\
&+e^{i\varphi_{13}\mu}\Psi(w_2,w_3,w_1)(|JM\mu; w_1w_2w_3; +-+\rangle \pm |JM\mu; w_1w_2w_3; -+-\rangle)\Big)\\
-\sigma(-1)^{J+\mu} \int \tfrac{\mathrm{d}w_1\mathrm{d}w_2\mathrm{d}w_3}{8} \Big(&\Psi(w_2,w_1,w_3)(|JM-\mu; w_1w_2w_3; +-+\rangle \pm |JM-\mu; w_1w_2w_3; -+-\rangle)\\
&+e^{-i\varphi_{13}\mu}\Psi(w_3,w_2,w_1)(|JM-\mu; w_1w_2w_3; ++-\rangle \pm |JM-\mu; w_1w_2w_3; --+\rangle)\\
&+e^{i\varphi_{23}\mu}\Psi(w_1,w_3,w_2)(|JM-\mu; w_1w_2w_3; -++\rangle \pm |JM-\mu; w_1w_2w_3; +--\rangle)\Big)
\end{aligned}
$$

end of Sec. IV A. Specifically, this involves replacing $|JM\mu; w_1w_2w_3; \lambda_1\lambda_2\lambda_3\rangle$ on the right-hand side of Eq. (97) with one of the states from Table IV. Due to their similarities, states from the first and third lines of Table IV can be treated together, as can those from the second and fourth sets. Notably, due to symmetrization, each glueball state combines multiple Berman states where the energy variables w_1, w_2, and w_3 appear in different orders. This difference can be transferred to the $\Psi(w_1, w_2, w_3)$ wave function by appropriately exchanging integration variables. The resulting combinations are presented in Table V. At this stage, the normalization of the symmetrized states is not guaranteed.

Table V shows that any J^{PC} quantum number can, in principle, be realized by a three-gluon system. However, it may be reasonable to assume that low-lying glueball states correspond to symmetric helicity-momentum wave functions,

$$\forall\, i,j,k \in \{1,2,3\}, \Psi(w_i, w_j, w_k) = \Psi(w_1, w_2, w_3). \quad (116)$$

Imposing this symmetry reduces the states in Table V to those in Table VI. Unlike the general case, states with a symmetric helicity-momentum wave function exhibit a selection rule for $\mu = 0$. Specifically, when $\sigma(-1)^J = 1$, terms involving $+\mu$ systematically cancel those with $-\mu$. This implies that states with $\mu = 0$ and negative (positive) charge conjugation only exist for odd (even) J values. Since the following discussion primarily considers states with negative charge conjugation, $\mu = 0$ will always imply an odd J. This feature highlights two interesting properties of the spectrum. First, because the even value $J = 0$ can only be achieved by setting $\mu = 0$, no state with symmetric wave function, null total angular momentum, and negative charge conjugation can be constructed. Color-singlet two-gluon states have only positive charge conjugation; therefore a 0^{P-} bound state of pure glue would either contradict hypothesis (116) or require at least four constituent gluons, a requirement consistent with group theory arguments [10]. Second, negative charge conjugation

TABLE VI. Total angular momentum, parity, and charge conjugation eigenstates for three-gluon systems. A symmetric helicity-momentum wave function $\Psi(w_1, w_2, w_3)$ is considered. Labels A_2' and A_2'' differentiate the two possible symmetrical combinations of helicity triplets. These labels are inspired by the notations in Ref. [42] and originate from crystallography [43].

$$
\begin{aligned}
|\Psi; A_2'; JM; C=-\sigma; P=\pm(-1)^\mu\rangle = \int \tfrac{\mathrm{d}w_1\mathrm{d}w_2\mathrm{d}w_3}{8} \Psi(w_1,w_2,w_3)\Big(&1 + e^{-i\varphi_{23}\mu} + e^{i\varphi_{13}\mu}\Big)\\
&(|JM\mu; w_1w_2w_3; +++\rangle \pm |JM\mu; w_1w_2w_3; ---\rangle)\\
-\sigma(-1)^{J+\mu} \int \tfrac{\mathrm{d}w_1\mathrm{d}w_2\mathrm{d}w_3}{8} \Psi(w_1,w_2,w_3)\Big(&1 + e^{-i\varphi_{13}\mu} + e^{i\varphi_{23}\mu}\Big)\\
&(|JM-\mu; w_1w_2w_3; +++\rangle \pm |JM-\mu; w_1w_2w_3; ---\rangle)
\end{aligned}
$$

$$
\begin{aligned}
|\Psi; A_2''; JM; C=-\sigma; P=\pm(-1)^\mu\rangle = \int \tfrac{\mathrm{d}w_1\mathrm{d}w_2\mathrm{d}w_3}{8} \Psi(w_1,w_2,w_3)\Big(&(|JM\mu; w_1w_2w_3; -++\rangle \pm |JM\mu; w_1w_2w_3; +--\rangle)\\
&+e^{-i\varphi_{23}\mu}(|JM\mu; w_1w_2w_3; ++-\rangle \pm |JM\mu; w_1w_2w_3; --+\rangle)\\
&+e^{i\varphi_{13}\mu}(|JM\mu; w_1w_2w_3; +-+\rangle \pm |JM\mu; w_1w_2w_3; -+-\rangle)\Big)\\
-\sigma(-1)^{J+\mu} \int \tfrac{\mathrm{d}w_1\mathrm{d}w_2\mathrm{d}w_3}{8} \Psi(w_1,w_2,w_3)\Big(&(|JM-\mu; w_1w_2w_3; +-+\rangle \pm |JM-\mu; w_1w_2w_3; -+-\rangle)\\
&+e^{-i\varphi_{13}\mu}(|JM-\mu; w_1w_2w_3; ++-\rangle \pm |JM-\mu; w_1w_2w_3; --+\rangle)\\
&+e^{i\varphi_{23}\mu}(|JM-\mu; w_1w_2w_3; -++\rangle \pm |JM-\mu; w_1w_2w_3; +--\rangle)\Big)
\end{aligned}
$$

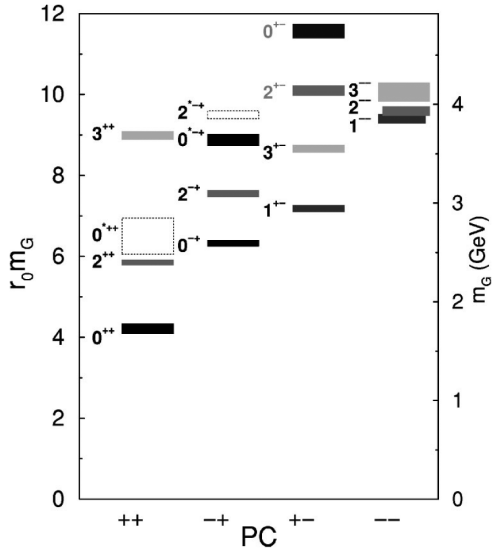

FIG. 8. Glueball spectrum obtained using LQCD. The picture is taken from Ref. [6].

states with $J = 2$ must at least have $\mu = 1$. Qualitatively, one may suppose that higher μ projection of the total angular momentum would result in higher energy states. If this is correct, the $\mu = 0$ selection rule would push $J = 2$ states to higher masses.

This analysis is supported by glueball spectrum calculations from other approaches. For instance, Fig. 8, taken from reference Ref. [6], shows glueball masses calculated using LQCD. In this spectrum, the first 0^{P-} state appears above 4.5 GeV, significantly higher than the lowest J^{P-} state, which lies below 3 GeV. This aligns with the preceding analysis. The $J = 0$ state may be interpreted as a first four-gluon state or a three-gluon state with a nonsymmetric helicity-momentum wave function $\Psi(w_1, w_2, w_3)$. Beyond $J = 0$, the hierarchy of even states follows the expected pattern: The $J = 1$ and $J = 3$ states, which allow $\mu = 0$, appear in order, while the $J = 2$ state is shifted to higher energies. However, the situation for odd states remains less clear. Further discussion is deferred until quantitative results are obtained.

The states from Tables V and VI are also consistent with results from Refs. [42,44]. In Ref. [44], it is argued that no general selection rules govern the decay of a particle into three massless spin-1 particles. This is consistent with the absence of selection rules in Table V. Reference [42] refines this discussion for symmetric decays into three photons, concluding that such a decay is not possible for $J = 0$ particles. This agrees with the analysis of states from Table VI. Moreover, the helicity triplet combinations constructed in [42] closely resemble those in the current work. For this reason, the labels A_2' and A_2'' from Ref. [42] have been adopted in Tables V and VI to distinguish these states.

C. Low-lying three-gluon glueballs with negative charge conjugation

The current description of the glueball spectrum has remained qualitative. To move toward quantitative analysis, the methodology based on the variational theorem applied to two-gluon glueballs in Sec. III will be extended to three-gluon glueballs. This approach involves, on one hand, constructing a set of trial states designed to approximate three-gluon glueballs accurately and, on the other hand, evaluating Hamiltonian MEs on this set. For the former, appropriate trial helicity-momentum wave functions Ψ must be chosen. For the latter, formulas to compute MEs on three-body helicity states are required. This subsection addresses both these tasks for the low-lying three-gluon glueball states with negative charge conjugation and with a symmetric Ψ function. Angular momenta up to $J = 3$ and μ projections up to $\mu = 1$ are considered. To keep the equations concise, reduced notations are introduced for Berman's J-helicity states and for the three-body helicity states defined in (97),

$$|\lambda_1\lambda_2\lambda_3\rangle^J_\mu = |JM\mu; w_1w_2w_3; \lambda_1\lambda_2\lambda_3\rangle,$$
$$|\Psi; \lambda_1\lambda_2\lambda_3\rangle^J_\mu = |\Psi; JM\mu; \lambda_1\lambda_2\lambda_3\rangle. \tag{117}$$

In $|\lambda_1\lambda_2\lambda_3\rangle^J_\mu$, the order of energy labels is tacitly assumed to be always $w_1w_2w_3$. For clarity in plain text, three-body states defined in Eq. (97) will be referred to as unsymmetrical states, while those from Table VI will be referred to as symmetrical states. Symmetrical states corresponding to the above-named low-lying three-gluon glueballs can be made explicit using these notations. Considering $\mu = 0$, the following states are obtained:

$$|\Psi; A_2'; \mu = 0; J^{PC} = (2k+1)^{\pm-}\rangle = \frac{1}{\sqrt{2}}\left(|\Psi; +++\rangle^{2k+1}_0 \pm |\Psi; ---\rangle^{2k+1}_0\right), \tag{118}$$

$$|\Psi; A_2''; \mu = 0; J^{PC} = (2k+1)^{\pm-}\rangle = \frac{1}{\sqrt{6}}\Big(|\Psi; -++\rangle^{2k+1}_0 \pm |\Psi; +--\rangle^{2k+1}_0 + |\Psi; ++-\rangle^{2k+1}_0$$
$$\pm |\Psi; --+\rangle^{2k+1}_0 + |\Psi; +-+\rangle^{2k+1}_0 \pm |\Psi; -+-\rangle^{2k+1}_0\Big) \tag{119}$$

where $k \in \mathbb{N}$ (even angular momenta are forbidden for $\mu = 0$). Notations of the states have slightly been adapted in comparison with those from Table VI. Considering $\mu = \pm 1$, the following states are obtained:

$$|\Psi; A_2'; |\mu| = 1; J^{PC} = J^{\mp-}\rangle = \Big(|\Psi(1 + e^{-i\varphi_{23}} + e^{i\varphi_{13}}); + + +\rangle_1^J \pm |\Psi(1 + e^{-i\varphi_{23}} + e^{i\varphi_{13}}); - - -\rangle_1^J + (-1)^J |\Psi(1 + e^{-i\varphi_{13}} + e^{i\varphi_{23}}); + + +\rangle_{-1}^J \pm (-1)^J |\Psi(1 + e^{-i\varphi_{13}} + e^{i\varphi_{23}}); - - -\rangle_{-1}^J\Big), \tag{120}$$

$$\begin{aligned}|\Psi; A_2''; |\mu| = 1; J^{PC} = J^{\mp-}\rangle = \frac{1}{\sqrt{12}}\Big(&|\Psi; - + +\rangle_1^J \pm |\Psi; + - -\rangle_1^J + |\Psi e^{i\varphi_{13}}; + - +\rangle_1^J \pm |\Psi e^{i\varphi_{13}}; - + -\rangle_1^J \\ &+ |\Psi e^{-i\varphi_{23}}; + + -\rangle_1^J \pm |\Psi e^{-i\varphi_{23}}; - - +\rangle_1^J \\ &+ (-1)^J(|\Psi; + - +\rangle_{-1}^J \pm |\Psi; - + -\rangle_{-1}^J + |\Psi e^{i\varphi_{23}}; - + +\rangle_{-1}^J \pm |\Psi e^{i\varphi_{23}}; + - -\rangle_{-1}^J \\ &+ |\Psi e^{-i\varphi_{13}}; + + -\rangle_{-1}^J \pm |\Psi e^{-i\varphi_{13}}; - - +\rangle_{-1}^J)\Big).\end{aligned} \tag{121}$$

In general, symmetrical states are linear combinations of unsymmetrical ones whose helicity-momentum wave function is potentially modified by an additional kinematic factor introduced during the symmetrization process. In (118), (119), and (121), square root factors have been added to ensure that symmetric states are normalized as long as unsymmetrical ones are. The question of the normalization of Eq. (120) is deferred to Sec. V C 4.

1. Selection of trial helicity-momentum wave functions

Let us start by selecting a suitable structure to use for trial helicity-momentum wave functions $\Psi(w_1, w_2, w_3)$. The most convenient choice is probably a Gaussian-shaped wave function for which calculations are reasonably simple and which often offers great convergence properties. Symmetrical states (118)–(121) are linear combinations of unsymmetrical ones, and this discussion takes place at the level of the latter. Gaussians may be constructed using different sets of coordinates, thereby leading to nonequivalent structures. The most straightforward choice is probably to consider a Gaussian-shaped helicity-momentum wave function in PMP coordinates,

$$\Psi_{\text{PMP}}(w_1, w_2, w_3) = A e^{-a((w_1-b)^2+(w_2-b)^2+(w_3-b)^2)}. \tag{122}$$

Above, A is a normalization constant used to ensure that (98) is respected. If an expansion with more than one trial state is to be used, for instance adapting Eq. (75), the normalization condition is replaced by the evaluation of an overlap matrix [37]. In that case, the constant A can be omitted. The structure (122) incorporates two nonlinear variational parameters, a and b. The former encodes the spreading in energy and has dimensions of inverse energy squared. The latter encodes the position of the energy peak and has energy dimension. Different constants for each term in the exponential cannot be used to keep the trial wave function symmetrical. The choice of wave function is, of course, arbitrary, and many modifications can be proposed. After several tests, adding a square root factor $\sqrt{8w_1w_2w_3}$ in front of the Gaussian was found to improve convergence. As a result, the following trial wave function is suggested:

$$\Psi_{a,b}(w_1, w_2, w_3) = A\sqrt{8w_1w_2w_3}e^{-a((w_1-b)^2+(w_2-b)^2+(w_3-b)^2)}, \tag{123}$$

and the corresponding unsymmetrical state reads

$$|\Psi_{\text{PMP}}; \lambda_1\lambda_2\lambda_3\rangle_\mu^J = A\int \frac{\mathrm{d}w_1\mathrm{d}w_2\mathrm{d}w_3}{8}\sqrt{8w_1w_2w_3}e^{-a((w_1-b)^2+(w_2-b)^2+(w_3-b)^2)}|\lambda_1\lambda_2\lambda_3\rangle_\mu^J. \tag{124}$$

Further calculations will require us to switch for the system of coordinates depicted in relation (113), namely $u = \sin(\phi_{12})$, p_{12}, and p_3. In these new coordinates, $\Psi_{a,b}(w_1, w_2, w_3)$ becomes

$$\Psi_{a,b}(u, p_{12}, p_3) = A\sqrt{p_3(8p_{12}^2 + 2p_3^2(1-u^2))}e^{-\frac{a}{2}(6b^2-4b(\sqrt{4p_{12}^2+p_3^2}+p_3)+4p_{12}^2+3p_3^2)}e^{-\frac{a}{2}u^2p_3^2}. \tag{125}$$

One can already anticipate why this system of coordinates will be helpful: The variable u is by definition the cosine of the angle that occurs in the change of basis formula (110), while the variable p_{12} is the relative momentum between particles 1 and 2 in their c.m.f., a variable of great interest for the evaluation of two-body potential MEs. Symmetric states from Eqs. (120) and (121) supplement the helicity-momentum wave function with kinematics factors that depend on the angles φ_{ij} defined in (77). To complete the picture of the wave function, these additional kinematic factors should be made explicit in u, p_{12}, p_3 coordinates,

$$\cos\varphi_{12}=\frac{(1-u^2)p_3^2-4p_{12}^2}{(1-u^2)p_3^2+4p_{12}^2},\qquad \cos\varphi_{13}=-\frac{u\sqrt{4p_{12}^2+p_3^2}+p_3}{\sqrt{4p_{12}^2+p_3^2}+up_3},$$
$$\cos\varphi_{23}=\frac{u\sqrt{4p_{12}^2+p_3^2}-p_3}{\sqrt{4p_{12}^2+p_3^2}-up_3}. \tag{126}$$

On one hand, in states (120), the following combinations of φ_{ij} appear:

$$1+e^{\pm i\varphi_{13}}+e^{\mp i\varphi_{23}}=\frac{(1-u^2)(p_3^2-2\sqrt{(4p_{12}^2+p_3^2)p_3^2})+4p_{12}^2}{(1-u^2)p_3^2+4p_{12}^2}\mp i\frac{4p_{12}u\sqrt{(1-u^2)p_3^2}}{(1-u^2)p_3^2+4p_{12}^2}. \tag{127}$$

On the other hand, in states (121), φ_{ij} angles are taken in complex exponential,

$$e^{i\varphi_{13}}=-\frac{u\sqrt{4p_{12}^2+p_3^2}+p_3}{\sqrt{4p_{12}^2+p_3^2}+up_3}+i\frac{2p_{12}\sqrt{1-u^2}}{\sqrt{4p_{12}^2+p_3^2}+up_3},$$
$$e^{i\varphi_{23}}=\frac{u\sqrt{4p_{12}^2+p_3^2}-p_3}{\sqrt{4p_{12}^2+p_3^2}-up_3}+i\frac{2p_{12}\sqrt{1-u^2}}{\sqrt{4p_{12}^2+p_3^2}-up_3}. \tag{128}$$

2. Evaluation of matrix elements on unsymmetrical states

To acquire an approximate energy spectrum by using the variational theorem requires the evaluation of Hamiltonian MEs on trial states. Therefore, it requires deriving formulas for performing such calculations on symmetrical states. Since symmetrical states decompose as linear combinations of unsymmetrical ones [cf. Eqs. (118)–(121)], establishing formulas for the latter will give support to the evaluation of the MEs for the former. Extension to symmetrical states will be discussed further in the next subsection.

Because helicity states are momentum eigenstates, the evaluation of kinetic energy operators is the most straightforward to perform. To encompass many different kinematics at once, a generic $T(w_1,w_2,w_3)$ kinetic energy is considered for now. This function is only supposed to depend on the three w energies and not on the angles α,β,γ. First, definition (97) can be used for both the bra and the ket,

$${}^J_{\bar\mu}\langle\bar\Psi;\bar\lambda_1\bar\lambda_2\bar\lambda_3|T|\Psi;\lambda_1\lambda_2\lambda_3\rangle^J_\mu=\int\frac{d\bar w_1 d\bar w_2 d\bar w_3}{8}\frac{dw_1dw_2dw_3}{8}\bar\Psi^*(\bar w_1,\bar w_2,\bar w_3)\Psi(w_1,w_2,w_3){}^J_{\bar\mu}\langle\bar\lambda_1\bar\lambda_2\bar\lambda_3|T|\lambda_1\lambda_2\lambda_3\rangle^J_\mu. \tag{129}$$

With Berman's J-helicity states being eigenstates of the three w energies, the evaluation of $T(w_1,w_2,w_3)$ on these comes down to a simple scalar multiplication,

$${}^J_{\bar\mu}\langle\bar\Psi;\bar\lambda_1\bar\lambda_2\bar\lambda_3|T|\Psi;\lambda_1\lambda_2\lambda_3\rangle^J_\mu=\int\frac{d\bar w_1 d\bar w_2 d\bar w_3}{8}\frac{dw_1dw_2dw_3}{8}\bar\Psi^*(\bar w_1,\bar w_2,\bar w_3)\Psi(w_1,w_2,w_3)$$
$$T(w_1,w_2,w_3){}^J_{\bar\mu}\langle\bar\lambda_1\bar\lambda_2\bar\lambda_3|\lambda_1\lambda_2\lambda_3\rangle^J_\mu. \tag{130}$$

Finally, using the orthonormalization relation of Berman's J-helicity states, three Dirac deltas are produced and remove the integrations on bar variables,

$${}^J_{\bar\mu}\langle\bar\Psi;\bar\lambda_1\bar\lambda_2\bar\lambda_3|T|\Psi;\lambda_1\lambda_2\lambda_3\rangle^J_\mu=\delta_{\bar\mu\mu}\delta_{\bar\lambda_1\lambda_1}\delta_{\bar\lambda_2\lambda_2}\delta_{\bar\lambda_3\lambda_3}\int\frac{dw_1dw_2dw_3}{8}\bar\Psi^*(w_1,w_2,w_3)\Psi(w_1,w_2,w_3)T(w_1,w_2,w_3). \tag{131}$$

As a reminder, both w_1 and w_2 vary from 0 to $+\infty$ while w_3 varies between $|w_1-w_2|$ and w_1+w_2. This formula allows for reasonably easy evaluations of kinetic energy MEs on unsymmetrical states.

Let us turn to the evaluation of two-body potential MEs. For symmetric states, MEs of the three two-body interactions are shown to be equal each other. As a result, computing a single two-body interaction ME and multiplying it by 3 is sufficient to evaluate the entire potential energy of the system. Because the current goal is to perform evaluations on such symmetric states, calculations will only be developed for the interaction between particles 1 and 2. One may expect to reuse the method set up to compute potential MEs for two-body systems. To do so, the trial states have to be developed in Wick's helicity basis in order to introduce two-body subcouplings. From

definition (97), one can use the expansion (110) to develop the state in Wick's helicity basis,

$$|\Psi;\lambda_1\lambda_2\lambda_3\rangle^J_\mu = e^{i(\pi/2)(\lambda_2-\lambda_1-\mu)}\sum_{j_{12}=|\lambda_1-\lambda_2|}^{\infty}\sum_{\lambda_{12}=-j_{12}}^{j_{12}} i^{\lambda_{12}}\sqrt{\frac{2j_{12}+1}{2}}d^J_{\mu\lambda_{12}-\lambda_3}(\pi/2)$$
$$\times\int\frac{\mathrm{d}w_1\mathrm{d}w_2\mathrm{d}w_3}{8}\Psi(w_1,w_2,w_3)d^{j_{12}}_{\lambda_{12}\lambda_1-\lambda_2}(\pi/2-\phi_{12})|p_3;JM;j_{12}\lambda_{12}\lambda_3;p_{12}\lambda_1\lambda_2\rangle. \tag{132}$$

For the sake of readability, summation ranges are omitted in the next expressions. For further convenience, variables u, p_{12}, and p_3 are introduced in the integral [cf. relations (113) and (D27)],

$$|\Psi;\lambda_1\lambda_2\lambda_3\rangle^J_\mu = e^{i(\pi/2)(\lambda_2-\lambda_1-\mu)}\sum_{j_{12}}\sum_{\lambda_{12}} i^{\lambda_{12}}\sqrt{\frac{2j_{12}+1}{2}}d^J_{\mu\lambda_{12}-\lambda_3}(\pi/2)$$
$$\times\int\frac{p_3p_{12}\mathrm{d}u\mathrm{d}p_{12}\mathrm{d}p_3}{4\sqrt{4p_{12}^2+p_3^2}}\Psi(u,p_{12},p_3)d^{j_{12}}_{\lambda_{12}\lambda_1-\lambda_2}(\arccos u)|p_3;JM;j_{12}\lambda_{12}\lambda_3;p_{12}\lambda_1\lambda_2\rangle. \tag{133}$$

As a reminder, the integration range is -1 to 1 for u while it is 0 to ∞ for both p_3 and p_{12}. Because this important result is relatively cumbersome, the following notation shortcuts are introduced:

$$\mathcal{C}^{j_{12}\lambda_{12}}_{J\mu;\lambda_1\lambda_2\lambda_3} = e^{i(\pi/2)(\lambda_2-\lambda_1-\mu+\lambda_{12})}\sqrt{\frac{2j_{12}+1}{2}}d^J_{\mu\lambda_{12}-\lambda_3}(\pi/2), \tag{134}$$

$$\Psi^{j_{12}}_{\lambda_{12}\lambda_1-\lambda_2}(u,p_{12},p_3) = \Psi(u,p_{12},p_3)d^{j_{12}}_{\lambda_{12}\lambda_1-\lambda_2}(\arccos u). \tag{135}$$

The above $\mathcal{C}$ coefficients should not be confused with those for two-body systems defined in relation (53). The difference should be clear depending on the context and looking at the index structure. With these notations, Eq. (133) shortens,

$$|\Psi;\lambda_1\lambda_2\lambda_3\rangle^J_\mu = \sum_{j_{12}}\sum_{\lambda_{12}}\mathcal{C}^{j_{12}\lambda_{12}}_{J\mu;\lambda_1\lambda_2\lambda_3}\int\frac{p_3p_{12}\mathrm{d}u\mathrm{d}p_{12}\mathrm{d}p_3}{4\sqrt{4p_{12}^2+p_3^2}}\Psi^{j_{12}}_{\lambda_{12}\lambda_1-\lambda_2}(u,p_{12},p_3)|p_3;JM;j_{12}\lambda_{12}\lambda_3;p_{12}\lambda_1\lambda_2\rangle. \tag{136}$$

This formula will be very helpful to evaluate two-body potential MEs associated with particles 1 and 2. This interaction, denoted $\mathcal{O}$, is supposed to solely depend on the relative distance between these two particles, $r_{12} = |\boldsymbol{r_1}-\boldsymbol{r_2}|$. This distance is assumed to be defined in the 12-c.m.f. First, Eq. (136) is used on both the bra and the ket,

$${}^J_{\bar\mu}\langle\bar\Psi;\bar\lambda_1\bar\lambda_2\bar\lambda_3|\mathcal{O}(r_{12})|\Psi;\lambda_1\lambda_2\lambda_3\rangle^J_\mu = \sum_{\bar j_{12}}\sum_{\bar\lambda_{12}}\sum_{j_{12}}\sum_{\lambda_{12}}(\mathcal{C}^{\bar j_{12}\bar\lambda_{12}}_{J\bar\mu;\bar\lambda_1\bar\lambda_2\bar\lambda_3})^*\mathcal{C}^{j_{12}\lambda_{12}}_{J\mu;\lambda_1\lambda_2\lambda_3}$$
$$\times\int\frac{\bar p_3\bar p_{12}\mathrm{d}\bar u\mathrm{d}\bar p_{12}\mathrm{d}\bar p_3}{4\sqrt{4\bar p_{12}^2+\bar p_3^2}}(\bar\Psi^{\bar j_{12}}_{\bar\lambda_{12}\bar\lambda_1-\bar\lambda_2}(\bar u,\bar p_{12},\bar p_3))^*\int\frac{p_3p_{12}\mathrm{d}u\mathrm{d}p_{12}\mathrm{d}p_3}{4\sqrt{4p_{12}^2+p_3^2}}\Psi^{j_{12}}_{\lambda_{12}\lambda_1-\lambda_2}(u,p_{12},p_3)$$
$$\times\langle\bar p_3;JM;\bar j_{12}\bar\lambda_{12}\bar\lambda_3;\bar p_{12}\bar\lambda_1\bar\lambda_2|\mathcal{O}(r_{12})|p_3;JM;j_{12}\lambda_{12}\lambda_3;p_{12}\lambda_1\lambda_2\rangle. \tag{137}$$

By doing so, the evaluation of $\mathcal{O}(r_{12})$ on Berman's J-helicity states comes down to its evaluation on Wick's J-helicity states. The latter, thanks to the intermediary coupling in Wick's definition, consists of evaluating $\mathcal{O}(r_{12})$ on two-body J-helicity states. Dividing up the normalization factor from (107) between both states and ensuring a normalization for two-body states consistent with Secs. II and III, one gets

$$\langle\bar p_3;JM;\bar j_{12}\bar\lambda_{12}\bar\lambda_3;\bar p_{12}\bar\lambda_1\bar\lambda_2|\mathcal{O}(r_{12})|p_3;JM;j_{12}\lambda_{12}\lambda_3;p_{12}\lambda_1\lambda_2\rangle$$
$$= \frac{\sqrt[4]{\bar p_3^2+4\bar p_{12}^2}\sqrt[4]{p_3^2+4p_{12}^2}}{\sqrt{\bar p_3\bar p_{12}}\sqrt{p_{12}p_3}}\delta(\bar p_3-p_3)\delta_{\bar\lambda_3\lambda_3}\langle\bar p_{12};\bar j_{12}\bar\lambda_{12};\bar\lambda_1\bar\lambda_2|\mathcal{O}(r_{12})|p_{12};j_{12}\lambda_{12};\lambda_1\lambda_2\rangle. \tag{138}$$

Because r_{12} is defined in the 12-c.m.f., the residual MEs on two-body states can be computed by using formulas developed in Sec. II. Such MEs for such central potentials have proven to cancel for $\bar j_{12}\neq j_{12}$ or $\bar\lambda_{12}\neq\lambda_{12}$ in Eq. (58). It has also been emphasized in this section that these MEs, as soon as nonzero, do not truly depend on the total angular momentum

projection λ_{12}. Equation (138) can be plugged into Eq. (137),

$$\begin{aligned}{}^{J}_{\bar{\mu}}\langle\bar{\Psi};\bar{\lambda}_1\bar{\lambda}_2\bar{\lambda}_3|\mathcal{O}(r_{12})|\Psi;\lambda_1\lambda_2\lambda_3\rangle^{J}_{\mu} &= \delta_{\bar{\lambda}_3\lambda_3}\sum_{j_{12}}\sum_{\lambda_{12}}\left(\mathcal{C}^{j_{12}\lambda_{12}}_{J\bar{\mu};\bar{\lambda}_1\bar{\lambda}_2\lambda_3}\right)^{*}\mathcal{C}^{j_{12}\lambda_{12}}_{J\mu;\lambda_1\lambda_2\lambda_3}\\ &\times\int\frac{p_3\sqrt{\bar{p}_{12}p_{12}}}{4\sqrt[4]{p_3^2+4\bar{p}_{12}^2}4\sqrt[4]{p_3^2+4p_{12}^2}}\mathrm{d}\bar{u}\mathrm{d}\bar{p}_{12}\mathrm{d}u\mathrm{d}p_{12}\mathrm{d}p_3\left(\bar{\Psi}^{j_{12}}_{\lambda_{12}\bar{\lambda}_1-\bar{\lambda}_2}(\bar{u},\bar{p}_{12},p_3)\right)^{*}\Psi^{j_{12}}_{\lambda_{12}\lambda_1-\lambda_2}(u,p_{12},p_3)\\ &\times\langle\bar{p}_{12};j_{12}\lambda_{12};\bar{\lambda}_1\bar{\lambda}_2|\mathcal{O}(r_{12})|p_{12};j_{12}\lambda_{12};\lambda_1\lambda_2\rangle. \end{aligned}\tag{139}$$

The lower boundary in the summation on j_{12} must now fulfill both the constraints $j_{12}\geq|\lambda_1-\lambda_2|$ and $j_{12}\geq|\bar{\lambda}_1-\bar{\lambda}_2|$. This integral can be reorganized as follows:

$$\begin{aligned}{}^{J}_{\bar{\mu}}\langle\bar{\Psi};\bar{\lambda}_1\bar{\lambda}_2\bar{\lambda}_3|\mathcal{O}(r_{12})|\Psi;\lambda_1\lambda_2\lambda_3\rangle^{J}_{\mu} &= \delta_{\bar{\lambda}_3\lambda_3}\sum_{j_{12}}\sum_{\lambda_{12}}\left(\mathcal{C}^{j_{12}\lambda_{12}}_{J\bar{\mu};\bar{\lambda}_1\bar{\lambda}_2\lambda_3}\right)^{*}\mathcal{C}^{j_{12}\lambda_{12}}_{J\mu;\lambda_1\lambda_2\lambda_3}\\ &\times\int p_3\mathrm{d}p_3\int\frac{\mathrm{d}\bar{p}_{12}}{2}\frac{\mathrm{d}p_{12}}{2}\tilde{\Psi}(\bar{p}_{12},p_3;j_{12},\lambda_{12},\bar{\lambda}_1-\bar{\lambda}_2;\bar{\Psi}^{*})\tilde{\Psi}(p_{12},p_3;j_{12},\lambda_{12},\lambda_1-\lambda_2;\Psi)\\ &\times\langle\bar{p}_{12};j_{12}\lambda_{12};\bar{\lambda}_1\bar{\lambda}_2|\mathcal{O}(r_{12})|p_{12};j_{12}\lambda_{12};\lambda_1\lambda_2\rangle \end{aligned}\tag{140}$$

where

$$\tilde{\Psi}(p_{12},p_3;j_{12},\lambda_{12},\Delta\lambda;\Psi)=\frac{\sqrt{p_{12}}}{2\sqrt[4]{4p_{12}^2+p_3^2}}\int\mathrm{d}u\Psi^{j_{12}}_{\lambda_{12}\Delta\lambda}(u,p_{12},p_3)\tag{141}$$

and where the product of three-body $\mathcal{C}$ coefficients can be made a bit more explicit,

$$\begin{aligned}\left(\mathcal{C}^{j_{12}\lambda_{12}}_{J\bar{\mu};\bar{\lambda}_1\bar{\lambda}_2\lambda_3}\right)^{*}\mathcal{C}^{j_{12}\lambda_{12}}_{J\mu;\lambda_1\lambda_2\lambda_3} &= e^{i\frac{\pi}{2}((\lambda_2-\bar{\lambda}_2)+(\bar{\lambda}_1-\lambda_1)+(\bar{\mu}-\mu))}\frac{2j_{12}+1}{2}d^{J}_{\bar{\mu}\lambda_{12}-\lambda_3}(\pi/2)d^{J}_{\mu\lambda_{12}-\lambda_3}(\pi/2)\\ &=(-1)^{(\lambda_2-\bar{\lambda}_2)/2+(\bar{\lambda}_1-\lambda_1)/2+(\bar{\mu}-\mu)/2}\frac{2j_{12}+1}{2}d^{J}_{\bar{\mu}\lambda_{12}-\lambda_3}(\pi/2)d^{J}_{\mu\lambda_{12}-\lambda_3}(\pi/2). \end{aligned}\tag{142}$$

In Eq. (140), the function $\tilde{\Psi}$ acts like an unnormalized two-body helicity-momentum wave function that would depend on three parameters (a, b, and p_3). Therefore, the evaluation of the integrals on p_{12} and $\bar{p}_{12}$ is fully analogous to what has been done to compute potential MEs for two-body systems.

Equations (140)–(142) are key formulas for the current work as they allow computation of two-body potential MEs on three-body helicity states. However, these formulas involve the evaluation of an infinite series of four-dimensional integrals. Even when truncating this series, calculating such a large number of integrals remains a significant challenge. Gaining deeper insight into the components of this formula may help mitigate this complexity. Appendix E is dedicated to this analysis.

3. Evaluation of matrix elements on symmetrical states

The previous subsection worked at obtaining formulas to compute Hamiltonian MEs on unsymmetrical states. In the current one, this technology is used to compute MEs for symmetric states. Starting with kinetic MEs, a formula for both symmetric states having $\mu=0$ can easily be obtained thanks to the absence of mixing between helicities in (131). The situation is even simpler because nonzero terms prove to be independent of the actual value of λ_1, λ_2, or λ_3. Only a single integral has to be evaluated,

$$\begin{aligned}\langle\bar{\Psi};A_2';0;(2k+1)^{\pm-}|T|\Psi;A_2';0;(2k+1)^{\pm-}\rangle &= \langle\bar{\Psi};A_2'';0;(2k+1)^{\pm-}|T|\Psi;A_2'';0;(2k+1)^{\pm-}\rangle\\ &=\int\frac{\mathrm{d}w_1\mathrm{d}w_2\mathrm{d}w_3}{8}\bar{\Psi}^{*}(w_1,w_2,w_3)\Psi(w_1,w_2,w_3)T(w_1,w_2,w_3). \end{aligned}\tag{143}$$

Concerning states based on $\mu=\pm1$, the presence of Kronecker deltas in (131) still simplifies the evaluation of kinetic energy. For the A_2' states [cf. Eq. (120)], due to the additional kinematic factors arising from the symmetrization, the result requires the evaluation of a slightly different integral,

$$\langle\bar{\Psi};A_2';1;J^{\mp-}|T|\Psi;A_2';1;J^{\mp-}\rangle=\int\frac{\mathrm{d}w_1\mathrm{d}w_2\mathrm{d}w_3}{2}\bar{\Psi}^*(w_1,w_2,w_3)\Psi(w_1,w_2,w_3)|1+e^{-i\varphi_{13}}+e^{i\varphi_{23}}|^2T(w_1,w_2,w_3). \quad (144)$$

For the A_2'' states [cf. Eq. (121)], the kinetic energy MEs are again provided by the previous integral,

$$\langle\bar{\Psi};A_2'';1;J^{\mp-}|T|\Psi;A_2'';1;J^{\mp-}\rangle=\int\frac{\mathrm{d}w_1\mathrm{d}w_2\mathrm{d}w_3}{8}\bar{\Psi}^*(w_1,w_2,w_3)\Psi(w_1,w_2,w_3)T(w_1,w_2,w_3). \quad (145)$$

For each symmetric state, kinetic energy ME can be evaluated in a single integral. Notice that Eqs. (143)–(145) allow us to infer formulas for the overlap between symmetrical states by plugging in $T(w_1,w_2,w_3)=1$.

Let us move on to the case of two-body potential MEs. Due to the $\delta_{\bar{\lambda}_3\lambda_3}$ factor in (140), some MEs on unsymmetrical states are directly shown to cancel. For state (118), the resulting expression only requires us to evaluate two MEs,

$$\begin{aligned}\langle\bar{\Psi};A_2';0;(2k+1)^{\pm-}|\mathcal{O}(r_{12})|\Psi;A_2';0;(2k+1)^{\pm-}\rangle=\frac{1}{2}\big({}_0^{2k+1}\langle\bar{\Psi};+++|\mathcal{O}(r_{12})|\Psi;+++\rangle_0^{2k+1}\\ +{}_0^{2k+1}\langle\bar{\Psi};---|\mathcal{O}(r_{12})|\Psi;---\rangle_0^{2k+1}\big).\end{aligned} \quad (146)$$

One can immediately observe that the potential MEs for these states are parity degenerated. Concerning state (119), this sum is composed of 12 MEs, including nondiagonal ones,

$$\begin{aligned}&\langle\bar{\Psi};A_2'';0;(2k+1)^{\pm-}|\mathcal{O}(r_{12})|\Psi;A_2'';0;(2k+1)^{\pm-}\rangle\\ &\quad=\frac{1}{6}\big({}_0^{2k+1}\langle\bar{\Psi};-++|\mathcal{O}(r_{12})|\Psi;-++\rangle_0^{2k+1}+{}_0^{2k+1}\langle\bar{\Psi};+-+|\mathcal{O}(r_{12})|\Psi;+-+\rangle_0^{2k+1}\\ &\quad+{}_0^{2k+1}\langle\bar{\Psi};--+|\mathcal{O}(r_{12})|\Psi;--+\rangle_0^{2k+1}+{}_0^{2k+1}\langle\bar{\Psi};++-|\mathcal{O}(r_{12})|\Psi;++-\rangle_0^{2k+1}\\ &\quad+{}_0^{2k+1}\langle\bar{\Psi};+--|\mathcal{O}(r_{12})|\Psi;+--\rangle_0^{2k+1}+{}_0^{2k+1}\langle\bar{\Psi};+++|\mathcal{O}(r_{12})|\Psi;+++\rangle_0^{2k+1}\big)\\ &\quad+\frac{1}{3}\big({}_0^{2k+1}\langle\bar{\Psi};+-+|\mathcal{O}(r_{12})|\Psi;-++\rangle_0^{2k+1}+{}_0^{2k+1}\langle\bar{\Psi};+--|\mathcal{O}(r_{12})|\Psi;-+-\rangle_0^{2k+1}\\ &\quad\pm{}_0^{2k+1}\langle\bar{\Psi};--+|\mathcal{O}(r_{12})|\Psi;-++\rangle_0^{2k+1}\pm{}_0^{2k+1}\langle\bar{\Psi};--+|\mathcal{O}(r_{12})|\Psi;+-+\rangle_0^{2k+1}\\ &\quad\pm{}_0^{2k+1}\langle\bar{\Psi};-+-|\mathcal{O}(r_{12})|\Psi;++-\rangle_0^{2k+1}\pm{}_0^{2k+1}\langle\bar{\Psi};++-|\mathcal{O}(r_{12})|\Psi;+--\rangle_0^{2k+1}\big).\end{aligned} \quad (147)$$

Finally, concerning states with $\mu=\pm1$, calculations will only be illustrated with $|\Psi;A_2';1;J^{-\pm}\rangle$ because it is less cumbersome to decompose than $|\Psi;A_2'';1;J^{-\pm}\rangle$,

$$\begin{aligned}&\langle\bar{\Psi};A_2';1;J^{\mp-}|\mathcal{O}(r_{12})|\Psi;A_2';1;J^{\mp-}\rangle\\ &\quad=\big({}_1^J\langle(1+e^{i\varphi_{13}}+e^{-i\varphi_{23}})\bar{\Psi}|;+++\mathcal{O}(r_{12})|(1+e^{i\varphi_{13}}+e^{-i\varphi_{23}})\Psi;+++\rangle_1^J\\ &\quad+{}_1^J\langle(1+e^{i\varphi_{13}}+e^{-i\varphi_{23}})\bar{\Psi}|;---\mathcal{O}(r_{12})|(1+e^{i\varphi_{13}}+e^{-i\varphi_{23}})\Psi;---\rangle_1^J\\ &\quad+{}_{-1}^J\langle(1+e^{-i\varphi_{13}}+e^{i\varphi_{23}})\bar{\Psi};+++|\mathcal{O}(r_{12})|(1+e^{-i\varphi_{13}}+e^{i\varphi_{23}})\Psi;+++\rangle_{-1}^J\\ &\quad+{}_{-1}^J\langle(1+e^{-i\varphi_{13}}+e^{i\varphi_{23}})\bar{\Psi};---|\mathcal{O}(r_{12})|(1+e^{-i\varphi_{13}}+e^{i\varphi_{23}})\Psi;---\rangle_{-1}^J\\ &\quad+2(-1)^J{}_1^J\langle(1+e^{i\varphi_{13}}+e^{-i\varphi_{23}})\bar{\Psi};+++|\mathcal{O}(r_{12})|(1+e^{-i\varphi_{13}}+e^{i\varphi_{23}})\Psi;+++\rangle_{-1}^J\\ &\quad+2(-1)^J{}_1^J\langle(1+e^{i\varphi_{13}}+e^{-i\varphi_{23}})\bar{\Psi}|;---\mathcal{O}(r_{12})|(1+e^{-i\varphi_{13}}+e^{i\varphi_{23}})\Psi;---\rangle_{-1}^J\big).\end{aligned} \quad (148)$$

In general, the symmetry properties depicted in Appendix E facilitate in evaluating these MEs. They show that some MEs on unsymmetrical states are strictly equal, while some others involve the same integrals but combine them differently [see Eq. (140)]. This significantly reduces the overall computational cost. This is especially true if the helicity-momentum wave function Ψ is even in u. Apart from diagonal MEs, symmetric states are also shown to mix with each other. For instance, mixing MEs between $|\Psi;A_2';0;(2k)^{\pm-}\rangle$ and $|\Psi;A_2'';0;(2k)^{\pm-}\rangle$ is given by

$$\begin{aligned}\langle\bar{\Psi};A_2';0;(2k+1)^{\pm-}|\mathcal{O}(r_{12})|\Psi;A_2'';0;(2k+1)^{\pm-}\rangle \\ =\frac{1}{\sqrt{12}}\big({}_0^{2k+1}\langle\bar{\Psi};+++|\mathcal{O}(r_{12})|\Psi;-++\rangle_0^{2k+1}+{}_0^{2k+1}\langle\bar{\Psi};+++|\mathcal{O}(r_{12})|\Psi;+-+\rangle_0^{2k+1} \\ \pm{}_0^{2k+1}\langle\bar{\Psi};+++|\mathcal{O}(r_{12})|\Psi;--+\rangle_0^{2k+1}+{}_0^{2k+1}\langle\bar{\Psi};---|\mathcal{O}(r_{12})|\Psi;+--\rangle_0^{2k+1} \\ \pm{}_0^{2k+1}\langle\bar{\Psi};---|\mathcal{O}(r_{12})|\Psi;++-\rangle_0^{2k+1}+{}_0^{2k+1}\langle\bar{\Psi};---|\mathcal{O}(r_{12})|\Psi;-+-\rangle_0^{2k+1}\big).\end{aligned} \tag{149}$$

However, it will be shown in the next section that this mixing is quite small for three-gluon glueballs and only affects masses very slightly.

4. Determination of the low-lying glueball spectrum

Trial states and formulas set up all along the previous subsections will now be used to compute a true mass spectrum for $1^{\pm-}$ three-gluon glueballs. It will require us to evaluate MEs of a Hamiltonian that should model three-gluon glueballs. This work considers the following structure for the latter:

$$H=T(w_1,w_2,w_3)+V(r_{12})+V(r_{13})+V(r_{23}) \tag{150}$$

with $r_{ij}=|\boldsymbol{r}_i-\boldsymbol{r}_j|$. Different kinematics T can be envisaged for gluons. Although these particles are formally massless, they acquire a constituent mass in some potential models. In the following, calculations will be performed considering ultrarelativistic kinematics,

$$T(w_1,w_2,w_3)=w_1+w_2+w_3. \tag{151}$$

Concerning potential, Cornell interactions will be assumed,

$$V(r)=\sigma r-\frac{3\alpha_s}{2r}. \tag{152}$$

Above, σ is the meson string tension, generally set around 0.185 GeV^2, and α_s is the strong coupling constant. In the following, the latter is fixed at 0.450 (as in Sec. III and Ref. [11]). The mesonic string tension is used as a confinement constant because each gluon is supposed to provide both a 3 and a $\bar{3}$ flux tube. The six flux tubes join two by two in a Δ shape, as illustrated in Fig. 9. Because each junction connects 3 and $\bar{3}$ flux tubes, the meson string tension has not to be rescaled. The factor $3/2$ is the color factor corresponding with three gluons in a color singlet. The use of this potential and its comparison with a Y junction is explained in Appendix F. To avoid reproducing many evaluations for different mesonic string tensions σ, dimensionless variables are introduced by rescaling the current ones with the square root of the string tension,

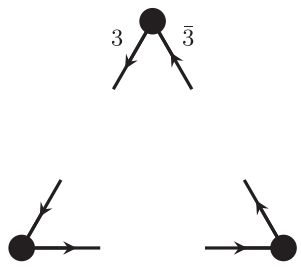

FIG. 9. Schematic representation of the Δ junction modeling three-gluon glueballs in the current work. Gluons bounds two by two by pooling 3 and $\bar{3}$ flux tubes.

$$\mathbb{w}_i=w_i/\sqrt{\sigma},\qquad \mathbb{r}_{ij}=\sqrt{\sigma}r_{ij}. \tag{153}$$

Dimensionless equivalents for p_3 and p_{12} are also defined

$$\mathbb{p}_3=p_3/\sqrt{\sigma},\qquad \mathbb{p}_{12}=p_{12}/\sqrt{\sigma}. \tag{154}$$

Because u is already dimensionless, it remains unchanged. Relation (113) still relates variables $\mathbb{w}_1$, $\mathbb{w}_2$, $\mathbb{w}_3$, and $u,\mathbb{p}_{12},\mathbb{p}_3$. Using these new coordinates, a dimensionless version $\mathbb{H}$ of the Hamiltonian (150) is introduced,

$$\mathbb{H}=H/\sqrt{\sigma},=\mathbb{T}(\mathbb{w}_1,\mathbb{w}_2,\mathbb{w}_3)+\mathbb{V}(\mathbb{r}_{12})+\mathbb{V}(\mathbb{r}_{13})+\mathbb{V}(\mathbb{r}_{23}) \tag{155}$$

where

$$\mathbb{T}(\mathbb{w}_1,\mathbb{w}_2,\mathbb{w}_3)=\mathbb{w}_1+\mathbb{w}_2+\mathbb{w}_3,\qquad \mathbb{V}(\mathbb{r})=\mathbb{r}-\frac{3\alpha_s}{2\mathbb{r}}. \tag{156}$$

This Hamiltonian will be evaluated on different symmetric trial states. To start with, a single trial state is considered. As a reminder, the reasonable trial wave function that is chosen is

$$\Psi_{a,b}(w_1,w_2,w_3)=A\sqrt{8w_1w_2w_3}e^{-a((w_1-b)^2+(w_2-b)^2+(w_3-b)^2)}. \tag{157}$$

For states (118) and (119), this trial wave function remains unmodified. For states (120) and (121), it has to be multiplied by different kinematic factors to ensure the right symmetry properties. In the following, calculations will be made explicit for a generic kinematic factor denoted $\Gamma(w_1,w_2,w_3)$. These trial wave functions are to be turned into the new dimensionless coordinate system. The change simply rescales the a parameter by a factor σ and modifies the value of the normalization constant A,

$$\mathbb{a} = \sigma a, \qquad \mathbb{b} = b/\sqrt{\sigma}, \qquad \mathbb{A} = \sigma^{\frac{3}{4}} A. \tag{158}$$

The rescaling factor for the normalization constant has been chosen to eliminate the dimensions of the wave function. The use of a dimensionless wave function also suggests rescaling Berman's and Wick's bases to make them dimensionless,

$$|JM\mu;\mathbb{w}_1\mathbb{w}_2\mathbb{w}_3;\lambda_1\lambda_2\lambda_3\rangle = \sigma^{\frac{3}{4}}|JM\mu;w_1w_2w_3;\lambda_1\lambda_2\lambda_3\rangle, \tag{159}$$

$$|\mathbb{p}_3;JM;j_{12}\lambda_{12}\lambda_3;\mathbb{p}_{12}\lambda_1\lambda_2\rangle = \sigma^{\frac{3}{4}}|p_3;JM;j_{12}\lambda_{12}\lambda_3;p_{12}\lambda_1\lambda_2\rangle. \tag{160}$$

All the formulas set up to evaluate MEs can now be switched to the new coordinates. Taking every change into account, all the rescaling factors cancel each other. As a result, each formula can be naively turned into dimensionless coordinates by replacing A, a, w_i, p_3, and/or p_{12} by their dimensionless counterpart.

First, let us investigate the normalization of the symmetric trial states. For states (118), (119), and (121), the normalization constant A is fixed by imposing the normalization of the unsymmetrical trial states, implying that $\Psi_{a,b}$ must satisfy (98). Switching to dimensionless coordinates, one has to evaluate the following integral:

$$|\mathbb{A}|^2 = \left(\int \mathrm{d}\mathbb{w}_1\mathrm{d}\mathbb{w}_2\mathrm{d}\mathbb{w}_3\mathbb{w}_1\mathbb{w}_2\mathbb{w}_3 e^{-2\mathbb{a}((\mathbb{w}_1-\mathbb{b})^2+(\mathbb{w}_2-\mathbb{b})^2+(\mathbb{w}_3-\mathbb{b})^2)}\right)^{-1}, \tag{161}$$

where both $\mathbb{w}_1$ and $\mathbb{w}_2$ are integrated between 0 and ∞ while $\mathbb{w}_3$ is integrated between $|\mathbb{w}_1 - \mathbb{w}_2|$ and $\mathbb{w}_1 + \mathbb{w}_2$. Generic multidimensional integration techniques provide fast and accurate evaluations of $\mathbb{A}$. As inferred from (144), the situation is slightly more complicated for state (120) due to the additional kinematic factor. For the A_2' state, the normalization involves the integral

$$|\mathbb{A}|^2 = \left(4\int \mathrm{d}\mathbb{w}_1\mathrm{d}\mathbb{w}_2\mathrm{d}\mathbb{w}_3\mathbb{w}_1\mathbb{w}_2\mathbb{w}_3 e^{-2\mathbb{a}((\mathbb{w}_1-\mathbb{b})^2+(\mathbb{w}_2-\mathbb{b})^2+(\mathbb{w}_3-\mathbb{b})^2)}|1+e^{-i\varphi_{13}}+e^{i\varphi_{23}}|^2\right)^{-1}. \tag{162}$$

It is possible to evaluate these two integrals numerically, with any desired accuracy.

The evaluation of kinetic energy MEs is analogous to the normalization. States (118), (119), and (121) require us to evaluate a single three-dimensional integral, as demonstrated in relations (143) and (145). For the current trial wave function, it equates to computing the following integral:

$$\langle\mathbb{T}\rangle = |\mathbb{A}|^2\int \mathrm{d}\mathbb{w}_1\mathrm{d}\mathbb{w}_2\mathrm{d}\mathbb{w}_3\mathbb{w}_1\mathbb{w}_2\mathbb{w}_3 e^{-2\mathbb{a}((\mathbb{w}_1-\mathbb{b})^2+(\mathbb{w}_2-\mathbb{b})^2+(\mathbb{w}_3-\mathbb{b})^2)}(\mathbb{w}_1+\mathbb{w}_2+\mathbb{w}_3). \tag{163}$$

On the other hand, kinetic energy MEs for state (120) are provided by relation (144), which complements the integrand with a kinematic factor,

$$\begin{aligned}&\langle\Psi_{a,b};A_2';\pm;1^{\pm-}|\mathbb{T}|\Psi_{a,b};A_2';\pm;1^{\pm-}\rangle\\ &= 4|\mathbb{A}|^2\int \mathrm{d}\mathbb{w}_1\mathrm{d}\mathbb{w}_2\mathrm{d}\mathbb{w}_3\mathbb{w}_1\mathbb{w}_2\mathbb{w}_3 e^{-2\mathbb{a}((\mathbb{w}_1-\mathbb{b})^2+(\mathbb{w}_2-\mathbb{b})^2+(\mathbb{w}_3-\mathbb{b})^2)}|1+e^{-i\varphi_{13}}+e^{i\varphi_{23}}|^2(\mathbb{w}_1+\mathbb{w}_2+\mathbb{w}_3).\end{aligned} \tag{164}$$

It remains to evaluate potential MEs. As already mentioned, thanks to the symmetry of the state, the evaluation for the interaction between particles 1 and 2 is sufficient to infer the full potential energy of the Δ junction,

$$\langle\mathbb{V}(\mathbb{r}_{12})+\mathbb{V}(\mathbb{r}_{13})+\mathbb{V}(\mathbb{r}_{23})\rangle = 3\langle\mathbb{V}(\mathbb{r}_{12})\rangle. \tag{165}$$

Relations (146)–(148) reduce evaluations on symmetric states to several evaluations on unsymmetrical states, eventually with additional kinematic factors. The latter evaluations can be performed using formula (140). Specifying for the current trial wave function and using variables u, p_{12}, and p_3 defined in Eq. (112), one gets

$$\begin{aligned}\langle\Psi_{a,b}\bar{\Gamma};\bar{\lambda}_1\bar{\lambda}_2\bar{\lambda}_3|\mathbb{V}(\mathbb{r}_{12})|\Psi_{a,b}\Gamma;\lambda_1\lambda_2\lambda_3\rangle^J_\mu &= \delta_{\bar{\lambda}_3\lambda_3}\sum_{j_{12}}\sum_{\lambda_{12}}(\mathcal{C}^{j_{12}\lambda_{12}}_{J\mu;\bar{\lambda}_1\bar{\lambda}_2\lambda_3})^*\mathcal{C}^{j_{12}\lambda_{12}}_{J\mu;\lambda_1\lambda_2\lambda_3}\\ &\times\int \mathbb{p}_3\mathrm{d}\mathbb{p}_3\int\frac{\mathrm{d}\bar{\mathbb{p}}_{12}}{2}\frac{\mathrm{d}\mathbb{p}_{12}}{2}\tilde{\Psi}^*_{\mathbb{a},\mathbb{b}}(\bar{\mathbb{p}}_{12},\mathbb{p}_3;j_{12},\lambda_{12},\bar{\lambda}_1-\bar{\lambda}_2;\bar{\Gamma})\\ &\times\tilde{\Psi}_{\mathbb{a},\mathbb{b}}(\mathbb{p}_{12},\mathbb{p}_3;j_{12},\lambda_{12},\lambda_1-\lambda_2;\Gamma)\langle\bar{\mathbb{p}}_{12};j_{12}\lambda_{12};\bar{\lambda}_1\bar{\lambda}_2|\mathbb{V}(\mathbb{r}_{12})|\mathbb{p}_{12};j_{12}\lambda_{12};\lambda_1\lambda_2\rangle\end{aligned} \tag{166}$$

where

$$\tilde{\Psi}_{\mathbb{a},\mathbb{b}}(\mathbb{p}_{12},\mathbb{p}_3;j_{12},\lambda_{12},\Delta\lambda;\Gamma)=\mathbb{A}\frac{\sqrt{\mathbb{p}_{12}\mathbb{p}_3}}{2\sqrt[4]{4\mathbb{p}_{12}^2+\mathbb{p}_3^2}}e^{-\frac{\mathbb{a}}{2}(6\mathbb{b}^2-4\mathbb{b}(\sqrt{4\mathbb{p}_{12}^2+\mathbb{p}_3^2}+\mathbb{p}_3)+4\mathbb{p}_{12}^2+3\mathbb{p}_3^2)}$$
$$\times\int_{-1}^{1}\mathrm{d}u\sqrt{8\mathbb{p}_{12}^2+2\mathbb{p}_3^2(1-u^2)}d^{j_{12}}_{\lambda_{12}\Delta\lambda}(\arccos u)e^{-\frac{a}{2}\mathbb{p}_3^2u^2}\Gamma(u,\mathbb{p}_{12},\mathbb{p}_3). \tag{167}$$

These integrals must be evaluated. Performing efficient numerical integrations requires us to slightly modify the variables and to refine the definition of $\tilde{\Psi}$. First, because the integral on $\mathbb{p}_3$ will be performed using a generalized Gauss-Laguerre quadrature, the variable $\mathbb{p}_3$ is modified as follows:

$$x=3\mathbb{a}\mathbb{p}_3^2,\qquad \mathbb{p}_3=\sqrt{\frac{x}{3\mathbb{a}}},\qquad \mathbb{p}_3\mathrm{d}\mathbb{p}_3=\frac{\mathrm{d}x}{6\mathbb{a}}. \tag{168}$$

After replacement and a bit of reorganization, the integrals to evaluate become

$$|\mathbb{A}|^2\sqrt{\frac{2}{(6\mathbb{a})^3}}\int\sqrt{x}e^{-x}\mathrm{d}x\int\frac{\mathrm{d}\bar{\mathbb{p}}_{12}}{2}\frac{\mathrm{d}\mathbb{p}_{12}}{2}\Theta_{\mathbb{a},\mathbb{b}}(\bar{\mathbb{p}}_{12},x;j_{12},\lambda_{12},\bar{\lambda}_1-\bar{\lambda}_2;\bar{\Gamma}^*)$$
$$\times\Theta_{\mathbb{a},\mathbb{b}}(\mathbb{p}_{12},x;j_{12},\lambda_{12},\lambda_1-\lambda_2;\Gamma)\langle\bar{\mathbb{p}}_{12};j_{12}\lambda_{12};\bar{\lambda}_1\bar{\lambda}_2|\mathbb{V}(\mathbb{r}_{12})|\mathbb{p}_{12};j_{12}\lambda_{12};\lambda_1\lambda_2\rangle \tag{169}$$

with a function Θ that replaces $\tilde{\Psi}$,

$$\Theta_{\mathbb{a},\mathbb{b}}(\mathbb{p}_{12},x;j_{12},\lambda_{12},\Delta\lambda;\Gamma)=\mathcal{F}_{\mathbb{a},\mathbb{b}}(\mathbb{p}_{12},x)\int\mathrm{d}u\mathcal{K}_{\mathbb{a}}(u,\mathbb{p}_{12},x;j_{12},\lambda_{12},\Delta\lambda;\Gamma) \tag{170}$$

where

$$\mathcal{F}_{\mathbb{a},\mathbb{b}}(\mathbb{p}_{12},x)=\frac{\sqrt{\mathbb{p}_{12}}}{2\sqrt[4]{4\mathbb{p}_{12}^2+\frac{x}{3\mathbb{a}}}}e^{-\frac{\mathbb{a}}{2}(6\mathbb{b}^2-4\mathbb{b}(\sqrt{4\mathbb{p}_{12}^2+x/(3\mathbb{a})}+\sqrt{x/(3\mathbb{a})})+4\mathbb{p}_{12}^2)} \tag{171}$$

and where

$$\mathcal{K}_{\mathbb{a}}(u,\mathbb{p}_{12},x;j_{12},\lambda_{12},\Delta\lambda;\Gamma)=\sqrt{8\mathbb{p}_{12}^2+\frac{2x}{3\mathbb{a}}(1-u^2)}d^{j_{12}}_{\lambda_{12}\Delta\lambda}(\arccos u)e^{-\frac{x}{6}u^2}\Gamma(u,\mathbb{p}_{12},\sqrt{x/(3\mathbb{a})}). \tag{172}$$

The symmetry properties of Θ under modifications of indices λ_{12} and $\Delta\lambda$ are the same as the ones of $\tilde{\Psi}$. They are compiled in Appendix E. Integrals (169) and (170) can be computed using a series of Gauss quadratures. The following procedure is applied.

(i) Choose a definite number of points to use in each of the integrals on x, $\mathbb{p}_{12}$, $\bar{\mathbb{p}}_{12}$, and u. Notice that the integrals on $\mathbb{p}_{12}$ and $\bar{\mathbb{p}}_{12}$ will be turned into integrals on $\mathbb{v}=\mathbb{p}_{12}+\bar{\mathbb{p}}_{12}$ and $\bar{\mathbb{v}}=\mathbb{p}_{12}-\bar{\mathbb{p}}_{12}$, as suggested in Sec. II B 3. Because the integral on $\bar{\mathbb{v}}$ is the most sensitive, it is recommended to assign the greatest number of points to it.

(ii) Accuracies being chosen, identify the different x values and $\mathbb{p}_{12}$ values at which an evaluation of the function Θ will be required and perform all the necessary evaluations. Gauss-Legendre quadrature works very well for the integral on u. The result is stored for further use.

(iii) For each x value, compute the two-body ME in the same way it has been done in Sec. III. Thanks to the previous step, two-body wave functions Θ have already been tabulated. Again, the result is stored for further use.

(iv) At this stage, only the integral on x remains. Perform this last integral by using the evaluations of two-body MEs stored during the last step. As already mentioned, a Gauss-Laguerre quadrature is the most adapted.

For each value of j_{12} and λ_{12}, that is for each term in the sum in Eq. (166), four integrals are evaluated numerically.

Since the sum extends to $j_{12} \to \infty$, the number of required integrals would be infinite. In practice, the sum on j_{12} is truncated at a given level denoted $j_{\max}$. Plugging the computed integrals into Eq. (166) allows for an approximate evaluation of two-body potential MEs on unsymmetrical trial states. Because of the multiple quadratures and because of this truncation, the exactness of the evaluation cannot be guaranteed. The MEs on unsymmetrical states can be combined following expressions (146)–(149) in order to compute potential MEs on symmetrical trial states. To get the full potential energy, the factor 3 from Eq. (165) is not to be forgotten. Once potential MEs on symmetrical states have been computed, the contribution from kinetic energy is added and Hamiltonian MEs are obtained. This calculation is repeated for many different couples $(\mathbb{a}, \mathbb{b})$ and only the minimum value is retained as an approximation for the true spectrum.

Since these states are the simplest to handle, convergence properties are illustrated using $|\Psi_{a,b}; A_2'; 0; 1^{\pm-}\rangle$ and $|\Psi_{a,b}; A_2''; 0; 1^{\pm-}\rangle$. All the following evaluations will be performed with $\alpha_s = 0.450$ [11]. To start with, calculations are performed for various numbers of points used in the different quadratures. All these computations employ for now the same cutoff at $j_{12} = 20$. The minimization process is executed for each configuration. The results are summarized in Table VII. As expected, the integrals over u and x converge with as few as 30 points. While slightly more sensitive, the integral on $\mathbb{v}$ does not require more than 50 points for sufficient accuracy in the current context. The key parameter for ensuring precision is the number of points used in the integral over $\mathbb{v}$. Using 100 points, the energy stabilizes to two significant digits. The search for a minimum in the variational parameters can also be illustrated. Figure 10 shows energy evaluations over a range of $(\mathbb{a}, \mathbb{b})$ pairs. Clear minima are observed for each state. Lastly, the convergence of the sum over j_{12} can be examined by repeating evaluations with various cutoff values. The result is displayed in Fig. 11. Although the convergence behavior differs slightly between states, a reasonable convergence is achieved in all cases. Notice that the j_{12} convergence can also be assessed by calculating normalization by means of Eq. (166), substituting $\mathbb{V}(r_{12})$ with the identity operator.

Before we move on to the determination of a complete spectrum, the mixing between different symmetric states is to be investigated. This issue will be illustrated using $|\Psi_{a,b}; A_2'; 0; 1^{+-}\rangle$ and $|\Psi_{a,b}; A_2''; 0; 1^{+-}\rangle$. Without allowing for mixing, approximate energies are simply obtained by evaluating the Hamiltonian on each state separately,

$$E_{A_2';0} = 10.020, \qquad E_{A_2'';0} = 10.269. \tag{173}$$

Introducing mixing between these states requires the evaluation of off-diagonal Hamiltonian MEs and solving the corresponding eigenvalue problem. The off-diagonal kinetic MEs cancel, while the off-diagonal potential MEs are calculated using formula (149). The splitting is found to be maximal when both states share the same variational parameters. The resulting optimal eigenvalues of the Hamiltonian matrix are

$$E_1 = 9.9902, \qquad E_2 = 10.3319. \tag{174}$$

As shown, the mixing slightly affects the energies, but this effect does not exceed 1% of the original value. Mixing with states of higher mass is expected to have an even

TABLE VII. Evaluations of the glueball masses in units of $\sqrt{\sigma}$ for different numbers of points for the quadratures. For $|\Psi; A_2'; 0; 1^{\pm-}\rangle$, energies are given for $(\mathbb{a}, \mathbb{b}) = (0.35, 1.8)$. For $|\Psi; A_2'; 0; 1^{+-}\rangle$, energies are given for $(\mathbb{a}, \mathbb{b}) = (0.45, 1.95)$. For $|\Psi; A_2'; 0; 1^{--}\rangle$, energies are given for $(\mathbb{a}, \mathbb{b}) = (0.35, 1.9)$. A cutoff at $j_{12} = 20$ has been used.

For $|\Psi; A_2'; 0; 1^{\pm-}\rangle$:

$(N_u, N_{\mathbb{v}}, N_{\bar{\mathbb{v}}}, N_x)$	Energy
(30, 30, 30, 30)	9.9499
(50, 30, 30, 30)	9.9499
(100, 30, 30, 30)	9.9499
(30, 50, 30, 30)	9.9536
(30, 100, 30, 30)	9.9536
(30, 30, 50, 30)	9.9895
(30, 30, 100, 30)	10.0202
(30, 30, 30, 50)	9.9499
(30, 30, 30, 100)	9.9499

For $|\Psi; A_2''; 0; 1^{+-}\rangle$:

$(N_u, N_{\mathbb{v}}, N_{\bar{\mathbb{v}}}, N_x)$	Energy
(30, 30, 30, 30)	10.1793
(50, 30, 30, 30)	10.1793
(100, 30, 30, 30)	10.1793
(30, 50, 30, 30)	10.1817
(30, 100, 30, 30)	10.1817
(30, 30, 50, 30)	10.2297
(30, 30, 100, 30)	10.2689
(30, 30, 30, 50)	10.1793
(30, 30, 30, 100)	10.1793

For $|\Psi; A_2''; 0; 1^{--}\rangle$:

$(N_u, N_{\mathbb{v}}, N_{\bar{\mathbb{v}}}, N_x)$	Energy
(30, 30,30,30)	10.0566
(50, 30, 30, 30)	10.0566
(100, 30, 30, 30)	10.0566
(30, 50, 30, 30)	10.0616
(30, 100, 30, 30)	10.0616
(30, 30, 50, 30)	10.1097
(30, 30, 100, 30)	10.1512
(30, 30, 30, 50)	10.0566
(30, 30, 30, 100)	10.0566

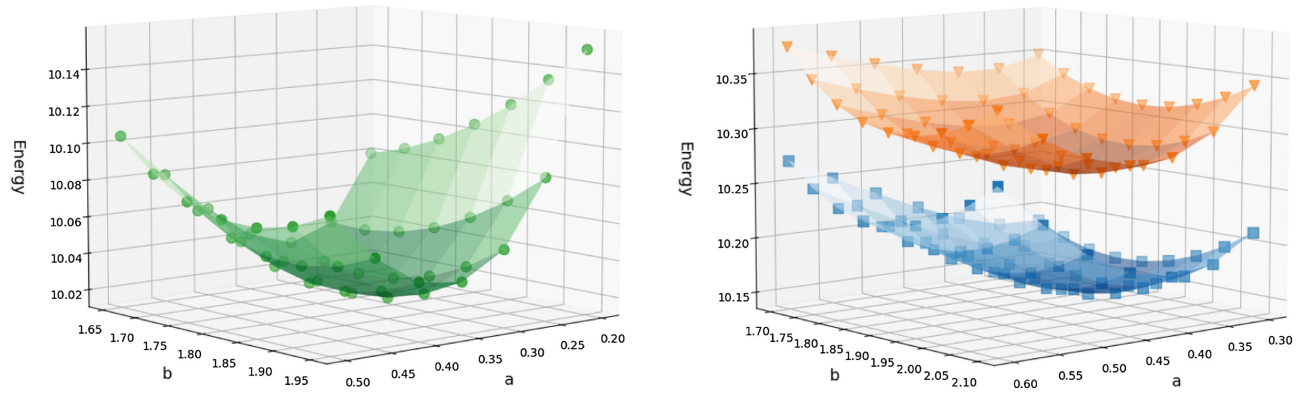

FIG. 10. Plot of Hamiltonian MEs for a single trial state depending on the nonlinear variational parameters $\mathbb{a}$ and $\mathbb{b}$. Left: a symmetric state $|\Psi_{a,b}; A_2'; 0; 1^{\pm-}\rangle$ is considered. Right: symmetric states $|\Psi_{a,b}; A_2''; 0; 1^{\pm-}\rangle$ are considered (even with orange triangles and odd with blue squares). Quadrature with 30 points has always been used except for $\bar{\mathbb{v}}$ where 100 points have been used. A cutoff $j_{\max} = 20$ has been chosen.

smaller impact due to the increasing energy gap. Consequently, the following calculations will be performed using pure symmetric states.

A concrete three-gluon glueball spectrum can now be computed. Again, $\alpha_s = 0.450$ is used. Calculations are performed with a cutoff at $j_{12} = 20$ for the summation and with 30 points for each quadrature, except for $\bar{\mathbb{v}}$ where 100 points are used. Full optimizations of the variational parameters $\mathbb{a}$ and $\mathbb{b}$ are performed. The states $|\Psi_{a,b}; A_2'; 0; J^{\pm-}\rangle$, $|\Psi_{a,b}; A_2''; 0; J^{\pm-}\rangle$, and $|\Psi_{a,b}; A_2'; 1; J^{\pm-}\rangle$ are investigated up to $J = 3$. However, states $|\Psi_{a,b}; A_2''; 1; J^{\pm-}\rangle$ are not considered, as they involve significantly more ME computations on unsymmetrical states, leading to a substantial increase in computational cost. The resulting three-gluon glueball masses expressed in units of $\sqrt{\sigma}$ are presented in Table VIII. For comparison, Fig. 12 displays these masses alongside results from LQCD. In Fig. 12, masses are normalized to the lowest state, 1^{+-}. Several observations support a relatively good agreement between the current calculation and LQCD results [5,6].

(i) The lowest 1^{+-} and 3^{+-} three-gluon glueballs obtained using the helicity formalism appear at the correct energy. However, the helicity formalism predicts a pair of states, whereas LQCD predicts only a single state [5,6].

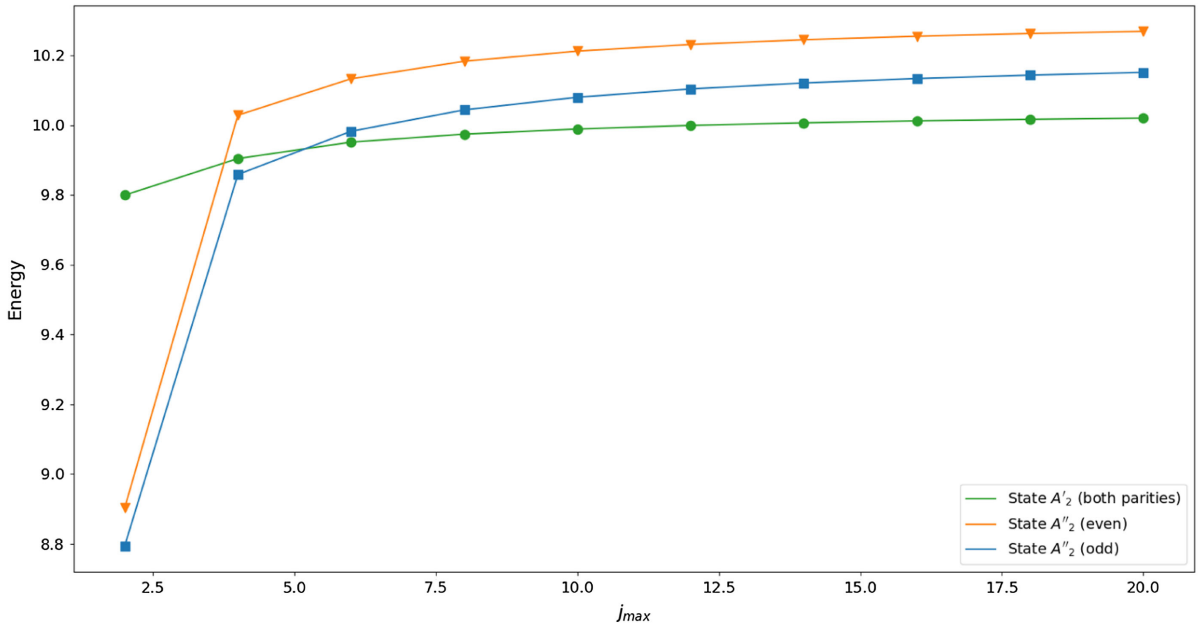

FIG. 11. Evolution of the lowest three-gluon glueball masses depending on the cutoff for the sum in j_{12}. Results for $|\Psi_{a,b}; A_2'; 0; 1^{\pm-}\rangle$ use $(\mathbb{a}, \mathbb{b}) = (0.35, 1.8)$ and are displayed with green circles. Results for $|\Psi_{a,b}; A_2''; 0; 1^{+-}\rangle$ use $(\mathbb{a}, \mathbb{b}) = (0.45, 1.95)$ and are displayed with orange triangles. Results for $|\Psi_{a,b}; A_2''; 0; 1^{--}\rangle$ use $(\mathbb{a}, \mathbb{b}) = (0.35, 1.9)$ and are displayed with blue squares.

TABLE VIII. Display of the dimensionless three-gluon glueball spectrum obtained by using the three-body helicity formalism. Energies are given in units of $\sqrt{\sigma}$. Only a single trial state is considered and the optimization on variational parameters $\mathbb{a}$ and $\mathbb{b}$ is performed. Calculations are performed until $J = 3$ and $|\mu| = 1$. Only one of the two states with $|\mu| = 1$ is considered (namely, A_0'). All integrals are computed with 30 points, except for those on $\bar{v}$ which use 100 points. The sum in j_{12} is truncated at $j_{12} = 20$.

State	Opt. $\mathbb{b}$	Opt. $\mathbb{a}$	E
$\|\Psi; A_2'; 0; 1^{\pm-}\rangle$	1.80	0.35	10.020
$\|\Psi; A_2''; 0; 1^{+-}\rangle$	1.95	0.45	10.269
$\|\Psi; A_2''; 0; 1^{--}\rangle$	1.90	0.35	10.151
$\|\Psi; A_2'; 0; 3^{\pm-}\rangle$	2.25	0.55	11.990
$\|\Psi; A_2''; 0; 3^{+-}\rangle$	2.30	0.55	12.090
$\|\Psi; A_2''; 0; 3^{--}\rangle$	2.25	0.50	11.881
$\|\Psi; A_2'; 1; 1^{\mp-}\rangle$	2.40	0.6	12.305
$\|\Psi; A_2'; 1; 2^{\mp-}\rangle$	2.40	0.6	12.742
$\|\Psi; A_2'; 1; 3^{\mp-}\rangle$	2.65	0.95	14.113

(ii) The lowest 2^{+-} glueball is found with the same hierarchy in both approaches. However, its energy is 10% lower using the helicity formalism. Unlike the lowest 1^{+-} and 3^{+-}, the 2^{+-} does not exhibit a nearby secondary state, but this is an artifact resulting from the omission of $|\Psi_{a,b}; A_2''; 1; J^{\pm-}\rangle$ states in the analysis. The 10% discrepancy may be explained by this omission: Including $|\Psi_{a,b}; A_2''; 1; 2^{+-}\rangle$ could slightly shift the 2^{+-} average energy. It may also stem from the simplicity of the Hamiltonian used, which does not account for spin interactions.

(iii) For negative parity, the first excited 1^{--} state predicted by the helicity formalism appears similar to the lowest 1^{--} observed in LQCD. As for 2^{+-}, the relative energy is around 5% too low. This discrepancy can likely be explained with the same arguments as for the 2^{+-} state.

(iv) Finally, a 3^{--} state analogous to the one observed in LQCD is also predicted. In this case, energies from the helicity formalism and LQCD are in good agreement.

On the other hand, the spectrum depicted by the helicity formalism does not fully align with the LQCD results. In particular, the helicity formalism predicts states that are not observed in LQCD. Overall, the helicity spectrum appears to exhibit near-parity degeneracy, whereas the LQCD spectrum clearly separates into two distinct columns.

(i) Low-lying 1^{--} and 3^{--} three-gluon glueballs are predicted by the helicity formalism. These states appear, roughly speaking, at the same energy as their positive parity counterparts. According to [5,6], in LQCD, the lowest 1^{--} and 3^{--} lie well above the lowest 1^{+-} and 3^{+-}.

(ii) On the positive parity side, the helicity formalism predicts 1^{+-} and 3^{+-} states in the vicinity of the lowest 2^{+-} glueball. Again, such states are absent in Refs. [5,6].

Several explanations can be proposed for this discrepancy. On the one hand, constituent approaches are known to sometimes overestimate the number of resonances. However, this effect typically impacts excited states rather than low-lying ones. On the other hand, it is possible that LQCD methods have missed a few states due to the challenges in interpreting the signal and in performing the continuum limit. For example, it seems that a more recent study of LQCD results observes an excited 1^{+-} glueball state whose energy is consistent with the one obtained using the helicity formalism [45].

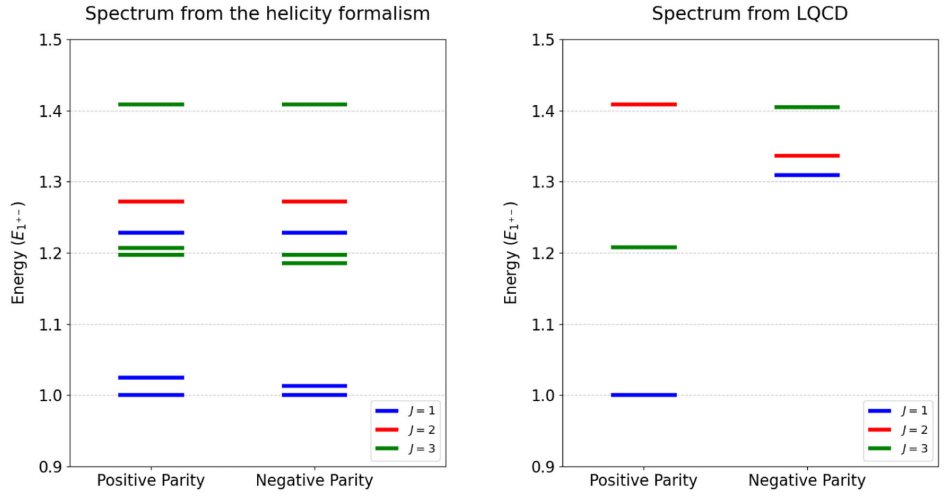

FIG. 12. Comparison of glueball spectra obtained using the helicity formalism (left, this work) and LQCD (right, Refs. [5,6]). In both cases, spectra are provided in units of the lowest mass. Concerning calculations with the helicity formalism, a strong coupling constant $\alpha_s = 0.450$ has been used.

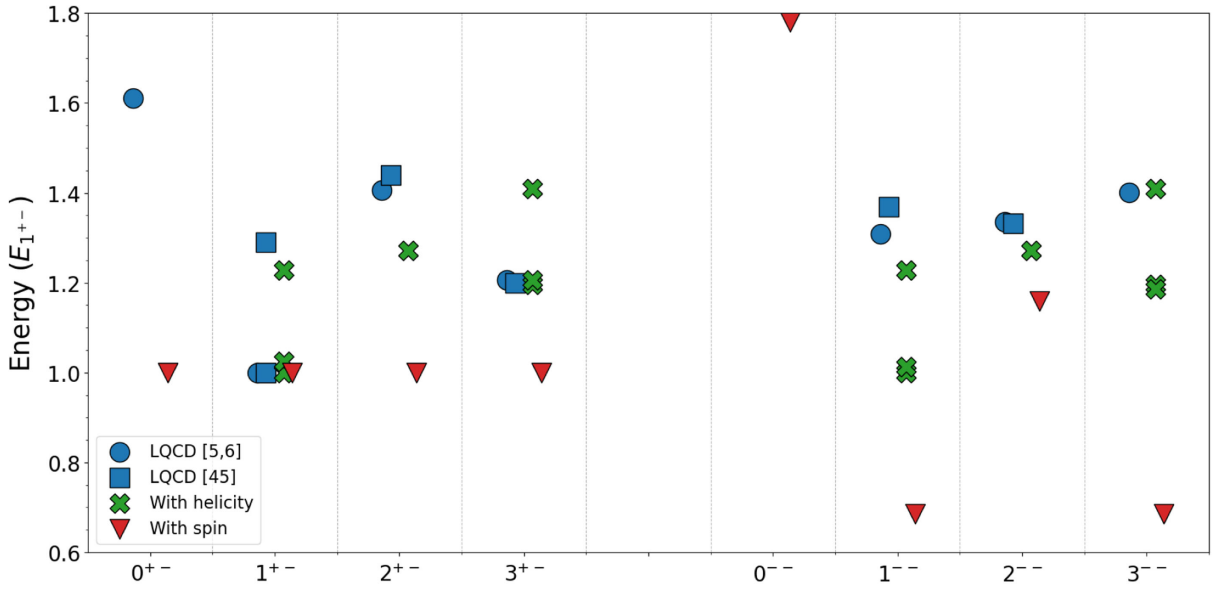

FIG. 13. Comparison of low-lying negative charge conjugation glueball spectra computed using different approaches. Blue dots and squares represent the results from the LQCD calculations from Refs. [5,6,45], respectively. Red triangles correspond to results obtained by considering three spin-1 particles governed by the Hamiltonian (155). Finally, green crosses are obtained by considering helicity degrees of freedom for the constituent gluons. Masses are normalized to the 1^{+-} state.

For two-gluon glueballs, which lie in the $C = +$ part of the spectrum, it is already known that helicity degrees of freedom are necessary to reproduce the lattice spectrum [11]. It would be interesting to compare the $C = -$ glueball spectrum obtained with helicity degrees of freedom in the present model to the $C = -$ spectrum obtained when longitudinal spin components for the gluon are included. Fortunately, such results have already been published [32,46]. However, the Hamiltonian considered in these studies includes spin interactions. To ensure a fair comparison, eigenenergies from the dimensionless Hamiltonian (155) are computed considering three spin-1 particles and using oscillator bases expansions [47,48]. Figure 13 illustrates the comparison. Energies are again given in units of the lowest 1^{+-} state. LQCD results from Ref. [45] are also included. It is immediately apparent that the spectrum computed with spin degrees of freedom exhibits several flaws.

(i) Positive parity states are all degenerate, whereas LQCD predicts a definite hierarchy for the lowest J^{+-} glueball states. In particular, spin degrees of freedom predict a low-lying 0^{+-} glueball, which LQCD calculations place at a higher energy.
(ii) On the negative parity side, the 1^{--} and 3^{--} spin eigenstates share the same energy, while the 2^{--} state lies significantly higher. In contrast, LQCD calculations predict nearly degenerate states with a soft ordering in ascending total angular momentum.

On the other hand, using helicity degrees of freedom better reproduces the overall spectrum, apart from the aforementioned inaccuracies and extra states. As with two-gluon glueballs [11], it appears that constituent gluons should be treated as particles endowed with massless helicity quantum numbers.

The previous analysis focused on the relative spectrum. To obtain a genuine energy spectrum requires us to fix the mesonic string tension σ. The best agreement with LQCD results is achieved for a value of $\sigma = 0.086$ GeV^2, which seems a factor 2 smaller compared to the values found in the literature (see for instance [11,49–51]). This issue can be addressed by reasonably modifying the Hamiltonian (150). In baryon studies, it is common to complement the potential with a constant term, particularly when dealing with light quarks [51]. Replacing the potential (152) with

$$V(r) = \sigma r - \frac{3\alpha_s}{2r} + C \tag{175}$$

were $\sigma = 0.150$ GeV^2, $\alpha_s = 0.450$, and $C = -0.375$ GeV results in the spectrum displayed in Fig. 14. The agreement between absolute spectra is as good as that for relative spectra, and the parameters used are more consistent with values typically found in the literature. It is also important to notice that the methodology employed in this work inherently provides approximate results. This approximate character may also explain the discrepancies observed in both spectra.

VI. CONCLUSION

In the framework of constituent approaches, the current work exploited the two- and three-body helicity formalism to acquire two- and three-gluon glueball spectra. It required

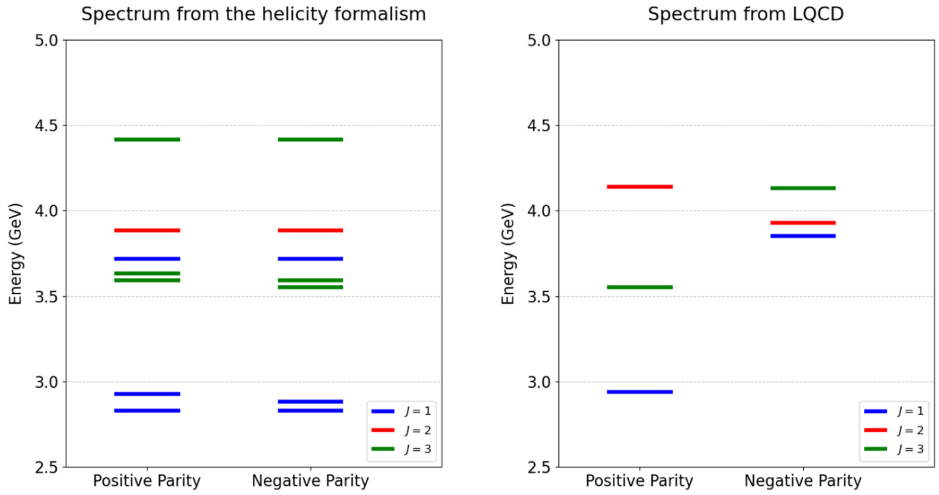

FIG. 14. Comparison of glueball spectra obtained using the helicity formalism with the modified potential (175) (left, this work) and quenched LQCD (right, Refs. [5,6]). In both cases, spectra are provided in GeV.

us to sum up different properties from the existing literature as well as to complement them with innovative results. A definite methodology able to infer a spectrum for helicity states and based on the variational theorem has been set up for both two- and three-body systems.

Concerning two-gluon glueballs, the spectrum obtained using the helicity formalism is compatible with LQCD calculations. This agreement gives credit for the methodology implemented and motivates the generalization to three-gluon glueballs. Although similar calculations were already present in the literature [11–13], the current work proposed a new perspective on this spectrum.

The situation concerning three-gluon glueballs is less conclusive. In summary, in units of the meson string tension, the helicity formalism proves it is able to reproduce the spectrum from LQCD with a satisfying accuracy but predicts supplementary states whose origin remains elusive. The comparison with calculations involving three spin-1 particles favored the use of helicity degrees of freedom. When comparing spectra in physical units, a mesonic string tension too low by a factor of 2 compared to its standard value is to be used. This flaw can be overcome by adding a constant term in the potential in agreement with the potential used in baryons [51]. Although it allows us to use parameter values in their physical range, it slightly deteriorates the agreement with LQCD. In addition, this parameter was not necessary to describe two-gluon glueballs.

Additional research may help unveil the origin of these discrepancies. Improvements on the accuracy of the resolution method in the case of three-gluon glueballs may give credit to the spectrum obtained using the helicity formalism. Including more trial states in the resolution to test the convergence, truly implementing the possibility of mixing between the different symmetrical states, and increasing the number of points in the quadrature or increasing the cutoff in j_{12} are all trails to reach this goal. Hamiltonian (150) may also be refined and complemented, for instance, with spin-based interactions. A more detailed study of the role of three-body forces could also be considered. This may help to decide whether the extra states predicted by the current methodology are artifacts of the resolution method or not.

Setting aside the question of the extra states, the solutions obtained using the helicity formalism may also yield additional insights into glueball properties. For instance, effort could be directed toward evaluating observables beyond the energy, such as decay rates.

ACKNOWLEDGMENTS

C. C. would like to thank the Fonds de la Recherche Scientifique—FNRS for the financial support. V. M. acknowledges support from the Spanish National Grants No. PID2023-147112NB-C21 and No. CNS2022-136085. The authors thank C. Semay and F. Buisseret for advice and a careful reading of the manuscript.

DATA AVAILABILITY

The data supporting this study's findings are available within the article.

APPENDIX A: HELICITY STATES FOR MASSLESS PARTICLES

In Sec. II, massive particle states were discussed. For massless ones, the Pauli-Lubanski Casimir operator is identically zero while helicity proves to be Lorentz invariant. As a result, a general massless state $|\phi;0;\lambda\rangle$ is by definition an eigenstate of the squared-momentum operator with a null eigenvalue and of the helicity operator,

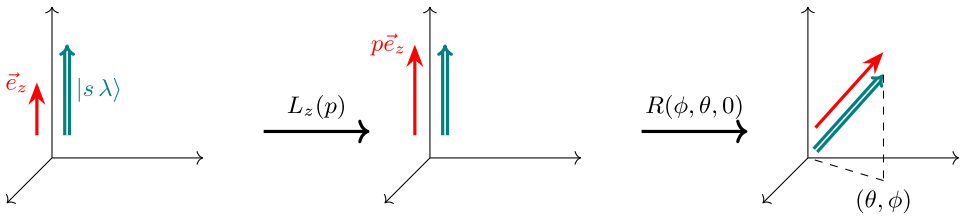

FIG. 15. Graphic illustration for the definition (A3) of massless one-body p-helicity states.

$$P^2|\psi;0;\lambda\rangle = 0|\psi;0;\lambda\rangle, \qquad \Lambda|\psi;0;\lambda\rangle = \lambda|\psi;0;\lambda\rangle. \quad \text{(A1)}$$

If helicity is truly Lorentz invariant, it is nevertheless reversed by a parity transformation, meaning that massless states always come in pairs, one with helicity λ and the other one with helicity $-\lambda$. This feature justifies the aforementioned simplification of reality: Although spin is not formally defined in the massless case, these two states with the same nature but opposed helicities are often considered as the two facets of a spin λ particle whose intermediary projections are forbidden. This is the case when someone considers left-handed and right-handed photons as unique spin-1 particles whose 0 projection is forbidden.

To describe the actual state of a massless particle, complete orthonormal sets are again necessary. Since massless particles have no rest frame, the corresponding states are defined as eigenstates of the helicity operator, and only the p-helicity states are suitable to describe them. These are eigenstates of the exact same operators as massive ones but with zero as the eigenvalue for both Casimir operators,

$$\begin{aligned} P^2|0;p\theta\phi;s\lambda\rangle &= 0|0;p\theta\phi;s\lambda\rangle, \\ W^2|0;p\theta\phi;s\lambda\rangle &= 0|0;p\theta\phi;s\lambda\rangle. \end{aligned} \quad \text{(A2)}$$

Above, rather than being a true quantum number, s specifies the possible values of λ. Massless p-helicity states significantly differ from massive ones in the sense that, because massless particles cannot be taken at rest, relation (14) cannot remain valid for these. A similar relation can nevertheless be obtained by turning the rest state into another reference state having a more suitable four-momentum for massless particles. Choosing this reference four-momentum as $k = (1,0,0,1)$ and denoting the associated reference state $|0;s\lambda\rangle$, the adapted relation reads

$$\begin{aligned} |0;p\theta\phi;s\lambda\rangle &= U(L_h(0,p,\theta,\phi))|0;s\lambda\rangle \\ &= U(R(\phi,\theta,0)L_z(0,p))|0;s\lambda\rangle. \end{aligned} \quad \text{(A3)}$$

Above, $L_z(0,p)$ refers to a boost that provides a momentum of modulus p along the z axis to a massless particle having initially the dimensionless reference four-momentum k. Notice that, because $|0;s\lambda\rangle$ has a unit spatial momentum along the z axis, this state proves to be the eigenstate of both W_3 and Λ, these two operators being equal in the current circumstances.

Because of this adaptation, the graphic interpretation of massive p-helicity states must slightly be adapted, the initial state having a nonzero spatial momentum. The new diagram is shown in Fig. 15. Apart from this modification in the initial state, both diagrams are to be understood similarly.

Let us now focus on the adaptation of properties (19) and (23) to massless particles. First, for the definition of intrinsic parity (19) making use of rest states, it must be adapted to a massless reference state. Applying parity on this state reverses its nonzero spatial momentum and, as already mentioned, opposes the helicity quantum number. It results in the following relation for the action of parity on a reference state:

$$\Pi|0;s\lambda\rangle = \eta U(R(0,\pi,0))|0;s-\lambda\rangle \quad \text{(A4)}$$

where η is defined as the intrinsic parity of the massless particle. This modification considered, one can roughly follow the same calculation steps as in the massive case to demonstrate that

$$\Pi|0;p\theta\phi;s\lambda\rangle = \eta(-1)^{\lambda}|0;p(\pi-\theta)(\pi+\phi);s-\lambda\rangle. \quad \text{(A5)}$$

Formula (A5) replaces (18) in the presence of massless particles. The discussion of relation (23) must also partially be revised. In the massive case, the Wigner rotations R_W defined in relation (24) are shown to belong to $SO(3)$, namely the massive little group. Setting $m = 0$, the combination (24) turns out to no longer belong to the massive little group but to the massless one, ISO(2). Therefore, the transformation is no longer parametrized by Euler angles but by three ISO(2) parameters, such as the α, β, and θ parameters suggested in Ref. [18], and the action of R_W on physical states is no longer provided by $SU(2)$ Wigner D matrices but instead reduces to [41]

$$D^s_{\lambda'\lambda}(\alpha_W,\beta_W,\theta_W) = e^{i\theta_W\lambda}\delta_{\lambda'\lambda}. \quad \text{(A6)}$$

The $\delta_{\lambda'\lambda}$ factor ensures that, as expected for massless states, the helicity quantum number remains invariant while boosting the state. This replacement done, relation (23) can be freely used even while dealing with massless

particles. Although R_W is no longer a true spatial rotation, this transformation is still called Wigner rotation through misuse of language.

As already mentioned in the main text, helicity states for two massless bodies behave quite similarly to those of massive ones. The demonstrations are very similar to their massive counterparts, with the main differences generally arising from the phase factor in definition (27), which must be adapted by replacing s_2 with $|\lambda_2|$. The one-body parity transformation rule (18) must also be replaced by the massless version (A5). The rest of the demonstrations remain analogous to the massive case, taking advantage of the fact that the reference helicity states for the massless particles, $|0; s\lambda\rangle$, are also J_3 eigenstates.

APPENDIX B: EXAMPLES OF TWO-BODY CALCULATIONS IN MOMENTUM SPACE

To simplify, evaluations will be performed on pure two-body canonical states. Three different two-body systems will be considered,

$$\mathcal{H}_{\text{Coul}}(p,r) = \frac{p^2}{2\mu} - \frac{g}{r}, \tag{B1}$$

$$\mathcal{H}_{\text{lin}}(p,r) = \frac{p^2}{2\mu} + \lambda r, \tag{B2}$$

$$\mathcal{H}_{\text{Ful}}(p,r) = \sqrt{m_1^2+p^2} + \sqrt{m_2^2+p^2} + Ar - \frac{\kappa}{r}, \tag{B3}$$

with $\mu = m_1 m_2/(m_1+m_2)$ denoting the reduced mass. For convenience, in all cases, both particles are chosen with equal nonzero masses, $m_1 = m_2 = m$ and $\mu = m/2$. Natural units are used. Hamiltonian MEs will be computed for a Gaussian-like Ξ helicity wave function with one parameter,

$$\Xi_a(p) = 2\left(\frac{(2a)^3}{\pi}\right)^{1/4} p e^{-ap^2}. \tag{B4}$$

Above, the constant has been fixed to ensure that the condition (47) holds. The variational theorem ensures that, for any angular momentum ℓ and for all value of the parameter a, this ME consists of an upper bound for the ground state energy with angular momentum ℓ of the corresponding Hamiltonian. This approximated eigenenergy is the one referred to as SGA in Sec. III.

Concerning kinetic energies, the integral from relation (50) can be solved analytically for both non- and semi-relativistic kinematics,

$$|A|^2 \int \mathrm{d}p\, p^2 e^{-2ap^2} \frac{p^2}{2\mu} = \frac{3}{8}\frac{1}{a\mu}, \tag{B5}$$

TABLE IX. Spectra comparison for the Coulomb Hamiltonian (B1). Upper bounds obtained with the SGA, (E_{SGA}), are compared to the analytical spectrum from [55], E_{exact}, for various angular momenta ℓ. Optimized values of the variational parameter a_{opt} are also displayed in the fourth column. Arbitrary units are used: $m = 2$ and $g = 1$.

ℓ	E_{exact}	E_{SGA}	a_{opt}
0	−0.50	−0.42	0.89
1	−0.25	−0.12	3.16
2	−0.125	−0.05	6.99

$$|A|^2 \int \mathrm{d}p\, p^2 e^{-2ap^2} 2\sqrt{m^2+p^2} = \sqrt{\frac{8a}{\pi}} m^2 e^{am^2} K_1(am^2). \tag{B6}$$

Above K_n refers to a modified Bessel function of the second kind. Potential MEs are managed using relations (63) and (67) from previous sections. As already mentioned, numerical integration methods based on Gauss-Legendre quadrature are used.[5] Results for the potential and the kinetic energy are then gathered to compute Hamiltonian matrix elements and the obtained upper bounds are minimized on the variational parameter a. With a single trial state, this method only provides approximations for the lowest state of a given angular momentum ℓ.

Let us now focus on the results of the three tests. Table IX displays the upper bounds obtained for the Hamiltonian $\mathcal{H}_{\text{Coul}}$. For this test, the mass m of the particles has been fixed to 2 while the constant of the Coulomb potential g has been fixed to 1, both in arbitrary units. One will notice that the obtained upper bounds are far from accurate, especially for $\ell = 3$. This is a regular feature when using a Gaussian trial wave function to solve a divergent potential. One can check that turning the trial wave function into the exact one for the $\ell = 0$ ground state [52],

$$\Xi^{\text{Coul}}(p) \propto \frac{p}{(1+p^2)^2}, \tag{B7}$$

allows us to exactly reproduce its eigenenergy, as expected. Concerning the pure linear Hamiltonian $\mathcal{H}_{\text{lin}}$, the results in arbitrary units are displayed in Table X for unit masses and the linear potential constant. An analytical spectrum for $\ell = 0$ is provided in [53]. For $\ell > 0$, the SGA is compared to the spectrum provided by another approximation method, the Lagrange-mesh method [36]. One can see that a single Gaussian provides a quite accurate upper

[5]For both potentials, to compute MEs using (63) and (67), Gauss-Legendre quadratures with 1000 points are used for integrals on $\bar{v}$ while integrals on v are handled with a change of variables $v = v_t/(1-v_t)$ and only 300 points. Integrals on v turn out to be clearly less sensitive than the ones on $\bar{v}$.

TABLE X. Spectra comparison for the linear Hamiltonian (B2). Upper bounds obtained with the SGA, (E_{SGA}), are compared to the analytical spectrum from [53] for $\ell = 0$ (E_{exact}) and to the spectrum from the Lagrange-mesh method [36] for various angular momenta, (E_{LM}). Optimized values of the variational parameter, a_{opt} are also displayed in the fourth column. Arbitrary units are used: $m = 1$ and $\lambda = 1$.

ℓ	E_{exact}	E_{LM}	E_{SGA}	a_{opt}
0	2.338	2.338	2.345	0.960
1	⋯	3.361	3.472	0.648
2	⋯	4.248	4.556	0.494

bound for the $\ell = 0$ ground state. For $\ell > 0$, as expected, the very accurate results provided by the Lagrange-mesh method lie below those obtained with the SGA. Finally, the Hamiltonian $\mathcal{H}_{\mathrm{Ful}}$ is investigated. This Hamiltonian has been used in [54] to model bottomonium and charmonium systems. Table XI compares the results obtained with the SGA to the spectrum provided in the reference. In both cases and for each ℓ value, the single Gaussian upper bound achieves an accuracy below 2%.

TABLE XI. Spectra comparison for Fulcher's Hamiltonian $\mathcal{H}_{\mathrm{Ful}}$ [54] (bottomonium at top, charmonium at bottom). Upper bounds obtained with the SGA, (E_{SGA}), are compared to the spectrum from [53] for various angular momenta ℓ. Optimized values of the variational parameter, a_{opt} are also displayed in the fourth column. Energy results and a values are respectively provided in GeV and GeV^{-1}. Relatives errors ε are indicated in square brackets.

ℓ	E_{exact}	E_{SGA}	$[\varepsilon]$	a_{opt}
0	9.448	9.499	[0.5%]	0.391
1	9.900	9.920	[0.2%]	0.450
2	10.150	10.204	[0.5%]	0.397

ℓ	E_{exact}	E_{SGA}	$[\varepsilon]$	a_{opt}
0	3.067	3.094	[0.9%]	1.383
1	3.504	3.531	[0.8%]	1.141
2	3.811	3.886	[2%]	0.903

APPENDIX C: PROPERTIES OF BERMAN'S STATES

This appendix is devoted to the demonstration of some properties of Berman's states that are missing in the literature. Let us start with property (83), which is about the modification of the reference plane in the definition of Berman's J-helicity states. For the sake of conciseness, in the following, $R(\alpha, \beta, \gamma)$ will be denoted R and $\mathrm{d}\alpha \mathrm{d}\cos\beta \mathrm{d}\gamma$ will be denoted $\mathrm{d}R$. First, an arbitrary rotation $\bar{R}$ is artificially introduced in (81). The $\bar{R}$ rotation is applied on the reference state $|w_1 w_2 w_3; \lambda_1\lambda_2\lambda_3\rangle$ while its inverse is composed with the rotation R,

$$|JM\mu; w_1 w_2 w_3; \lambda_1\lambda_2\lambda_3\rangle = \sqrt{\frac{2J+1}{8\pi^2}} \int \mathrm{d}R D^{J*}_{M\mu}(R) U(R\bar{R}^{-1})(U(\bar{R})|w_1 w_2 w_3; \lambda_1\lambda_2\lambda_3\rangle). \tag{C1}$$

Turning the integration on R Euler angles into an integration on $R\bar{R}^{-1}$ Euler angles, one gets

$$|JM\mu; w_1 w_2 w_3; \lambda_1\lambda_2\lambda_3\rangle = \sum_{\mu'=-J}^{J} D^{J*}_{\mu'\mu}(\bar{R}) \sqrt{\frac{2J+1}{8\pi^2}} \int \mathrm{d}(R\bar{R}^{-1}) D^{J*}_{M\mu'}(R\bar{R}^{-1}) U(R\bar{R}^{-1})(U(\bar{R})|w_1 w_2 w_3; \lambda_1\lambda_2\lambda_3\rangle). \tag{C2}$$

On the right-hand side of this equation, one recognize the definition of a Berman's J-helicity state whose reference state would have been tilted with the rotation $\bar{R}$. Denoting this state $|JM\mu'; w_1 w_2 w_3; \lambda_1\lambda_2\lambda_3\rangle_{\bar{R}}$, one finally gets formula (83),

$$|JM\mu; w_1 w_2 w_3; \lambda_1\lambda_2\lambda_3\rangle = \sum_{\mu'=-J}^{J} D^{J}_{\mu\mu'}(\bar{R}^{-1}) |JM\mu'; w_1 w_2 w_3; \lambda_1\lambda_2\lambda_3\rangle_{\bar{R}}. \tag{C3}$$

This property can be used to relate different conventions for Berman's states. In Ref. [38], Berman's reference states are defined considering the momentum of the third particle as opposite to the x axis in [38] while it is opposite to the y axis in the current work. In light of the previous developments, these two definitions for Berman's J-helicity states have a chance to differ from each other. The rotation $\bar{R}$ that conveys from one convention to the other brings the y axis along the x one, meaning

$$\bar{R} = R(0, 0, -\pi/2). \tag{C4}$$

Applying the aforementioned relation to this case, one gets

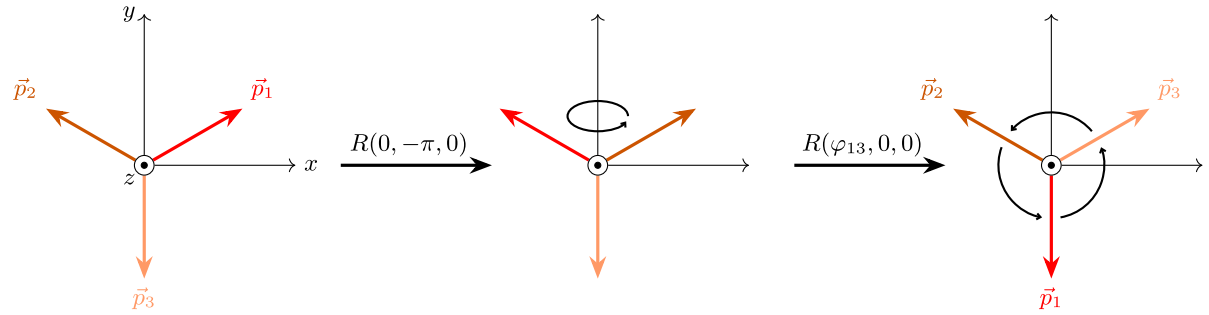

FIG. 16. Diagram justifying the role of $R(\varphi_{13},-\pi,0)$ in the application of $\mathbb{P}_{13}$ on Berman's states.

$$|JM\mu;w_1w_2w_3;\lambda_1\lambda_2\lambda_3\rangle = \sum_{\mu'=-J}^{J} D^J_{\mu\mu'}(0,0,\pi/2)|JM\mu';w_1w_2w_3;\lambda_1\lambda_2\lambda_3\rangle_{\text{var.}}$$
$$= i^{-\mu}|JM\mu;w_1w_2w_3;\lambda_1\lambda_2\lambda_3\rangle_{[38]}, \tag{C5}$$

where the notation $|\ldots\rangle_{\text{var.}}$ refers to an helicity state that uses conventions from [38]. Although both states have the same physical meaning, they differ by their phase conventions.

The action of $\mathbb{P}_{13}$ on Berman's J-helicity states also deserves a few explanations. The interest of symmetry being limited to the study of identical particles, spins, and masses of the three particles will be supposed equal, $s_1 = s_2 = s_3 = s$ and $m_1 = m_2 = m_3 = m$. Calculations have to be performed first at the p-helicity states level. The permutation operator exchanges the states of particles 1 and 3,

$$\mathbb{P}_{13}|\alpha\beta\gamma;w_1w_2w_3;\lambda_1\lambda_2\lambda_3\rangle = U(R(\alpha,\beta,\gamma))(U(R(\phi_3,\pi/2,0)L_z(p_3))|s\lambda_3\rangle$$
$$\otimes\, U(R(\phi_2,\pi/2,0)L_z(p_2))|s\lambda_2\rangle$$
$$\otimes\, U(R(\phi_1,\pi/2,0)L_z(p_1))|s\lambda_1\rangle). \tag{C6}$$

It is not clear if the left-hand side of this equation fits the structure of Berman's p-helicity states because for now relations (77) and (78) are not verified. This difficulty can be overcome by the insertion of a rotation $R(\varphi_{13},-\pi,0)$. The angles are chosen to mimic the action of $\mathbb{P}_{13}$ on the momenta, as illustrated on Fig. 16. Algebraically, one gets

$$\mathbb{P}_{13}|\alpha\beta\gamma;w_1w_2w_3;\lambda_1\lambda_2\lambda_3\rangle = U(R(\alpha,\beta,\gamma)R(\varphi_{13},-\pi,0))(U(R(0,\pi,-\varphi_{13})R(\phi_3,\pi/2,0)L_z(p_3))|s\lambda_3\rangle$$
$$\otimes\, U(R(0,\pi,-\varphi_{13})R(\phi_2,\pi/2,0)L_z(p_2))|s\lambda_2\rangle$$
$$\otimes\, U(R(0,\pi,-\varphi_{13})R(\phi_1,\pi/2,0)L_z(p_1))|s\lambda_1\rangle). \tag{C7}$$

The $SO(3)$ multiplication law can be used to reduce the previous expression

$$R(\alpha,\beta,\gamma)R(\varphi_{13},-\pi,0) = R(\pi+\alpha,\pi-\beta,-(\pi+\gamma+\varphi_{13})), \tag{C8}$$

$$R(0,\pi,-\varphi_{13})R(\phi,\pi/2,0) = R(\pi+\varphi_{13}-\phi,\pi/2,\pi) \quad (\forall\ \phi\in\mathbb{R}). \tag{C9}$$

With these relations the action of $\mathbb{P}_{13}$ on $|\alpha\beta\gamma;Ww_1w_2;\lambda_1\lambda_2\lambda_3\rangle$ becomes

$$\mathbb{P}_{13}|\alpha\beta\gamma;w_1w_2w_3;\lambda_1\lambda_2\lambda_3\rangle = U(R(\pi+\alpha,\pi-\beta,-(\pi+\gamma+\varphi_{13})))(U(R(\pi+\varphi_{13}-\phi_3,\pi/2,\pi)L_z(p_3))|s\lambda_3\rangle$$
$$\otimes\, U(R(\pi+\varphi_{13}-\phi_2,\pi/2,\pi)L_z(p_2))|s\lambda_2\rangle$$
$$\otimes\, U(R(\pi+\varphi_{13}-\phi_1,\pi/2,\pi)L_z(p_1))|s\lambda_1\rangle). \tag{C10}$$

This relation can be even further simplified using expression (78) for ϕ_1, ϕ_2, and ϕ_3,

$$\begin{aligned}\mathbb{P}_{13}|\alpha\beta\gamma; w_1w_2w_3; \lambda_1\lambda_2\lambda_3\rangle &= U(R(\pi+\alpha,\pi-\beta,-(\pi+\gamma+\varphi_{13})))(U(R(\varphi_{13}-\pi/2,\pi/2,\pi)L_z(p_3))|s\lambda_3\rangle \\ &\otimes U(R(3\pi/2-\varphi_{12},\pi/2,\pi)L_z(p_2))|s\lambda_2\rangle \\ &\otimes U(R(3\pi/2,\pi/2,\pi)L_z(p_1))|s\lambda_1\rangle) \\ &= U(R(\pi+\alpha,\pi-\beta,-(\pi+\gamma+\varphi_{13})))(U(R(\varphi_{13}-\pi/2,\pi/2,\pi)L_z(p_3))|s\lambda_3\rangle \\ &\otimes U(R(\varphi_{13}+\varphi_{23}-\pi/2,\pi/2,\pi)L_z(p_2))|s\lambda_2\rangle \\ &\otimes U(R(3\pi/2,\pi/2,\pi)L_z(p_1))|s\lambda_1\rangle). \end{aligned} \tag{C11}$$

The last equality makes use of $\varphi_{12}+\varphi_{23}+\varphi_{13}=2\pi$. The three angles in the reference state now satisfy relations (77) and (78) with w_1 and w_3 exchanged. To definitely obtain a true p-helicity state, the π rotations around the z axis have to be absorbed in the $|s\lambda_i\rangle$. This operation produces three $(-1)^{-\lambda_i}$ phase factors,

$$\mathbb{P}_{13}|\alpha\beta\gamma; w_1w_2w_3; \lambda_1\lambda_2\lambda_3\rangle = (-1)^{-\lambda_1-\lambda_2-\lambda_3}|(\pi+\alpha)(\pi-\beta)(-\pi-\gamma-\varphi_{13}); w_3w_2w_1; \lambda_3\lambda_2\lambda_1\rangle. \tag{C12}$$

Now that the relation has been written for Berman's p-helicity states, the corresponding relation for Berman's J-helicity states can be obtained,

$$\begin{aligned}\mathbb{P}_{13}|JM\mu; w_1w_2w_3; \lambda_1\lambda_2\lambda_3\rangle &= \sqrt{\frac{2J+1}{8\pi^2}}\int \mathrm{d}\alpha\mathrm{d}\cos\beta\mathrm{d}\gamma D^{J*}_{M\mu}(\alpha,\beta,\gamma)\mathbb{P}_{13}|\alpha\beta\gamma; w_1w_2w_3; \lambda_1\lambda_2\lambda_3\rangle \\ &= (-1)^{-\lambda_1-\lambda_2-\lambda_3}\sqrt{\frac{2J+1}{8\pi^2}}\int \mathrm{d}\alpha\mathrm{d}\cos\beta\mathrm{d}\gamma D^{J*}_{M\mu}(\alpha,\beta,\gamma) \\ &\quad\times|(\pi+\alpha)(\pi-\beta)(-\pi-\gamma-\varphi_{13}); w_3w_2w_1; \lambda_3\lambda_2\lambda_1\rangle. \end{aligned} \tag{C13}$$

The integration variables can be changed to fit the new angles in the p-helicity state,

$$\begin{aligned}\mathbb{P}_{13}|JM\mu; w_1w_2w_3; \lambda_1\lambda_2\lambda_3\rangle &= (-1)^{-\lambda_1-\lambda_2-\lambda_3}\sqrt{\frac{2J+1}{8\pi^2}}\int \mathrm{d}\alpha'\mathrm{d}\cos\beta'\mathrm{d}\gamma' D^{J*}_{M\mu}(\alpha'-\pi,\pi-\beta',-\pi-\gamma'-\varphi_{13}) \\ &\quad\times|\alpha'\beta'\gamma'; w_3w_2w_1; \lambda_3\lambda_2\lambda_1\rangle. \end{aligned} \tag{C14}$$

Making use of the Wigner D matrices' properties [15], the aforementioned relation can be reduced,

$$\begin{aligned}\mathbb{P}_{13}|JM\mu; w_1w_2w_3; \lambda_1\lambda_2\lambda_3\rangle &= (-1)^{-\lambda_1-\lambda_2-\lambda_3}\sqrt{\frac{2J+1}{8\pi^2}}\int \mathrm{d}\alpha'\mathrm{d}\cos\beta'\mathrm{d}\gamma'((-1)^{J-\mu}e^{-i\varphi_{13}\mu}D^{J*}_{M-\mu}(\alpha',\beta',\gamma')) \\ &\quad\times|\alpha'\beta'\gamma'; w_3w_2w_1; \lambda_3\lambda_2\lambda_1\rangle \\ &= (-1)^{J-\mu-\lambda_1-\lambda_2-\lambda_3}e^{-i\varphi_{13}\mu}|JM-\mu; w_3w_2w_1; \lambda_3\lambda_2\lambda_1\rangle. \end{aligned} \tag{C15}$$

This closes the demonstration of the property. The action of $\mathbb{P}_{23}$ is demonstrated in a similar way.

APPENDIX D: DEMONSTRATION OF THE CHANGE OF BASIS FORMULA FROM BERMAN'S TO WICK'S STATES

This appendix is dedicated to the derivation of relation (108). It is divided in three parts. First, Berman's p-helicity states are restructured to include a state for particles 1 and 2 in their c.m.f. Then, this rewriting is used to prove the change of basis formula. Finally, a consistency check concerning normalization of the states is suggested.

1. Rewriting of p-helicity states

To fit with Wick's structure, particles 1 and 2 in Berman's states are to be brought in their own c.m.f. This operation is performed on the reference states (79) at first. The boost that transitions between the c.m.f. of the entire system and the 12-c.m.f. is the one that imparts a momentum $\boldsymbol{p_3}$ to a particle of mass m_{12} initially at rest. It writes down as follows:

$$L_3 = R(3\pi/2,\pi/2,0)L_z(m_{12},p_3)R^{-1}(3\pi/2,\pi/2,0). \tag{D1}$$

This L_3 boost can be artificially inserted into the definition of Berman's reference states (79),

$$\begin{aligned}|w_1w_2w_3;\lambda_1\lambda_2\lambda_3\rangle &= U(L_3^{-1}L_3)[U(R(\phi_1,\pi/2,0)L_z(p_1))|s_1\lambda_1\rangle \otimes U(R(\phi_2,\pi/2,0)L_z(p_2))|s_2\lambda_2\rangle] \\ &\quad \otimes U(R(\phi_3,\pi/2,0)L_z(p_3))|s_3\lambda_3\rangle \\ &= U(L_3)^{-1}[U(L_3)U(R(\phi_1,\pi/2,0)L_z(p_1))|s_1\lambda_1\rangle \otimes U(L_3)U(R(\phi_2,\pi/2,0)L_z(p_2))|s_2\lambda_2\rangle] \\ &\quad \otimes U(R(\phi_3,\pi/2,0)L_z(p_3))|s_3\lambda_3\rangle. \end{aligned} \tag{D2}$$

Inside the brackets, both particle 1 and particle 2 are subjected to the L_3 boost. The subsequent development focuses on the first particle but the same applies to the second one. The expression to simplify the results from applying a Lorentz boost on a one-body helicity state (14) is

$$\begin{aligned}&U(L_3)U(R(\phi_1,\pi/2,0)L_z(p_1))|s_1\lambda_1\rangle \\ &= U(L_3)|p_1\pi/2\phi_1;s_1\lambda_1\rangle_0. \end{aligned} \tag{D3}$$

For further clarification, the third angle convention is written as an index. The situation is the one handled by property (23),

$$U(L_3)|p_1\pi/2\phi_1;s_1\lambda_1\rangle_0 = \sum_{\lambda_1'} D^{s_1}_{\lambda_1'\lambda_1}(R_W^1)|p_{12}\theta_{12}\phi_{12};s_1\lambda_1'\rangle_0. \tag{D4}$$

By construction, after applying the L_3 boost, the momentum ends in the 12-c.m.f. Corresponding coordinates have been denoted p_{12}, θ_{12}, and ϕ_{12}, in agreement with notations from Wick's definition (99). Because the momenta in the reference state are chosen to lie in the xy plane, and because L_3 is a boost along the y axis, the boosted momenta remain in that same plane. As a consequence, the polar angle θ_{12} is shown to be identically equal to $\pi/2$. Concerning the expressions of p_{12} and ϕ_{12} in terms of the energies w_1, w_2, and w_3, these are obtained by evaluating different Lorentz-invariant combinations of four-momenta[6] in both the 12-c.m.f. and the e.c.m.f. This allows us to show that

$$\begin{aligned}2p_{12} &= \sqrt{(w_1+w_2)^2-w_3^2}, \\ \cos(\pi/2-\phi_{12}) &= \frac{w_1-w_2}{w_3}. \end{aligned} \tag{D5}$$

The Wigner rotation R_W^1 is obtained by specifying expression (24) to the current situation,

$$R_W^1 = (R(\phi_{12},\pi/2,0)L_z(m_1,p_{12}))^{-1}L_3(R(\phi_1,\pi/2,0)L_z(m_1,p_1)). \tag{D6}$$

This expression for R_W^1 and the knowledge of each particle mass and energy theoretically allow us to determine the parameters for the Wigner rotation and to deduce the corresponding D matrix. The same calculation is applied to the second particle. By collecting the results, the following intermediate expression is obtained for the three-body reference state:

$$\begin{aligned}|w_1w_2w_3;\lambda_1\lambda_2\lambda_3\rangle &= \sum_{\lambda_1',\lambda_2'} D^{s_1}_{\lambda_1'\lambda_1}(R_W^1)D^{s_2}_{\lambda_2'\lambda_2}(R_W^2)(U(L_3)^{-1}[|p_{12}(\pi/2)(\phi_{12});s_1\lambda_1'\rangle_0 \otimes |p_{12}(\pi/2)(\pi+\phi_{12});s_2\lambda_2'\rangle_0] \\ &\quad \otimes |p_3(\pi/2)\phi_3;s_3\lambda_3\rangle_0). \end{aligned} \tag{D7}$$

Above, the definition of one-body helicity state (14) has also been used for the last particle. By using the definition of L_3, its invert can be written as

$$L_3^{-1} = R(5\pi/2,\pi/2,0)L_z(m_{12},p_3)R^{-1}(5\pi/2,\pi/2,0). \tag{D8}$$

The boost L_3^{-1} proves to fit the definition of a canonical boost (8). A helicity boost would be more convenient to subsequently construct helicity states. To perform the conversion, the rotation on the right can be absorbed into both one-body helicity states, using the invariance of helicity under rotations (17),

$$R^{-1}(5\pi/2,\pi/2,0)|p_{12}(\pi/2)(\phi_{12});s_1\lambda_1'\rangle_0 = e^{i\xi_1\lambda_1'}|p_{12}(\pi/2-\phi_{12})(3\pi/2);s_1\lambda_1'\rangle_0, \tag{D9}$$

$$R^{-1}(5\pi/2,\pi/2,0)|p_{12}(\pi/2)(\pi+\phi_{12});s_2\lambda_2'\rangle_0 = e^{i\xi_2\lambda_2'}|p_{12}(\pi/2+\phi_{12})(5\pi/2);s_2\lambda_2'\rangle_\pi. \tag{D10}$$

[6]Namely $(\boldsymbol{P_1}+\boldsymbol{P_2})^2$, $(\boldsymbol{P_1}+\boldsymbol{P_3})^2$ and $(\boldsymbol{P_1}+\boldsymbol{P_2}+\boldsymbol{P_3})^2$.

In definition (99), since the second particle is considered opposed to the first one, it is brought in the π convention instead of the 0 one. Above, the expressions for the polar and azimuth angles from the right-hand-side state are obtained by applying $R^{-1}(5\pi/2,\pi/2,0)$ on both particle momenta. Concerning ξ_1 and ξ_2, their values are obtained by explicitly multiplying both rotations that provide their angles to the one-body helicity states by $R^{-1}(5\pi/2,\pi/2,0)$,

$$\begin{aligned} R^{-1}(5\pi/2,\pi/2,0)R(\phi_{12},\pi/2,0) &= R(3\pi/2,\pi/2-\phi_{12},\pi/2) \\ R^{-1}(5\pi/2,\pi/2,0)R(\pi+\phi_{12},\pi/2,0) &= R(5\pi/2,\pi/2+\phi_{12},-\pi/2). \end{aligned} \tag{D11}$$

Noticing that ϕ_{12} itself lies between $-\pi/2$ and $\pi/2$, these two formulas have been tuned so that the second Euler angle of both combined rotations lies between 0 and π. The combined rotations are neither in the 0 nor the π convention. This issue is resolved by adding the suitable rotation around the z axis. After acting on the helicity state, this results in a simple phase factor,

$$e^{i\lambda_1'\xi_1} = e^{-i\lambda_1'\pi/2}, \qquad e^{i\lambda_2'\xi_2} = e^{3i\lambda_2'\pi/2}. \tag{D12}$$

At this stage, the reference state has been restructured as follows:

$$\begin{aligned} |w_1w_2w_3;\lambda_1\lambda_2\lambda_3\rangle = &\sum_{\lambda_1',\lambda_2'} D^{s_1}_{\lambda_1'\lambda_1}(R_W^1)D^{s_2}_{\lambda_2'\lambda_2}(R_W^2)e^{-i(\lambda_1'-3\lambda_2')\pi/2}(U(R(5\pi/2,\pi/2,0)L_z(m_{12},p_3)) \\ &\times[|p_{12}(\pi/2-\phi_{12})(3\pi/2);s_1\lambda_1'\rangle_0 \otimes |p_{12}(\pi/2+\phi_{12})(5\pi/2);s_2\lambda_2'\rangle_\pi] \otimes |p_3(\pi/2)(3\pi/2);s_3\lambda_3\rangle_0). \end{aligned} \tag{D13}$$

Two small modifications remain to be performed. First, the third particle is for now in the 0 convention but, because the momentum of particle 3 will be considered opposed, its third angle convention should be changed to the π one, thereby adding an $e^{i\lambda_3\pi}$ phase factor. Lastly, the state inside the brackets can be rewritten as a two-body helicity state (26b). This only requires an additional phase $(-1)^{s_2-\lambda_2'}$. The final expression for the reference state is

$$\begin{aligned} |w_1w_2w_3;\lambda_1\lambda_2\lambda_3\rangle = &\sum_{\lambda_1',\lambda_2'} D^{s_1}_{\lambda_1'\lambda_1}(R_W^1)D^{s_2}_{\lambda_2'\lambda_2}(R_W^2)e^{i(2s_2+\lambda_2'-\lambda_1'+2\lambda_3)\pi/2} \\ &\times (U(R(5\pi/2,\pi/2,0)L_z(m_{12},p_3))|p_{12}(\pi/2-\phi_{12})(3\pi/2);s_1\lambda_1's_2\lambda_2'\rangle \\ &\otimes |p_3(\pi/2)(3\pi/2);s_3\lambda_3\rangle_\pi). \end{aligned} \tag{D14}$$

This expression has the desired structure: Particles 1 and 2 are coupled in their own c.m.f., and this subsystem is boosted toward the e.c.m.f. to be coupled with the third particle.

2. Rewriting of J-helicity states

Now that an intermediary coupling has been added in Berman's p-helicity states, the development of Berman's J-helicity states in Wick's J-helicity states can be performed. By inserting relation (D14) into the definition (81), the following expression is obtained:

$$\begin{aligned} |JM\mu;w_1w_2w_3;\lambda_1\lambda_2\lambda_3\rangle = &\sqrt{\frac{2J+1}{8\pi^2}}\sum_{\lambda_1',\lambda_2'} D^{s_1}_{\lambda_1'\lambda_1}(R_W^1)D^{s_2}_{\lambda_2'\lambda_2}(R_W^2)e^{i(2s_2+\lambda_2'-\lambda_1'+2\lambda_3)\pi/2} \\ &\times \int \mathrm{d}\alpha\mathrm{d}\cos\beta\mathrm{d}\gamma D^{J*}_{M\mu}(\alpha,\beta,\gamma)U(R(\alpha,\beta,\gamma))(U(R(5\pi/2,\pi/2,0)L_z(m_{12},p_3)) \\ &\times |p_{12}(\pi/2-\phi_{12})(3\pi/2);s_1\lambda_1's_2\lambda_2'\rangle \otimes |p_3(\pi/2)(3\pi/2);s_3\lambda_3\rangle_\pi). \end{aligned} \tag{D15}$$

To fit Wick's definition, eigenstates of the total angular momentum relative to particles 1 and 2 would be preferable to the current $|p_{12}(\pi/2-\phi_{12})(3\pi/2);s_1\lambda_1's_2\lambda_2'\rangle$. Such two-body states are related to each other by relation (33). By omitting some passive coefficients for brevity, the following expression is obtained:

$$|JM\mu;w_1w_2w_3;\lambda_1\lambda_2\lambda_3\rangle = \sum_{\lambda_1',\lambda_2'}[\ldots]\int \mathrm{d}\alpha\mathrm{d}\cos\beta\mathrm{d}\gamma(\ldots)\sum_{j_{12}=|\lambda_1'-\lambda_2'|}^{\infty}\sum_{\lambda_{12}=-j_{12}}^{j_{12}}\sqrt{\frac{2j_{12}+1}{4\pi}}D^{j_{12}}_{\lambda_{12}\lambda_1'-\lambda_2'}(3\pi/2,\pi/2-\phi_{12},0)U(R(\alpha,\beta,\gamma))$$
$$\times\left(U(R(5\pi/2,\pi/2,0)L_z(m_{12},p_3))|p_{12};j_{12}\lambda_{12};\lambda_1'\lambda_2'\rangle\otimes|p_3(\pi/2)(3\pi/2);s_3\lambda_3\rangle_\pi\right). \tag{D16}$$

The structure of the state inside the large parentheses almost follows the pattern of Wick's p-helicity states (101). The main difference lies in the rotation that acts on the two-body state. It involves a $5\pi/2$ rotation around the z axis where a rotation in between 0 and 2π is expected. For bosonic states, 2π rotations are identified by the identity and can freely be ignored. For fermionic states, these rotations give rise to minus signs which have to be taken into account. Both cases can be taken into account at once by adding a $(-1)^{2\lambda_1'+2\lambda_2'}$ factor. A $(-1)^{\lambda_3-s_3}$ phase factor has to be added also to truly correspond to Wick's p-helicity state definition,

$$|JM\mu;w_1w_2w_3;\lambda_1\lambda_2\lambda_3\rangle = \sum_{\lambda_1',\lambda_2'}[\ldots]\int \mathrm{d}\alpha\mathrm{d}\cos\beta\mathrm{d}\gamma(\ldots)\sum_{j_{12}=|\lambda_1'-\lambda_2'|}^{\infty}\sum_{\lambda_{12}=-j_{12}}^{j_{12}}\sqrt{\frac{2j_{12}+1}{4\pi}}D^{j_{12}}_{\lambda_{12}\lambda_1'-\lambda_2'}(3\pi/2,\pi/2-\phi_{12},0)$$
$$\times U(R(\alpha,\beta,\gamma))(-1)^{2\lambda_1'+2\lambda_2'+s_3-\lambda_3}|p_3(\pi/2)(\pi/2);j_{12}\lambda_{12}s_3\lambda_3;p_{12}s_1\lambda_1's_2\lambda_2'\rangle. \tag{D17}$$

A second use of relation (33) allows us to replace this state with defined momenta by a sum of states with defined total angular momentum,

$$|JM\mu;w_1w_2w_3;\lambda_1\lambda_2\lambda_3\rangle = \sum_{\lambda_1',\lambda_2'}[\ldots]\int \mathrm{d}\alpha\mathrm{d}\cos\beta\mathrm{d}\gamma(\ldots)\sum_{j_{12}=|\lambda_1'-\lambda_2'|}^{\infty}\sum_{\lambda_{12}=-j_{12}}^{j_{12}}\{\ldots\}\sum_{\bar{J}=|\lambda_{12}-\lambda_3|}^{\infty}\sum_{\bar{M}=-\bar{J}}^{\bar{J}}\sqrt{\frac{2\bar{J}+1}{4\pi}}D^{\bar{J}}_{\bar{M}\lambda_{12}-\lambda_3}(\pi/2,\pi/2,0)$$
$$\times U(R(\alpha,\beta,\gamma))|p_3;\bar{J}\,\bar{M};j_{12}\lambda_{12}s_3\lambda_3;p_{12}s_1\lambda_1's_2\lambda_2'\rangle. \tag{D18}$$

Dots have again been used to replace passive coefficients in the expression. The relation can still be simplified. To start with, the transformation rule of angular momentum eigenstates under rotations [14,18] is used to eliminate the $U(R(\alpha,\beta,\gamma))$ operator,

$$|JM\mu;w_1w_2w_3;\lambda_1\lambda_2\lambda_3\rangle = \sum_{\lambda_1',\lambda_2'}[\ldots]\int \mathrm{d}\alpha\mathrm{d}\cos\beta\mathrm{d}\gamma(\ldots)\sum_{j_{12}=|\lambda_1'-\lambda_2'|}^{\infty}\sum_{\lambda_{12}=-j_{12}}^{j_{12}}\{\ldots\}\sum_{\bar{J}=|\lambda_{12}-\lambda_3|}^{\infty}\sum_{\bar{M}=-\bar{J}}^{\bar{J}}\sqrt{\frac{2\bar{J}+1}{4\pi}}D^{\bar{J}}_{\bar{M}\lambda_{12}-\lambda_3}(\pi/2,\pi/2,0)$$
$$\times\sum_{M'=-\bar{J}}^{\bar{J}}D^{\bar{J}}_{M'\bar{M}}(\alpha,\beta,\gamma)|p_3;\bar{J}M';j_{12}\lambda_{12}s_3\lambda_3;p_{12}s_1\lambda_1's_2\lambda_2'\rangle. \tag{D19}$$

Aforementioned passive coefficients will be reintroduced one after the other. Brackets, curly brackets, and parentheses are used consistently to trace their origin. The (α,β,γ) dependence is confined in two Wigner D matrices,

$$|JM\mu;w_1w_2w_3;\lambda_1\lambda_2\lambda_3\rangle = \sum_{\lambda_1',\lambda_2'}[\ldots]\sum_{j_{12}=|\lambda_1'-\lambda_2'|}^{\infty}\sum_{\lambda_{12}=-j_{12}}^{j_{12}}\{\ldots\}\sum_{\bar{J}=|\lambda_{12}-\lambda_3|}^{\infty}\sum_{\bar{M}=-\bar{J}}^{\bar{J}}\sqrt{\frac{2\bar{J}+1}{4\pi}}D^{\bar{J}}_{\bar{M}\lambda_{12}-\lambda_3}(\pi/2,\pi/2,0)$$
$$\times\sum_{M'=-\bar{J}}^{\bar{J}}\left(\int \mathrm{d}\alpha\mathrm{d}\cos\beta\mathrm{d}\gamma(D^{J*}_{M\mu}(\alpha,\beta,\gamma))D^{\bar{J}}_{M'\bar{M}}(\alpha,\beta,\gamma)\right)|p_3;\bar{J}M';j_{12}\lambda_{12}s_3\lambda_3;p_{12}s_1\lambda_1's_2\lambda_2'\rangle. \tag{D20}$$

The orthogonality of Wigner D matrices [15] can now be used. It produces three Kronecker deltas that eliminate three sums among the six,

$$|JM\mu;w_1w_2w_3;\lambda_1\lambda_2\lambda_3\rangle = \left[\sqrt{\frac{2J+1}{8\pi^2}}\right]\sum_{\lambda_1',\lambda_2'}[\ldots]\sum_{j_{12}=|\lambda_1'-\lambda_2'|}^{\infty}\sum_{\lambda_{12}=-j_{12}}^{j_{12}}\{\ldots\}\sqrt{\frac{2J+1}{4\pi}}D^{J}_{\mu\lambda_{12}-\lambda_3}(\pi/2,\pi/2,0)$$
$$\times\frac{8\pi^2}{2J+1}|p_3;JM;j_{12}\lambda_{12}s_3\lambda_3;p_{12}s_1\lambda_1's_2\lambda_2'\rangle. \tag{D21}$$

At this stage, reintroducing all the passive coefficients, the following expression has been obtained:

$$|JM\mu; w_1w_2w_3; \lambda_1\lambda_2\lambda_3\rangle = \sqrt{2\pi}\sum_{\lambda_1',\lambda_2'}[D^{s_1}_{\lambda_1'\lambda_1}(R_W^1)D^{s_2}_{\lambda_2'\lambda_2}(R_W^2)e^{i(2s_2+\lambda_2'-\lambda_1'+2\lambda_3)\pi/2}]$$
$$\times\sum_{j_{12}=|\lambda_1'-\lambda_2'|}^{\infty}\sum_{\lambda_{12}=-j_{12}}^{j_{12}}\left\{(-1)^{2\lambda_1'+2\lambda_2'+s_3-\lambda_3}\sqrt{\frac{2j_{12}+1}{4\pi}}D^{j_{12}}_{\lambda_{12}\lambda_1'-\lambda_2'}(3\pi/2,\pi/2-\phi_{12},0)\right\}$$
$$\times D^{J}_{\mu\lambda_{12}-\lambda_3}(\pi/2,\pi/2,0)|p_3;JM;j_{12}\lambda_{12}s_3\lambda_3;p_{12}s_1\lambda_1's_2\lambda_2'\rangle. \tag{D22}$$

Complex numbers inside the summation can be made explicit by turning complex Wigner D matrices into real d matrices and phases ([15] Sec. 4.3)

$$D^{j_{12}}_{\lambda_{12}\lambda_1'-\lambda_2'}(3\pi/2,\pi/2-\phi_{12},0)D^{J}_{\mu\lambda_{12}-\lambda_3}(\pi/2,\pi/2,0) = e^{-i(3\lambda_{12}+\mu)\pi/2}d^{j_{12}}_{\lambda_{12}\lambda_1'-\lambda_2'}(\pi/2-\phi_{12})d^{J}_{\mu\lambda_{12}-\lambda_3}(\pi/2). \tag{D23}$$

Compiling phase factors and noticing that λ_{12} and $\lambda_1'-\lambda_2'$ have the same integer or half-integer nature, one gets the final expression,

$$|JM\mu; w_1w_2w_3; \lambda_1\lambda_2\lambda_3\rangle = \sum_{\lambda_1',\lambda_2'}D^{s_1}_{\lambda_1'\lambda_1}(R_W^1)D^{s_2}_{\lambda_2'\lambda_2}(R_W^2)e^{i(2s_2+2s_3+\lambda_2'-\lambda_1'-\mu)\pi/2}$$
$$\times\sum_{j_{12}=|\lambda_1'-\lambda_2'|}^{\infty}\sum_{\lambda_{12}=-j_{12}}^{j_{12}}e^{i\lambda_{12}\pi/2}\sqrt{\frac{2j_{12}+1}{2}}d^{j_{12}}_{\lambda_{12}\lambda_1'-\lambda_2'}(\pi/2-\phi_{12})d^{J}_{\mu\lambda_{12}-\lambda_3}(\pi/2)$$
$$\times|p_3;JM;j_{12}\lambda_{12}s_3\lambda_3;p_{12}s_1\lambda_1's_2\lambda_2'\rangle. \tag{D24}$$

3. Normalization consistence

To confirm relations (108) and (110), one may try to deduce the orthonormalization of Berman's J-helicity states from the one of Wick's J-helicity states. This subsection is devoted to this consistency check supposing three massless particles. The scalar product of two arbitrary Berman J-helicity states is evaluated by making use of relation (110) while Wick's states orthonormalization (107) is assumed. After some algebra, one gets

$$\langle\bar{J}\,\bar{M}\,\bar{\mu};\bar{w}_1\bar{w}_2\bar{w}_3;\bar{\lambda}_1\bar{\lambda}_2\bar{\lambda}_3|JM\mu;w_1w_2w_3;\lambda_1\lambda_2\lambda_3\rangle$$
$$=\frac{4\sqrt{p_3^2+4p_{12}^2}}{p_3p_{12}}\delta(\bar{p}_3-p_3)\delta(\bar{p}_{12}-p_{12})\delta_{\bar{J}J}\delta_{\bar{M}M}\delta_{\bar{\lambda}_1\lambda_1}\delta_{\bar{\lambda}_2\lambda_2}\delta_{\bar{\lambda}_3\lambda_3}e^{i(\bar{\mu}-\mu)\pi/2}$$
$$\times\sum_{j_{12}=|\lambda_1-\lambda_2|}^{\infty}\sum_{\lambda_{12}=-j_{12}}^{j_{12}}\frac{2j_{12}+1}{2}d^{j_{12}}_{\lambda_{12}\lambda_1-\lambda_2}(\pi/2-\bar{\phi}_{12})d^{j_{12}}_{\lambda_{12}\lambda_1-\lambda_2}(\pi/2-\phi_{12})d^{J}_{\bar{\mu}\lambda_{12}-\lambda_3}(\pi/2)d^{J}_{\mu\lambda_{12}-\lambda_3}(\pi/2). \tag{D25}$$

Let us remind that a dependence on the energy variable w_1 ($\bar{w}_1$) is hidden inside the ϕ_{12} ($\bar{\phi}_{12}$) angle. Comparing with the announced orthonormalization of Berman's J-helicity states, the remaining summations on j_{12} and λ_{12} are expected to produce a Kronecker delta in μ and a Dirac delta in w_1. Using properties of d matrices [15], these summations can be reduced analytically,

$$\sum_{j_{12}=|\lambda_1-\lambda_2|}^{\infty}\sum_{\lambda_{12}=-j_{12}}^{j_{12}}\frac{2j_{12}+1}{2}d^{j_{12}}_{\lambda_{12}\lambda_1-\lambda_2}(\bar{u})d^{j_{12}}_{\lambda_{12}\lambda_1-\lambda_2}(u)d^{J}_{\bar{\mu}\lambda_{12}-\lambda_3}(\pi/2)d^{J}_{\mu\lambda_{12}-\lambda_3}(\pi/2) = \delta(u-\bar{u})\delta_{\mu\bar{\mu}}, \tag{D26}$$

where the shorter notation u for the variable $\cos(\pi/2-\phi_1')$ has been used. Dirac deltas on p_3, p_{12}, and u can also be turned into Dirac deltas on w_1, w_2, and w_3 using (113),

$$\delta(\bar{u}-u)\delta(\bar{p}_{12}-p_{12})\delta(\bar{p}_3-p_3) = \frac{2p_3p_{12}}{\sqrt{4p_{12}^2+p_3^2}}\delta(\bar{w}_1-w_1)\delta(\bar{w}_2-w_2)\delta(\bar{w}_3-w_3). \tag{D27}$$

As a result, one gets the expected orthonormalization of Berman's J-helicity states,

$$\langle \bar{J}\,\bar{M}\,\bar{\mu};\bar{w}_1\bar{w}_2\bar{w}_3;\bar{\lambda}_1\bar{\lambda}_2\bar{\lambda}_3|JM\mu;w_1w_2w_3;\lambda_1\lambda_2\lambda_3\rangle = 8\delta(\bar{w}_1-w_1)\delta(\bar{w}_2-w_2)\delta(\bar{w}_3-w_3)\delta_{\bar{J}J}\delta_{\bar{M}M}\delta_{\bar{\mu}\mu}\delta_{\lambda_1\bar{\lambda}_1}\delta_{\lambda_2\bar{\lambda}_2}\delta_{\lambda_3\bar{\lambda}_3}. \tag{D28}$$

APPENDIX E: SYMMETRY CONSIDERATIONS FOR EQ. (140)

First of all, let us have a quick look at coefficients (142),

$$(\mathcal{C}^{j_{12}\lambda_{12}}_{J\bar{\mu};\bar{\lambda}_1\bar{\lambda}_2\lambda_3})^*\mathcal{C}^{j_{12}\lambda_{12}}_{J\mu;\lambda_1\lambda_2\lambda_3} = (-1)^{(\lambda_2-\bar{\lambda}_2)/2+(\bar{\lambda}_1-\lambda_1)/2+(\bar{\mu}-\mu)/2}\frac{2j_{12}+1}{2}d^J_{\bar{\mu}\lambda_{12}-\lambda_3}(\pi/2)d^J_{\mu\lambda_{12}-\lambda_3}(\pi/2). \tag{E1}$$

These coefficients are easily shown to stay real, independent of the spin of the particles. If μ or $\bar{\mu}$ is null, the properties of Wigner d matrices allow us to show that, as long as $J-\lambda_{12}+\lambda_3$ is an odd number, the whole coefficient cancels [15]. Because λ_3 belongs to $\{+1,-1\}$ and because the total angular momentum of a symmetric state with $\mu=0$ must be odd, whenever μ or $\bar{\mu}$ is null, all terms with odd λ_{12} cancel, thereby avoiding evaluating them.

The dependence on helicity quantum numbers of the $\tilde{\Psi}$ function (141) can be investigated. The symmetry properties of Wigner d matrices allow us to equate different evaluations of $\tilde{\Psi}$. Following equalities immediately comes out of these symmetry properties,

$$\begin{aligned}\tilde{\Psi}(\ldots;j_{12},\lambda_{12},\Delta\lambda;\ldots) &= \tilde{\Psi}(\ldots;j_{12},-\Delta\lambda,-\lambda_{12};\ldots) = (-1)^{\lambda_{12}}\tilde{\Psi}(\ldots;j_{12},-\lambda_{12},-\Delta\lambda;\ldots)\\ &= (-1)^{\lambda_{12}}\tilde{\Psi}(\ldots;j_{12},\Delta\lambda,\lambda_{12};\ldots).\end{aligned} \tag{E2}$$

Other symmetries require Ψ to be an even function of u. In that case, performing the change of variables $u\to -u$ allows us to show that

$$\begin{aligned}\tilde{\Psi}(\ldots;j_{12},\lambda_{12},\Delta\lambda;\ldots) &= (-1)^{j_{12}}\tilde{\Psi}(\ldots;j_{12},-\lambda_{12},\Delta\lambda;\ldots) = (-1)^{j_{12}}\tilde{\Psi}(\ldots;j_{12},-\Delta\lambda,\lambda_{12};\ldots)\\ &= (-1)^{j_{12}+\lambda_{12}}\tilde{\Psi}(\ldots;j_{12},\Delta\lambda,-\lambda_{12};\ldots) = (-1)^{j_{12}+\lambda_{12}}\tilde{\Psi}(\ldots;j_{12},\lambda_{12},-\Delta\lambda;\ldots).\end{aligned} \tag{E3}$$

The assumption that requires Ψ to be even is consistent with the trial shape (125). However, it may be invalidated if kinematic factors such as those from relations (127) and (128) need to be included in order to ensure the symmetry of the state. Regardless of this precaution, relations (E2) and/or (E3) allow for the recycling of most evaluations of $\tilde{\Psi}$, thereby reducing computational cost. These eight symmetry relations can even show that $\tilde{\Psi}$ cancels for some combinations of quantum numbers, such as for $\Delta\lambda=0$, λ_{12} even and j_{12} odd.

Finally, the ME on two-body J-helicity states appearing in the integrand from Eq. (140) is also to be analyzed. Its dependence on helicity quantum numbers can be investigated by means of formula (58) from Sec. II B. Using properties of Clebsh-Gordan coefficients, it can be shown that

$$\mathcal{C}^{j_{12};11}_{l_{12}s_{12};\lambda_1\lambda_2} = (-1)^{s_{12}}\mathcal{C}^{j_{12};11}_{l_{12}s_{12};-\lambda_2-\lambda_1} = (-1)^{l_{12}-j_{12}}\mathcal{C}^{j_{12};11}_{l_{12}s_{12};-\lambda_1-\lambda_2} \tag{E4}$$

where $\mathcal{C}$ coefficients are those defined in Sec. II B. Applying this result to Eq. (58) reveals that certain helicity quadruplets $(\lambda_1,\lambda_2,\bar{\lambda}_1,\bar{\lambda}_2)$ yield identical values. Specifically, these quadruplets can be grouped into five families, within which MEs on two-body J-helicity states are equal to each other. These families are displayed in Table XII. For now, ignore the division of the fifth family into two distinct parts. Let us also mention that, again in view of (58), these matrix elements are real valued.

TABLE XII. Table of the different helicity quadruplets $(\lambda_1,\lambda_2,\bar{\lambda}_1,\bar{\lambda}_2)$ that give rise to the same ME on two-body J-helicity states $\langle \bar{p}_{12};j_{12}\lambda_{12};\bar{\lambda}_1\bar{\lambda}_2|\mathcal{O}(r_{12})|p_{12};j_{12}\lambda_{12};\lambda_1\lambda_2\rangle$.

First family		$(+,+,+,+)$	$(-,-,-,-)$	
Second family		$(+,+,-,-)$	$(-,-,+,+)$	
Third family		$(-,+,-,+)$	$(+,-,+,-)$	
Fourth family		$(+,-,-,+)$	$(-,+,+,-)$	
Fifth family (part 1)	$(+,-,+,+)$	$(+,+,+,-)$	$(+,-,-,-)$	$(-,-,+,-)$
Fifth family (part 2)	$(-,+,+,+)$	$(+,+,-,+)$	$(-,+,-,-)$	$(-,-,-,+)$

This allows us to freely exchange the bra and the ket,

$$\langle \bar{p}_{12}; j_{12}\lambda_{12}; \bar{\lambda}_1\bar{\lambda}_2|\mathcal{O}(r_{12})|p_{12}; j_{12}\lambda_{12}; \lambda_1\lambda_2\rangle = \langle p_{12}; j_{12}\lambda_{12}; \lambda_1\lambda_2|\mathcal{O}(r_{12})|\bar{p}_{12}; j_{12}\lambda_{12}; \bar{\lambda}_1\bar{\lambda}_2\rangle. \quad \text{(E5)}$$

Observations about $\tilde{\Psi}$ and about the two-body ME are to be combined to deduce symmetry properties of the whole integral from (140). Simplifications occur depending on the assumptions made on Ψ and $\bar{\Psi}$.

A special case of prime importance in the following concerns Ψ and $\bar{\Psi}$ being two equal real functions which are even for u. These assumptions imply two symmetry properties at the level of the integrals. First, the equality and reality hypothesis allows us to freely exchange $\Delta\lambda$ and $\Delta\bar{\lambda}$ by exchanging both integration variables. On the other hand, the hypothesis about the parity in u implies that the sign of each $\Delta\lambda$ can be flipped, at worst, at the cost of a phase factor $(-1)^{j_{12}+\lambda_{12}}$. These two properties imply that integrals line up with the five families of helicity quadruplets from Table XII, except for the fifth family in which quadruplets in both parts differ by a $(-1)^{j_{12}+\lambda_{12}}$ phase factor. Each evaluation of an integral from (140) for a given helicity quadruplet provides a value valid for any other quadruplet in the same family, potentially up to a minus sign.

Apart from this special case, a second simplification turns out relevant for the upcoming developments. In the first family from Table XII, both $\Delta\lambda$ and $\Delta\bar{\lambda}$ are always zero. As a result and without further conditions, calculations for both helicity quadruplets in this family will yield identical values for the integrals. This result will prove valuable, as the two helicity quadruplets in question are precisely those encountered during calculations with A_2'' states.

APPENDIX F: POTENTIAL FOR THREE-GLUON GLUEBALLS

The interactions between three gluons can be described in two main geometries. From the perspective discussed in the main text, each gluon generates two flux tubes that transform with the fundamental and the antifundamental representation of $SU(3)$. These flux tubes merge pairwise, in a so-called Δ junction. Alternatively, each gluon can be viewed as producing a single flux tube in the adjoint representation of $SU(3)$. In that case, the three flux tubes merge in a so-called Y junction [32], as illustrated in Fig. 17. The Y junction consists of a genuine three-body interaction. Differences between the Y and Δ junctions are discussed in [56,57], with the conclusions favoring the Δ junction.

For comparison, let us consider here a Y junction. In this configuration, the interaction potential used in constituent approaches writes down as follows:

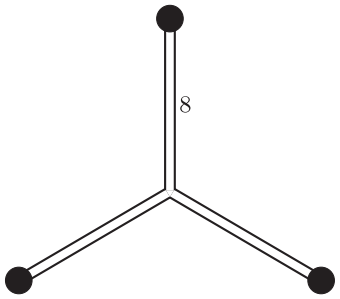

FIG. 17. Schematic representation of a Y junction modeling three-gluon glueballs. The three gluons bound at once by pooling their three eight-flux tubes.

$$V(\boldsymbol{r_1},\boldsymbol{r_2},\boldsymbol{r_3}) = \min_{\boldsymbol{Y}} \sum_{i=1}^{3} \beta\langle F_i^2\rangle|\boldsymbol{r_i}-\boldsymbol{Y}| + \sum_{i<j}^{3} \frac{\alpha_s\langle F_i\cdot F_j\rangle}{|\boldsymbol{r_i}-\boldsymbol{r_j}|}. \quad \text{(F1)}$$

Here, β is the fundamental string tension, and α_s is the strong coupling constant. The factor F_i^2 corresponds to the $SU(3)$ Casimir operator acting on the ith particle. Including this factor in the confining potential is known as the Casimir scaling hypothesis [35,58,59]. For flux tubes transforming under the fundamental or the antifundamental representation of $SU(3)$, this factor is shown to equal $4/3$, while for flux tubes transforming with the adjoint representation of $SU(3)$, it is shown to equal 3. The one-gluon exchange term includes a factor $F_i \cdot F_j$ which combines the $SU(3)$ generators of particles i and j. Its value can be deduced from those of the Casimir because

$$\langle F_i\cdot F_j\rangle = \frac{\langle (F_i+F_j)^2\rangle - \langle F_i^2\rangle - \langle F_j^2\rangle}{2}, \quad \text{(F2)}$$

where $(F_i+F_j)^2$ is the $SU(3)$ Casimir operator for the pair of particles i and j. Substituting these factors for a system of three gluons leads to the following expression:

$$V(\boldsymbol{r_1},\boldsymbol{r_2},\boldsymbol{r_3}) = 3\beta\min_{\boldsymbol{Y}} \sum_{i=1}^{3} |\boldsymbol{r_i}-\boldsymbol{Y}| - \sum_{i<j}^{3} \frac{3\alpha_s}{2|\boldsymbol{r_i}-\boldsymbol{r_j}|}. \quad \text{(F3)}$$

The Y junction introduces a genuine three-body interaction, which is incompatible with the formalism developed in the current work. As proposed in Ref. [60], this three-body interaction can be approximated by three effective two-body interactions with a rescaling parameter close to $1/2$. The interaction then becomes

$$V(\boldsymbol{r_1},\boldsymbol{r_2},\boldsymbol{r_3}) = \frac{3}{2}\beta \sum_{i<j}^{3} |\boldsymbol{r_i}-\boldsymbol{r_j}| - \sum_{i<j}^{3} \frac{3\alpha_s}{2|\boldsymbol{r_i}-\boldsymbol{r_j}|}. \quad \text{(F4)}$$

To compare this with the potential (152) used in the Δ junction, one must relate the mesonic and the fundamental string tensions. For mesons, the Casimir scaling factor is $4/3$ for both the quark and the antiquark flux tubes,

$$\sigma = \frac{4}{3}\beta. \tag{F5}$$

Expressing the interaction potential in terms of the mesonic string tension gives

$$V(\boldsymbol{r_1}, \boldsymbol{r_2}, \boldsymbol{r_3}) = \frac{9}{8}\sigma \sum_{i<j}^{3} |\boldsymbol{r_i} - \boldsymbol{r_j}| - \sum_{i<j}^{3} \frac{3\alpha_s}{2|\boldsymbol{r_i} - \boldsymbol{r_j}|}. \tag{F6}$$

This potential differs from the Δ junction potential (152) by a factor of $9/8$. This factor, a little higher than 1, slightly increases the overall energy of the glueball if the Y junction is considered. This conclusion aligns with the LQCD arguments from Ref. [57]. For this reason, a Δ junction is preferred in the present work.

[1] H. Fritzsch and M. Gell-Mann, Current algebra: Quarks and what else?, eConf **C720906V2**, 135 (1972).
[2] V. Mathieu, N. Kochelev, and V. Vento, The physics of glueballs, Int. J. Mod. Phys. E **18**, 1 (2009).
[3] F. Llanes-Estrada, Glueballs as the ithaca of meson spectroscopy, Eur. Phys. J. Spec. Top. **230**, 1575 (2021).
[4] V. Crede and C. Meyer, The experimental status of glueballs, Prog. Part. Nucl. Phys. **63**, 74 (2009).
[5] Y. Chen, A. Alexandru, S. Dong, T. Draper, I. Horváth, F. Lee, K. Liu, N. Mathur, C. Morningstar, M. Peardon, S. Tamhankar, B. Young, and J. Zhang, Glueball spectrum and matrix elements on anisotropic lattices, Phys. Rev. D **73**, 014516 (2006).
[6] C. Morningstar and M. Peardon, Glueball spectrum from an anisotropic lattice study, Phys. Rev. D **60**, 034509 (1999).
[7] H. Meyer and M. Teper, Glueball regge trajectories and the pomeron: A lattice study, Phys. Lett. B **605**, 344 (2005).
[8] D. Liu and J. Wu, The first calculation for the mass of the ground 4^{++} glueball state on lattice, Mod. Phys. Lett. A **17**, 1419 (2002).
[9] V. Petrov and N. Tkachenko, Odderon: Lost or/and found?, arXiv:2201.06948.
[10] N. Boulanger, V. Mathieu, F. Buisseret, and C. Semay, Constituent gluon interpretation of glueballs and gluelumps, Eur. Phys. J. A **38**, 317 (2008).
[11] V. Mathieu, F. Buisseret, and C. Semay, Gluons in glueballs: Spin or helicity?, Phys. Rev. D **77**, 114022 (2008).
[12] A. Szczepaniak and E. Swanson, The low-lying glueball spectrum, Phys. Lett. B **577**, 61 (2003).
[13] A. Szczepaniak, E. Swanson, C.-R. Ji, and S. Cotanch, Glueball spectroscopy in a relativistic many-body approach to hadronic structure, Phys. Rev. Lett. **76**, 2011 (1996).
[14] A. Martin and T. Spearman, *Elementary Particle Theory* (North-Holland Publishing Co., Amsterdam, 1970).
[15] V. Khersonskii, A. Moskalev, and D. Varshalovich, *Quantum Theory Of Angular Momentum* (World Scientific Publishing Co., Singapore, 1988).
[16] S.-U. Chung, Spin formalisms, Report No. CERN-71-08, 1971.
[17] M. Jacob and G. Wick, On the general theory of collisions for particles with spin, Ann. Phys. (N.Y.) **7**, 404 (1959).
[18] S. Weinberg, *The Quantum Theory of Fields* (Cambridge University Press, New York, 1995).
[19] D. Giebink, Relativity and spin in one-, two- and three-body systems, Phys. Rev. C **32**, 502 (1985).
[20] G. Wick, Angular momentum states for three relativistic particles, Ann. Phys. (N.Y.) **18**, 65 (1962).
[21] D. Eyre and J. Vary, Solving momentum-space integral equations for quarkonia spectra with confining potentials, Phys. Rev. D **34**, 3467 (1986).
[22] M. Abramowitz and I. Stegun, *Handbook of Mathematical Functions with Formulas, Graphs, and Mathematical Tables* (Dover Publications, Inc., New York, 1964).
[23] H. Hersbach, Relativistic linear potential in momentum space, Phys. Rev. D **47**, 3027 (1993).
[24] J. Norbury, D. Kahana, and K. Maung, Confining potential in momentum space, Can. J. Phys. **70**, 86 (1992).
[25] J. Cornwall, Dynamical mass generation in continuum quantum chromodynamics, Phys. Rev. D **26**, 1453 (1982).
[26] A. Cucchieri, T. Mendes, O. Oliveira, and P. Silva, Just how different are the $SU(2)$ and $SU(3)$ Landau-gauge propagators in the infrared regime?, Phys. Rev. D **76**, 114507 (2007).
[27] A. Aguilar, D. Binosi, and J. Papavassiliou, Gluon and ghost propagators in the Landau gauge: Deriving lattice results from Schwinger-Dyson equations, Phys. Rev. D **78**, 025010 (2008).
[28] A. C. Aguilar and J. Papavassiliou, Gluon mass generation without seagull divergences, Phys. Rev. D **81**, 034003 (2010).
[29] A. Aguilar, M. Ferreira, C. Figueiredo, and J. Papavassiliou, Gluon mass scale through nonlinearities and vertex interplay, Phys. Rev. D **100**, 094039 (2019).
[30] M. Huber, Correlation functions of Landau gauge Yang-Mills theory, Phys. Rev. D **101**, 114009 (2020).
[31] M. N. Ferreira and J. Papavassiliou, Gluon mass scale through the Schwinger mechanism, arXiv:2501.01080.
[32] V. Mathieu, C. Semay, and B. Silvestre-Brac, Semirelativistic potential model for three-gluon glueballs, Phys. Rev. D **77**, 094009 (2008).
[33] W.-S. Hou, C.-S. Luo, and G.-G. Wong, Glueball states in a constituent gluon model, Phys. Rev. D **64**, 014028 (2001).
[34] C. Semay and B. Silvestre-Brac, Comparison between relativistic, semirelativistic, and nonrelativistic approaches of quarkonium, Phys. Rev. D **46**, 5177 (1992).

[35] C. Semay, About the Casimir scaling hypothesis, Eur. Phys. J. A **22**, 353 (2004).
[36] C. Semay, D. Baye, M. Hesse, and B. Silvestre-Brac, Semirelativistic Lagrange mesh calculations, Phys. Rev. E **64**, 016703 (2001).
[37] Y. Suzuki and K. Varga, *Stochastic Variational Approach to Quantum-Mechanical Few-Body Problems* (Springer, Berlin, Heidelberg, 1998).
[38] S. Berman and M. Jacob, Systematics of angular and polarization distributions in three-body decays, Phys. Rev. **139**, B1023 (1965).
[39] J. Werle, Relativistic partial wave expansions for multiparticle processes, Phys. Lett. **4**, 127 (1963).
[40] M.Hesse, Three-body bound-state calculations by the Lagrange-mesh method: Selection of a coordinate system, Phys. Rev. E **65**, 046703 (2002).
[41] N. Lindner, A. Peres, and D. Terno, Wigner's little group and Berry's phase for massless particles, J. Phys. A **36**, L449 (2003).
[42] F. Fumi and L. Wolfenstein, Allowed final states for annihilation into three photons, Phys. Rev. **90**, 498 (1953).
[43] M. Hamermesh, *Group Theory and Its Application to Physical Problems* (Dover Publications, Inc., New York, 1989).
[44] D. Peaslee, Absolute selection rules for meson decay, Helv. Phys. Acta **23**, 845 (1950).
[45] A. Athenodorou and M. Teper, The glueball spectrum of $SU(3)$ gauge theory in $3+1$ dimensions, J. High Energy Phys. 11 (2020) 172.
[46] F. Llanes-Estrada, P. Bicudo, and S. Cotanch, J^{--} oddballs and a low odderon intercept, Phys. Rev. Lett. **96**, 081601 (2006).
[47] B. Silvestre-Brac, R. Bonnaz, C. Semay, and F. Brau, Quantum three body problems using harmonic oscillator bases with different sizes, arXiv:2003.11028, internal report ISN 0066.
[48] C. Chevalier and S. Khodja, Three-body forces in oscillator bases expansion, Few-Body Syst. **65**, 86 (2024).
[49] L. Theußl, R. Wagenbrunn, B. Desplanques, and W. Plessas, Hadronic decays of N and Δ resonances in a chiral quark model, Eur. Phys. J. A **12**, 91 (2001).
[50] F. Giannuzzi, Heavy pentaquark spectroscopy in the diquark model, Phys. Rev. D **99**, 094006 (2019).
[51] S. Capstick and N. Isgur, Baryons in a relativized quark model with chromodynamics, Phys. Rev. D **34**, 2809 (1986).
[52] S. Flügge, *Practical Quantum Mechanics* (Springer, Berlin, 1994).
[53] W. Lucha, F. Schöberl, and D. Gromes, Bound states of quarks, Phys. Rep. **200**, 127 (1991).
[54] L. Fulcher, Matrix representation of the nonlocal kinetic energy operator, the spinless salpeter equation and the cornell potential, Phys. Rev. D **50**, 447 (1994).
[55] R. Yàñez, W. V. Assche, and J. Dehesat, Position and momentum information entropies of the D-dimensional harmonic oscillator and hydrogen atom, Phys. Rev. A **50**, 3065 (1994).
[56] F. Buisseret, V. Mathieu, and C. Semay, Glueball phenomenology and the relativistic flux tube model, Phys. Rev. D **80**, 074021 (2009).
[57] M. Cardoso and P. Bicudo, First study of the three-gluon static potential in lattice QCD, Phys. Rev. D **78**, 074508 (2008).
[58] G. Bali, Casimir scaling of $SU(3)$ static potentials, Phys. Rev. D **62**, 114503 (2000).
[59] P. Bicudo, M. Cardoso, and O. Oliveira, Study of the gluon-quark-antiquark static potential in $SU(3)$ lattice QCD, Phys. Rev. D **77**, 091504 (2008).
[60] B. Silvestre-Brac, C. Semay, I. Narodetskii, and A. Veselov, The baryonic Y-shape confining potential energy and its approximants, Eur. Phys. J. C **32**, 385 (2004).